NUREG/CR-5429
Vol. 1

UDEC (Universal Distinct Element Code) Version ICG1.5

Software Summary

Prepared by Mark Board

Itasca Consulting Group, Inc.

Prepared for
U.S. Nuclear Regulatory Commission

AVAILABILITY NOTICE

Availability of Reference Materials Cited in NRC Publications

Most documents cited in NRC publications will be available from one of the following sources:

1. The NRC Public Document Room, 2120 L Street, NW, Lower Level, Washington, DC 20555

2. The Superintendent of Documents, U.S. Government Printing Office, P.O. Box 37082, Washington, DC 20013-7082

3. The National Technical Information Service, Springfield, VA 22161

Although the listing that follows represents the majority of documents cited in NRC publications, it is not intended to be exhaustive.

Referenced documents available for inspection and copying for a fee from the NRC Public Document Room include NRC correspondence and internal NRC memoranda; NRC Office of Inspection and Enforcement bulletins, circulars, information notices, inspection and investigation notices; Licensee Event Reports; vendor reports and correspondence; Commission papers; and applicant and licensee documents and correspondence.

The following documents in the NUREG series are available for purchase from the GPO Sales Program: formal NRC staff and contractor reports, NRC-sponsored conference proceedings, and NRC booklets and brochures. Also available are Regulatory Guides, NRC regulations in the *Code of Federal Regulations*, and *Nuclear Regulatory Commission Issuances*.

Documents available from the National Technical Information Service include NUREG series reports and technical reports prepared by other federal agencies and reports prepared by the Atomic Energy Commission, forerunner agency to the Nuclear Regulatory Commission.

Documents available from public and special technical libraries include all open literature items, such as books, journal and periodical articles, and transactions. *Federal Register* notices, federal and state legislation, and congressional reports can usually be obtained from these libraries.

Documents such as theses, dissertations, foreign reports and translations, and non-NRC conference proceedings are available for purchase from the organization sponsoring the publication cited.

Single copies of NRC draft reports are available free, to the extent of supply, upon written request to the Office of Information Resources Management, Distribution Section, U.S. Nuclear Regulatory Commission, Washington, DC 20555.

Copies of industry codes and standards used in a substantive manner in the NRC regulatory process are maintained at the NRC Library, 7920 Norfolk Avenue, Bethesda, Maryland, and are available there for reference use by the public. Codes and standards are usually copyrighted and may be purchased from the originating organization or, if they are American National Standards, from the American National Standards Institute, 1430 Broadway, New York, NY 10018.

DISCLAIMER NOTICE

NUREG/CR-5429
Vol. 1

UDEC (Universal Distinct Element Code) Version ICG1.5

Software Summary

Manuscript Completed: August 1989
Date Published: September 1989

Prepared by
Mark Board

Itasca Consulting Group, Inc.
1313 5th Street SE, Suite 210
Minneapolis, MN 55414

Prepared for
Division of High-Level Waste Management
Office of Nuclear Material Safety and Safeguards
U.S. Nuclear Regulatory Commission
Washington, DC 20555
NRC FIN D1016

ABSTRACT

UDEC (Universal Distinct Element Code) is a two-dimensional distinct element program written for the static and dynamic analysis of the mechanical, thermal and hydrologic behavior of jointed rock masses. This program has been applied to a wide variety of problems in civil construction, mining, nuclear waste disposal, and geologic modeling. This document presents the theoretical basis for the mathematical models, the details of solution procedures, user's manual and presentation of verification and example problems. A description of the program support and documentation methodology which is employed is also given. This document is given in three volumes: Volume 1 — Description of Mathematical Models and Numerical Methods, Volume 2 — User's Manual, and Volume 3 — Verification and Example Problems. These three volumes are intended to satisfy the requirements and guidelines set forth in Final Technical Position and Documentation of Computer Codes For High-Level Waste Management (NUREG-0856).

TABLE OF CONTENTS

VOLUME 1

SOFTWARE SUMMARY

TABLE OF CONTENTS

TABLE OF CONTENTS
(continued)

TABLE OF CONTENTS
(continued)

TABLE OF CONTENTS
(continued)

TABLE OF CONTENTS
(continued)

TABLE OF CONTENTS
(continued)

TABLE OF CONTENTS
(continued)

LIST OF FIGURES

LIST OF FIGURES
(continued)

LIST OF FIGURES
(continued)

LIST OF FIGURES
(continued)

LIST OF FIGURES
(continued)

LIST OF TABLES

1.1 STATEMENT AND DESCRIPTION OF THE PROBLEM

1.1.1 Introduction

The following report provides the quality assurance documentation suggested by the U.S. Nuclear Regulatory Commission (NRC) for computer codes which are to be used to meet, in part, the requirements of 10CFR Part 60. The report follows the format given in NUREG-0856, Final Technical Position on Documentation of Computer Codes for High-Level Waste Management (U.S. NRC, 1983). Disposal of high-level nuclear waste into an underground repository will result in thermal, mechanical and hydrologic effects to the surrounding, fractured rock mass. The UDEC code can be used to analyze the complex stress changes and rock mass deformations resulting from excavation and waste emplacement.

UDEC (Universal Distinct Element Code) is a two-dimensional computer program based on the distinct element method. The program, originally written by P. A. Cundall (Cundall 1980), has been under active development for over 10 years. The distinct element method is a recognized discontinuum modeling approach for simulating the behavior of jointed media subjected to quasi-static or dynamic boundary conditions. The method has three distinguishing features which make it well suited for discontinuum modeling.

1. The medium is simulated as an assemblage of blocks which interact through corner and edge contacts.

2. Discontinuities are regarded as boundary interactions between these blocks; discontinuity behavior is prescribed for these interactions.

3. The method utilizes an explicit timestepping (dynamic) algorithm which allows large displacements and rotations and general non-linear constitutive behavior for both the matrix and discontinuities.

UDEC is specifically designed to simulate the predominant features of fractured rock masses, including:

(a) complex joint structures;

(b) non-linear, inelastic joint behavior;

(c) elasto-plastic behavior of intact rock; and

(d) fluid flow and steady state pore pressure distribution in joints.

Additionally, transient heat transfer analysis and coupled thermal stress capabilities are available.

UDEC has been written in modular form for ease of modification. The coding has been performed in ANSI FORTRAN 77 with a minimum of machine-specific calls. The code, originally developed for use on mini- and mainframe computers has been modified for use on IBM compatible, 80386-based personal computers. The code makes use of a free-format, word-oriented input command structure, and is fully equipped with interactive graphics for screen or hard-copy plotting.

1.1.2 Program Capabilities Summary

UDEC has extensive capabilities for analysis of quasi-static and dynamic problems in solid mechanics, heat transfer and fracture fluid flow. Additionally, the code is equipped with an interactive or batch mode command interpreter and interactive graphical display capabilities. A summary of the code capabilities is given below.

1. Problem Geometry

   - Automatic Generation of Outer Boundary of the Problem
   - Statistically-Based Joint Generator — Joint sets are defined by their spacing, trace length, angle and gap between segments of the joints. Any of these variables may be defined by a mean value and some random variation from the mean, thus allowing virtually any jointing pattern to be generated with a minimum number of commands.
   - Automatic or Manual Finite Difference Zone Generator for Fully-Deformable Blocks
   - Automatic Excavation Generator for Formation of Excavation Geometries in the Block Structure

2. Model Solution Conditions

- Plane Strain
- Quasi-Static (dynamic solution damped to provide static solution)
- Dynamic (free field, non-reflecting boundaries, forced vibration)
- Thermal/Mechanical Analysis (optional explicit or implicit temperature calculation)
- Fluid Flow, Coupled Mechanical Analysis
- Damping — Damping constants may be selected automatically which is the usual case for static problems, or may be user-defined. Optional stiffness and/or mass proportional damping may be specified.

3. Block Mechanical Models

- Rigid (simplest formulation, no internal deformations)
- Simply Deformable (limited modes of internal deformation based on linear block stiffnesses)
- Fully Deformable — The blocks are internally discretized into triangular finite difference zones to allow complete determination of the internal stress and strain tensors)

4. Kinematics

- Large Displacement/Large Strain (no restriction on displacement or distortion of blocks). Blocks may slide past one another, or separate. Contacts between blocks are recognized and used for calculation of internal deformations.

5. Block Constitutive Models

- Simply Deformable - Elastic linear stiffness
  - Experimental elastic/brittle fracture by Griffith's theory

- Fully Deformable

  (a) Mechanical

  - general large-strain finite difference formulations
  - linearly-elastic, isotropic
  - elasto-plastic, Mohr-Coulomb yield criterion, non-associated flow rule (dilation may be specified separately from friction), optional tension cut-off
  - experimental null model (used to identify excavated regions)

  (b) Thermal

  - conductive heat transfer

  (c) Hydraulic

  - Fluid flow is confined to fractures, blocks are considered to be impermeable.

6. Joint Constitutive Models

(a) Mechanical

- Mohr-Coulomb failure criterion — Friction, cohesion, dilation and tensile strength of the surfaces may be set in addition to joint shear and normal stiffness.
- Mohr-Coulomb failure criteria — As above, but once shear or tensile strength exceeded, joint is considered to be fractured and cohesion and tensile strength set to zero thereafter.
- Continuously-yielding joint model (allows peak/residual stress-displacement behavior for joints).

(b) Hydraulic

- parallel plate model. Fluid may be considered to be:
  - Newtonian (cubic law)
  - Bingham (viscoplastic flow)

7. Boundary Conditions

(a) Mechanical

- velocity (displacement) in x- and/or y-coordinate directions
- free (no imposed velocity)
- force
- stress/pressure
- viscous (non-reflecting) boundary in x- and/or y-coordinate directions
- free-field boundary (performs function of viscous boundary, but allows unaffected translatory motion at vertical boundaries)
- boundary element (for static mechanical analysis (only) where infinite boundaries are necessary)
- options for velocity, force or stress boundary conditions — x and y gradients. (x and y constant multipliers and temporal histories may be applied to the boundary conditions. Several optional code-defined temporal histories include constant, linear, sine, cosine and arbitrary functions of time. Also, the user may manually define a temporal history of any of the boundary conditions in an external file which may then be read into the code.)

(b) Thermal

- fixed temperature
- free temperature (default adiabatic conditions)
- flux (optional exponential decay)
- volumetric source (optional exponential decay)
- radiative
- convective

(c) Hydraulic (fluid flow)

- fluid pressure on external boundaries (optional gradient)
- fixed or free fluid pressure in joints
- impermeable boundaries

8. Initial Conditions

(a) Mechanical

- initial stress (optional gradients)
- gravity

(b) Thermal

- temperature

(c) Hydraulic

- fluid pressure (optional water table)

9. Input/Output

- free-form, free-sequence English word command structure
- interactive or batch operation
- numerical data print to screen or hard disk
- interactive graphics to monitor or hardcopy to Hewlett Packard compatible pen plotter or PostScript compatible laser printer
- save and restart of problems
- pre-programmed error message facility for trapping of common errors

10. Special Features

- structural elements
  - beam elements (3 d.o.f. for each node) for representing rock support such as linings
  - cable elements (for representing grouted or ungrouted cable bolts or rock bolts; pre-tensioning optional)
  - reinforcement - spring stiffness logic for force/displacement relation across joint surfaces
- time histories (ability to sample any variable at any location within the body)
- multiple material types (any block may be given any mechanical or thermal material type)
- mass scaling (scaling of masses to decrease solution time for static analyses)

1.2 STRUCTURE OF THE SYSTEM MODEL

UDEC is a distinct element code which has been written specifically for examination of mechanical, thermal and fluid flow problems in fractured media (Cundall, 1980; Cundall and Hart, 1983; Lemos, 1987; Itasca, 1989). In particular, the code has been applied extensively to modeling of problems in rock mechanics, and many of the features in the code have been written to aid in the analysis of geotechnical problems. However, the code can be applied to general problems in solid body mechanics and heat transfer without adjustment. This section describes the overall structure of the code and the methods used for problem solution.

The distinct element method was developed by Cundall (1971) for analysis of stresses and deformations in blocky media. The user defines a body to be composed of a number of interacting blocks which are separated by the intervening interface planes. This is in contrast to other, better known, techniques such as the finite element, finite difference and boundary element methods where the material is assumed to be a continuum. In these methods, the effects of jointing are often accounted for through the use of nonlinear constitutive laws (e.g., Mohr-Coulomb plasticity, "ubiquitous" joint models). In the distinct element method, the joints are accounted for explicitly.

Initial versions of the distinct element code were restricted to rigid blocks in which deformations were restricted to the joint surfaces (Voegele, 1978; Lorig, 1984). Cundall et al. (1978) later modified the formulation to allow internal deformability in two fashions: (1) simple deformability (block deformations restricted to three translational/rotational degrees of freedom); and, (2) full deformability, where the blocks are discretized internally using finite difference zones to allow refinement of deformations and generalization of constitutive laws. It is noted that UDEC can solve problems of continuous materials simply by modeling few, widely spaced fractures.

1.2.1 Block System

UDEC requires that the body to be modeled be divided into blocks which are separated from neighboring blocks by joints or interfaces (Fig. 1.2-1). The blocks may be considered to be rigid or deformable. Deformable blocks are subdivided into triangular finite difference zones for calculation of internal stress and strain. The interfaces may be considered to conform to a standard Mohr-Coulomb slip condition or a displacement-weakening model. The system is subjected to static or dynamic boundary conditions and the blocks allowed to interact with one another across the interfaces. An explicit procedure is used to provide the static or dynamic solution.

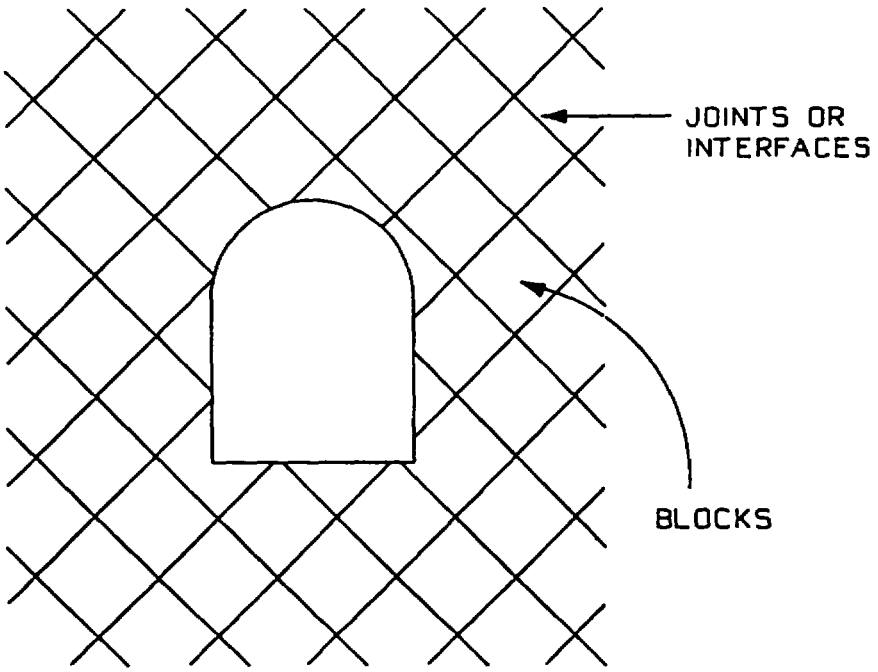

Fig. 1.2-1 Body Divided Into a System of Blocks Which May Be Rigid or Fully-Deformable

1.2.2 Explicit Solution Procedure

UDEC uses an explicit solution procedure as opposed to an implicit approach which is most common in finite element or boundary element methods. In the implicit approach, the equations describing the motion for all elements in the problem are solved simultaneously. For a linear-elastic, static analysis, the implicit solution is performed once but, for non-linear problems, several iterations of the complete set of equations may be required to converge to the equilibrium solution state. For non-linear dynamic analysis, the implicit scheme requires convergence to a solution state at each timestep. The timestep can be arbitrarily large with regard to numerical stability, but can still be restricted by the path dependency of the non-linear behavior of the system.

The system of equations in the implicit method is solved directly using a standard matrix solution method—for example, Gauss elimination. The solution method accounts for non-linearities by using an iterative procedure, such as the modified or unmodified Newton-Raphson method. The implicit approach is not well suited for problems that involve frequent changes to the connectivity between elements from, for example, highly non-linear behavior or dynamic loading. This is because the stiffness matrix must be reformulated every time a change in connectivity occurs.

In the explicit approach, unknown values of the variables relating to each element in the problem are calculated from known values in that element and its immediate neighbors. The equations relating these values are solved locally for each timestep* —there is no need to solve a complete system of equations. The reason for this independence of equations can be understood by considering that, in a physical system, there is a maximum speed at which information can propagate. For example, in an elastic solid, this speed corresponds to the compressional wave speed. In the explicit approach, the calculational timestep is selected sufficiently small that information cannot propagate further than one element during one timestep. If this timestep restriction is always satisfied, then the dependence of each element on its immediate neighbors is fulfilled, and the equations for each element can be solved independently.

The equations are solved in the explicit approach by direct integration† using a numerical differencing scheme. The central difference method is generally preferred over other differencing schemes because it is second-order accurate.

---

*This "timestep" may be a physically realistic timestep for dynamic analysis or a calculational increment progressing to an equilibrium state for a static analysis.

†For dynamic calculations, an alternative approach to direct integration for either implicit or explicit solution is a method called modal superposition [see, for example, Bathe and Wilson (1976)]. In this method, the equations of motion are first transformed into a generalized system of linear displacement equations known as a generalized eigenproblem. The eigenproblem yields n eigensolutions or n modes of displacement. Once these modes are known, they can be incorporated directly into each element and represent the response to loading. When many timesteps are required in the dynamic analysis, this approach can be more effective than direct integration. However, the approach is limited to problems involving linear behavior of the elements.

The timestep limitation in the explicit approach restricts the computation efficiency for solving linear problems because many calculational timesteps may be required to reach the equilibrium state. However, for non-linear analyses with an explicit program, there is little appreciable increase in computer time over the linear analysis, whereas an implicit program becomes much less efficient and may take several iterations to reach the solution, solving the complete system of equations at each step. The explicit approach, in this instance, proves more advantageous, particularly when the non-linear behavior is associated with a dynamic analysis.

The explicit solution approach is directly suitable for time domain dynamic analysis because the explicit time-marching scheme provides a reliable and efficient means for performing transient calculations. The method has also been adapted for static and quasi-static calculations by the use of two techniques, dynamic relaxation (Otter et al., 1966) and the conjugate gradient method (Consus et al., 1965), which facilitate the convergence to a static equilibrium or steady-state failure (collapse). In dynamic relaxation, as used in UDEC, the nodes of each element are moved in accordance to Newton's law of motion while, in the conjugate gradient method, convergence is achieved on the basis of a numerical iterative technique which does not involve reformulation of a stiffness matrix.

Cundall (1987) has shown that dynamic relaxation is better suited to model non-linear problems near failure than are iterative methods and can model collapse problems in a more realistic and efficient manner. With the conjugate gradient method, convergence for non-linear problems, particularly at failure, is not always guaranteed. While convergence is more certain with dynamic relaxation, the damping of inertial motion in this approach can still cause difficulties with problems at the collapse state because the viscous damping can introduce body forces which retard steady-state collapse. Cundall (1982 and 1987) describes the use of adaptive damping as an effective method to overcome this difficulty in dynamic relaxation. Adaptive damping continuously adjusts the viscosity such that the power absorbed by damping is a constant proportion of the rate of change of kinetic energy in the system. Therefore, as the kinetic energy approaches a constant or zero, the damping power also tends to zero.

Finally, because the explicit approach effectively "freezes" the strain-state of each element at each timestep, the non-linear material behavior can be followed directly, in incremental form, without the need for iterations.

1.2.3 General Solution Procedure in UDEC

The explicit algorithm used in the UDEC code is based on the use of force-displacement laws which specify the interactions between a block and its surrounding neighbors, and a law of motion which governs the displacements of the blocks as they are subjected to forces which are not in balance. As described above, the explicit method requires that a problem be solved in a time-marching procedure in which a calculation cycle is performed for each timestep. The basic mechanical calculation algorithms for rigid and fully-deformable (f.d.) blocks are shown in Figs. 1.2-2 and 1.2-3, respectively. Each of these calculation cycles perform the same basic calculations; the primary difference is that the law of motion is applied to the blocks themselves in the rigid block model, whereas it is applied to the grid points of the finite difference zones in the f.d. blocks. In each case, an initialization procedure is first performed in which the masses of the blocks or grid points and critical timestep is determined. The law of motion is applied to each block (grid point) using known force sums derived from boundary conditions, structural elements, fluid pressures (f.d. blocks), etc., to determine its velocity components. Coordinates of the block corners (rigid) or grid points (f.d.) are updated from the velocities. Since the UDEC code is a large strain model, there is no restriction in the deformation or motion of the blocks.

The normal and shear displacement increments across the contact are computed for each contact point. For rigid blocks, these increments are derived from rigid-body velocities of the blocks, while, for f.d. blocks, the increments come from the strain-rates of the contacting grid points. The normal and shear forces across the contacts are determined from the joint constitutive law. The normal force is linearly related to the normal displacement, and the shear force is limited by the Mohr-Coulomb slip condition for the default constitutive law. These forces are added into the force sums for the blocks or grid points involved in the contact. If f.d. blocks are used, the zone stresses are updated based on the constitutive relations for the block (intact) material.

The calculation cycle shown in Figs. 1.2-2 and 1.2-3 is performed once per timestep. For quasi-static problems, the timestep does not refer to real time, but a calculation increment and is more correctly viewed as a means of "cycling" a problem to the equilibrium or steady state. The primary goal is to bring the problem to the steady condition as rapidly as possible, thereby minimizing computational requirements. For quasi-static problems, viscous damping may be applied to the dynamic solution as in the dynamic relaxation method .

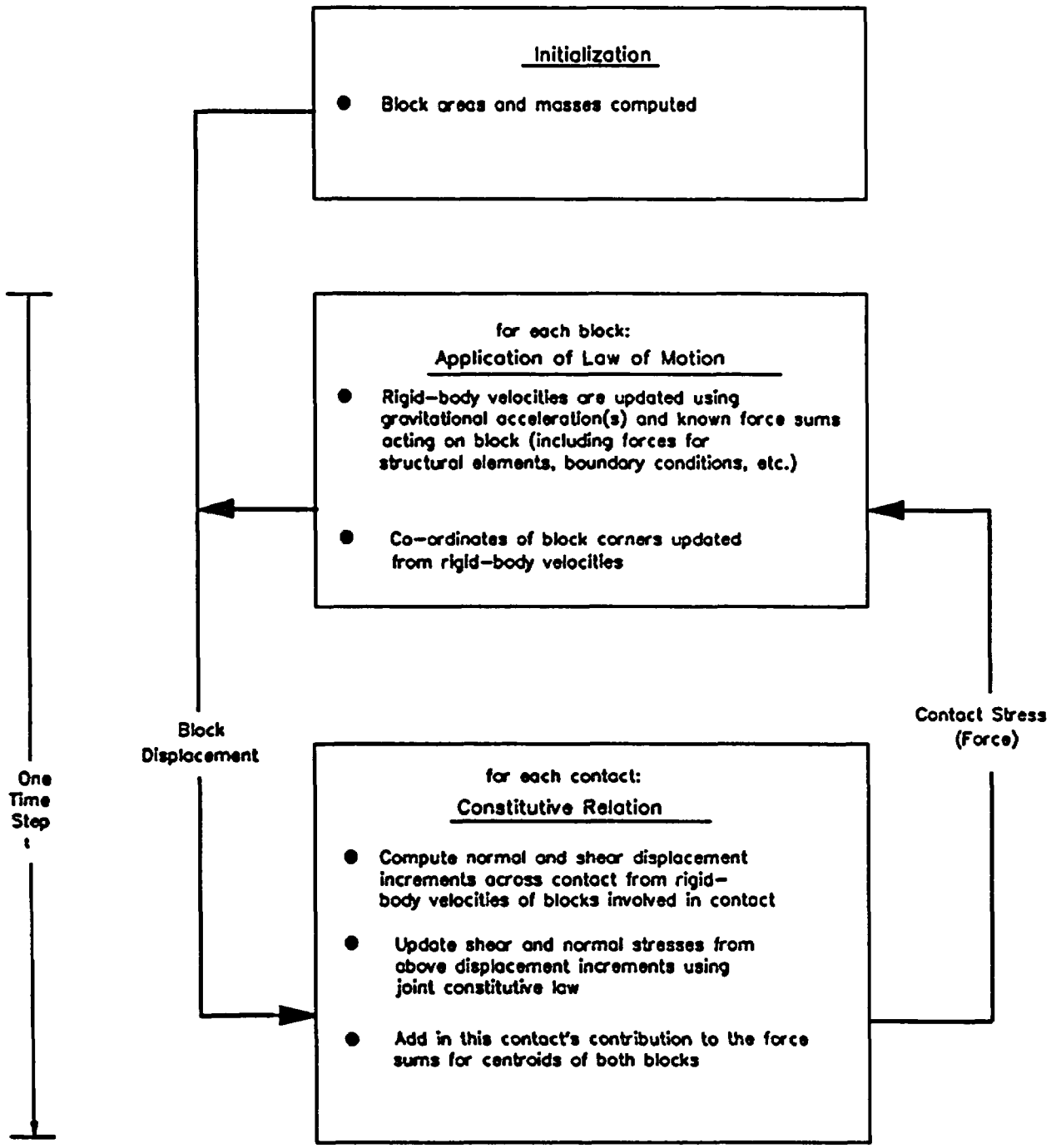

Fig. 1.2-2 Diagram Showing the Overall Calculation Flow For The Mechanical Portion of The UDEC Program For Rigid Blocks.

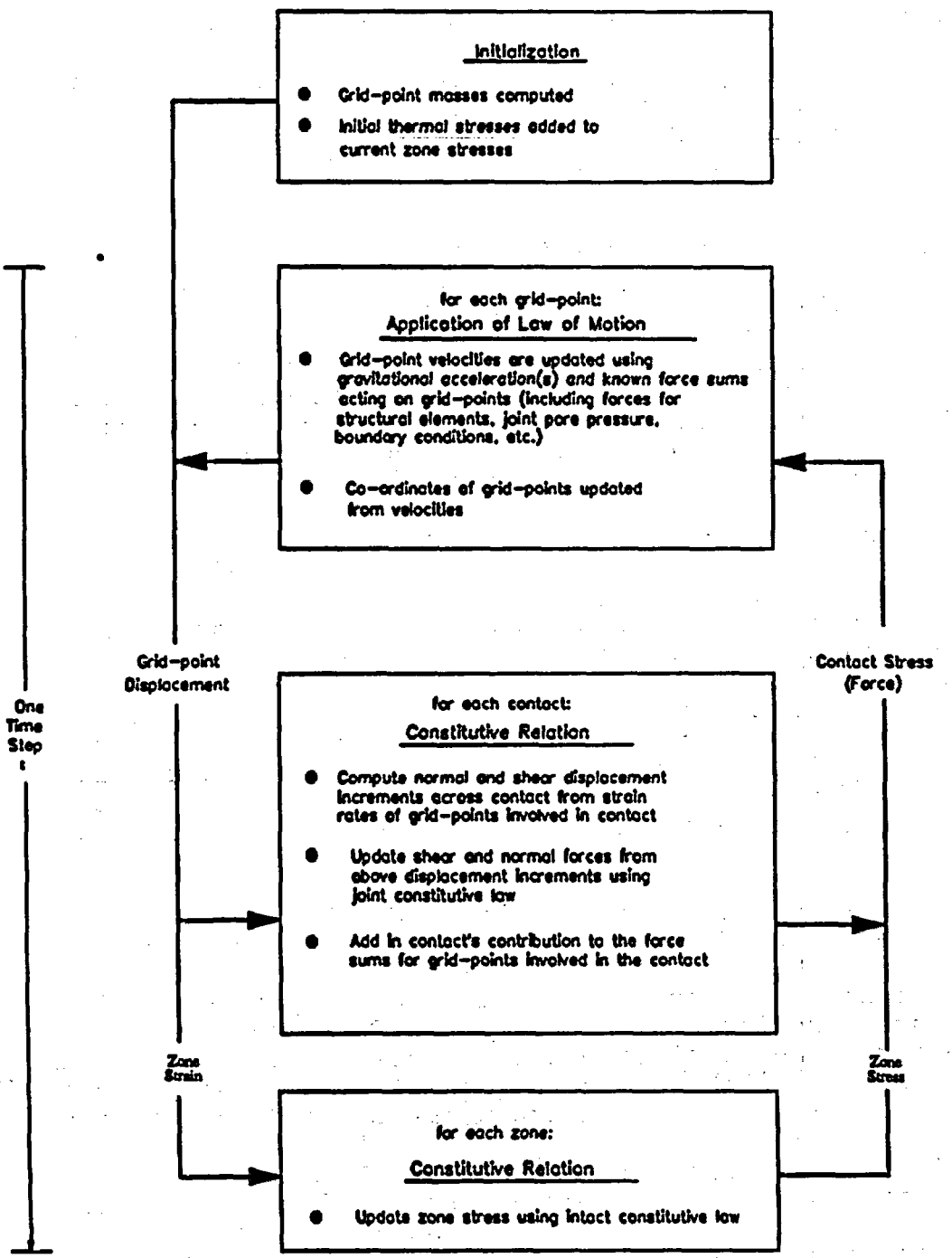

Fig. 1.2-3 Overall Calculation Flow for the Mechanical Portion of the UDEC Program for Fully-Deformable Blocks

Further detail on damping methodologies used in UDEC are provided in Chapter 1.3. In the case that a true dynamic problem is being solved, the timestep refers to real time, and a simulation is generally conducted for some explicit time period. Here, damping must be used with caution to avoid artificial transient effects to the numerical solution.

1.2.4 Thermal-Mechanical Analysis

UDEC contains finite difference logic for heat transfer analysis within and between blocks. This logic may be used as a standalone heat transfer code or may be applied to the mechanical portion of the code to conduct thermomechanical analyses. Thermal analysis may be conducted with rigid or fully deformable blocks, however, the coupled mechanical analysis requires the blocks to be subdivided into finite difference zones.

Heat flow in the body is assumed to be by conduction only (isotropic or transversely isotropic) and is governed by the standard two-dimensional diffusion equation. Thermal boundary conditions include convective, radiative, adiabatic (default) and constant temperature. UDEC offers a choice of explicit or implicit solution methods for heat transfer. For many of the typical problems examined in nuclear waste disposal, the implicit solution method can be advantageous since it is an unconditionally stable solution method, allowing larger time steps and shorter run times, particularly at late times in the run where temperature gradients are small. The explicit method may be better suited in cases where temperature gradients are larger.

The manner in which a coupled thermomechanical run is normally conducted is to first run the heat transfer analysis to the desired time (Fig. 1.2-4). At the end of the thermal analysis, each finite difference grid point in the problem will have a temperature associated with it. To perform the thermomechanical coupling, mechanical timesteps (cycles) are conducted until the body is at equilibrium as in the solution of standard quasi-static problems. The temperatures are used to determine out-of-balance thermo-elastic forces (f.d. blocks only) assuming isotropic linear volumetric expansion. As shown in Fig. 1.2-3, these thermally-induced forces are added into the force sums for each gridpoint prior to the mechanical timesteps. The heat transfer and mechanical analysis portions of the code act in a partially-coupled fashion. The temperatures are used to derive mechanical forces, but accelerations of the body do not, in turn, give rise to energy changes which may affect heat transfer.

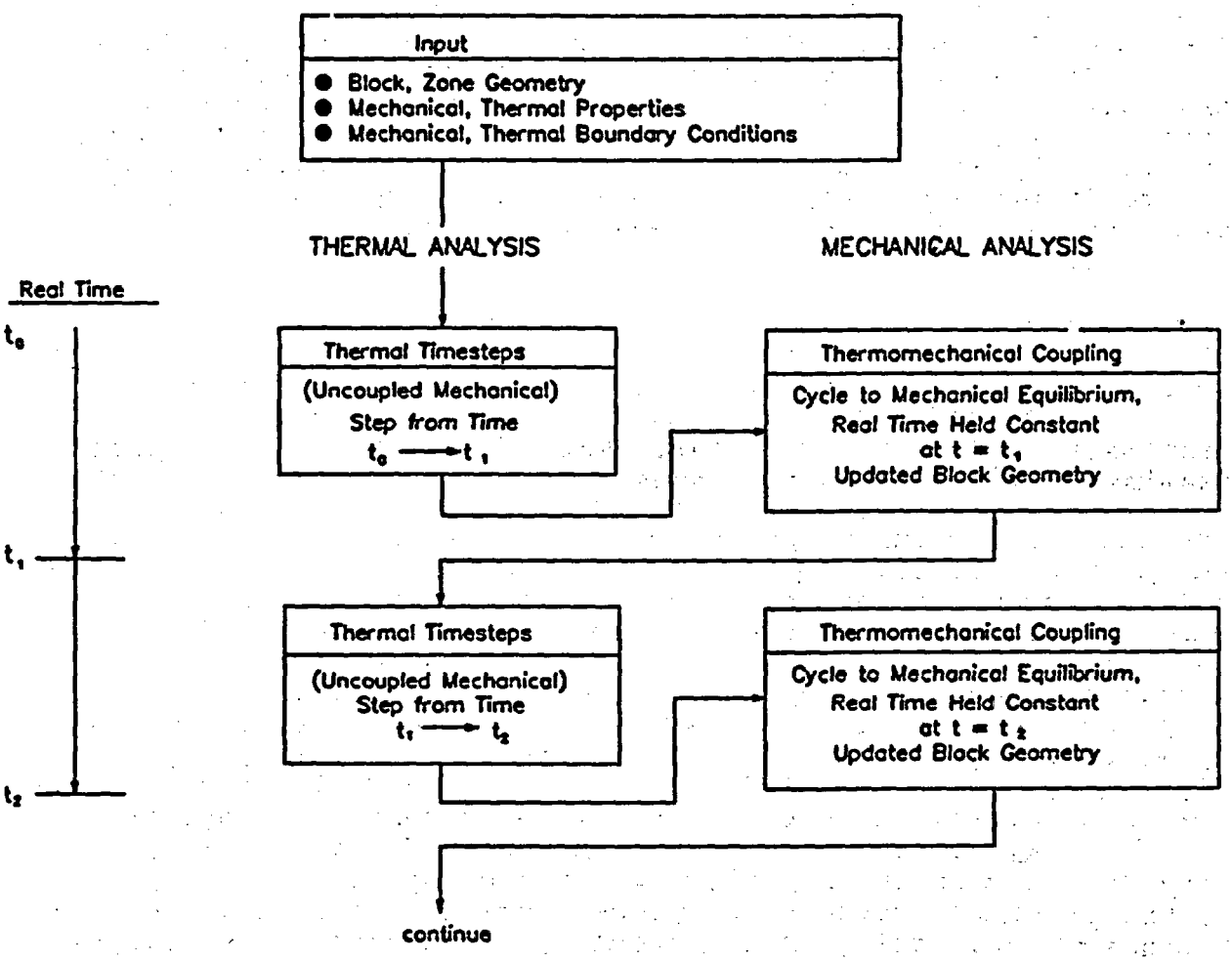

Fig. 1.2-4 Method of Running a Coupled Thermomechanical Simulation with UDEC

1.2.5 Fluid Flow in Joints

UDEC has the capability to perform analysis of fluid flow through a fracture system which separates impermeable blocks. Fully-saturated conditions are assumed to exist in the joints where fluid is present, but an unsaturated-saturated demarcation may exist in the model (e.g., at the phreatic surface). The fluid flow analysis is fully coupled to the mechanical analysis in that fracture aperture (and thus, its hydraulic conductivity) is dependent on mechanical deformations and conversely, joint water pressures affect the deformations of the block/joint system. Although transient fluid flow analyses are theoretically possible, the extremely small flow timestep and arbitrary volumes used at joint intersections make this procedure time consuming and inaccurate. Therefore, steady-state pore fluid distributions are generally used in coupled analyses. Full coupling of the fluid flow, mechanical computations and heat transfer is <u>not</u> provided in the code.

Figure 1.2-5 illustrates the calculation cycle for the fluid-mechanical coupling. Fluid-mechanical coupling requires a detailed knowledge of the aperture at and between block contacts. Elaborate procedures are required in UDEC to update the contact structure, detecting new contacts and deleting others. It is not computationally efficient to check for all possible block interactions, and therefore the concept of "domains" was developed. Domains are regions of space between blocks which are defined by the contact points. During any time increment, new contacts can only by formed between block edges and corners within a domain. These domains are also used to simplify the logic for fluid flow between blocks. Pore pressures are considered to be constant within any given domain, and pressure differentials can exist between adjacent domains. This pressure differential drives fluid flow according to the well known cubic law for parallel plate flow. As seen in Fig. 1.2-5, the gradient and flow rate are determined for each contact based on the current joint aperture. The flow sums of the domains are accumulated and the pressures updated based on the net flow and area change of the domain due to motion of the surrounding blocks during a timestep. The domain pressures acting on the blocks are converted to equivalent contact forces which are added into the force sums to be used in the motion law for the grid points. Details on the fluid flow logic are presented in Section 3 of this report.

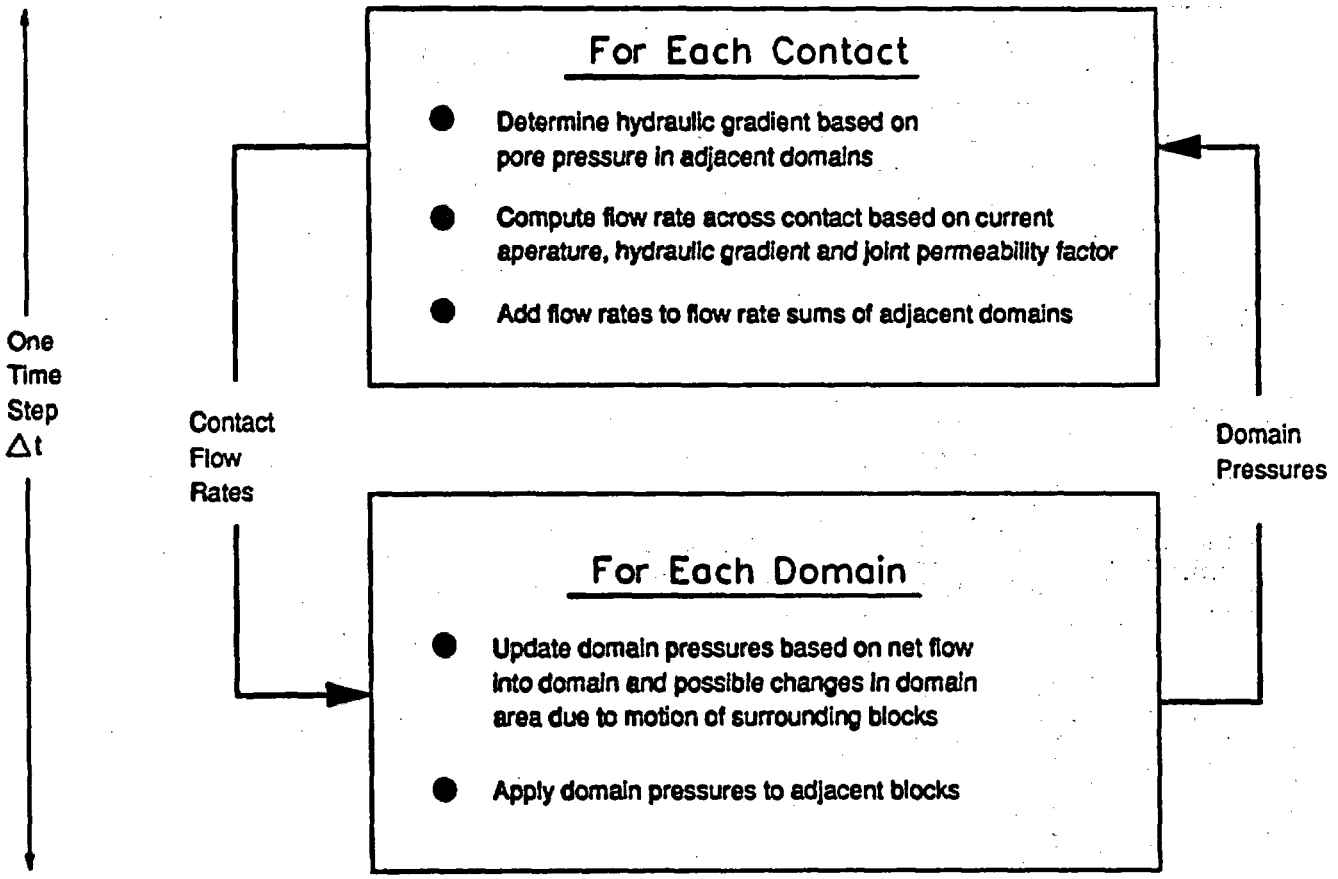

Fig. 1.2-5 Simplified Logic Diagram for the Fluid Flow Calculations in the UDEC Code

1.2.6 Structural Element Logic

Underground excavations in fractured rock are typically supported with a combination of rock bolts, cable anchors and interior support such as shotcrete, concrete arches, steel sets, etc. UDEC has the capability to model these supports using an optional structural element logic provided in the code. Three basic types of elements are available: beam elements to represent interior support types, cable elements for representation of grouted bolts which may be pretensioned and bolt elements used to represent "dowelling" and axial behavior of stiff bar reinforcement across joints. The beam elements use a standard matrix structural approach with three degrees of freedom at each end node (2 displacements, 1 moment). The interface of the beam nodes to the rock are represented by radial and tangential springs, allowing simulation of fully bonded or slipping connections to the rock mass.

UDEC provides a choice of two basic methods for representing rock or cable bolts. The first is a "local" reinforcement model across discontinuities; the second accounts for inelastic deformation of intact rock and shear behavior of a grout annulus. The first model restricts the effects of the reinforcment to the discontinuities themselves; large shear displacements are accounted for by assuming simple geometric changes develop locally in the reinforcement near a discontinuity. This model is therefore most suitable in cases where the deformation of individual rock blocks is negligible (i.e., the rigid block representation). In the second approach, the grout in the annulus between the rock and bolt is modeled as a Mohr-Coulomb material. This representation may only be used with fully-deformable blocks. Axial tensile forces are induced in the bolt through the interaction with the surrounding rock via the grout.

Figures 1.2-2 and 1.2-3 provide simple block diagrams reviewing the mechanical calculation methodology for a given timestep (or cycle for quasi-static solutions). The mechanical effect of rock reinforcement to the block structure can be seen as an addition to the out-of-balance forces for a given gridpoint or block. The forces along the reinforcement are lumped onto the adjacent finite difference grid points in the same manner as any other out-of-balance forces in the model. Greater detail regarding the formulations and solution algorithms are given in Section 1.3 of this report.

1.2.7 Simplified Flow Chart For the UDEC Code

Figures 1.2-6 to 1.2-12 are simplified flow charts for the structure and logic used in the UDEC code. Figure 1.2-6 shows the major control routines in the program which are used outside the main timestepping loop of the code. An English word command interpreter (in routine MON) is used in batch or interactive mode to interpret user commands and parse out program functions. An error trapping facility is provided which will recognize most common errors and inform the user without loss of the run. Many of the code sections shown in Figure 1.2-6 are used to set up the blocks and finite difference zones, structural elements, etc., and to assign properties and system control variables.

The primary calculation loop is given in the separate program branch denoted as "A". The minimum time step is determined first in routine INI, followed by the main calculation portion of the code, controlled by routine CYCLE. The general logic employed in the main cycing portion of the code is given in Figs. 1.2-7 to 1.2-9. These figures should be viewed in continuation. Further detail on implementation of the law of motion to blocks is given in Fig. 1.2-10, detection of block contacts in Fig. 1.2-11 and implementation of the joint contact laws in Fig. 1.2-12. In CYCLE, the main calculation loop runs over the total number of timesteps specified. For each timestep, the main mechanical functions of the code (application of the law of motion, checking for all block contacts and invoking the interface constitutive laws) are conducted for all blocks.

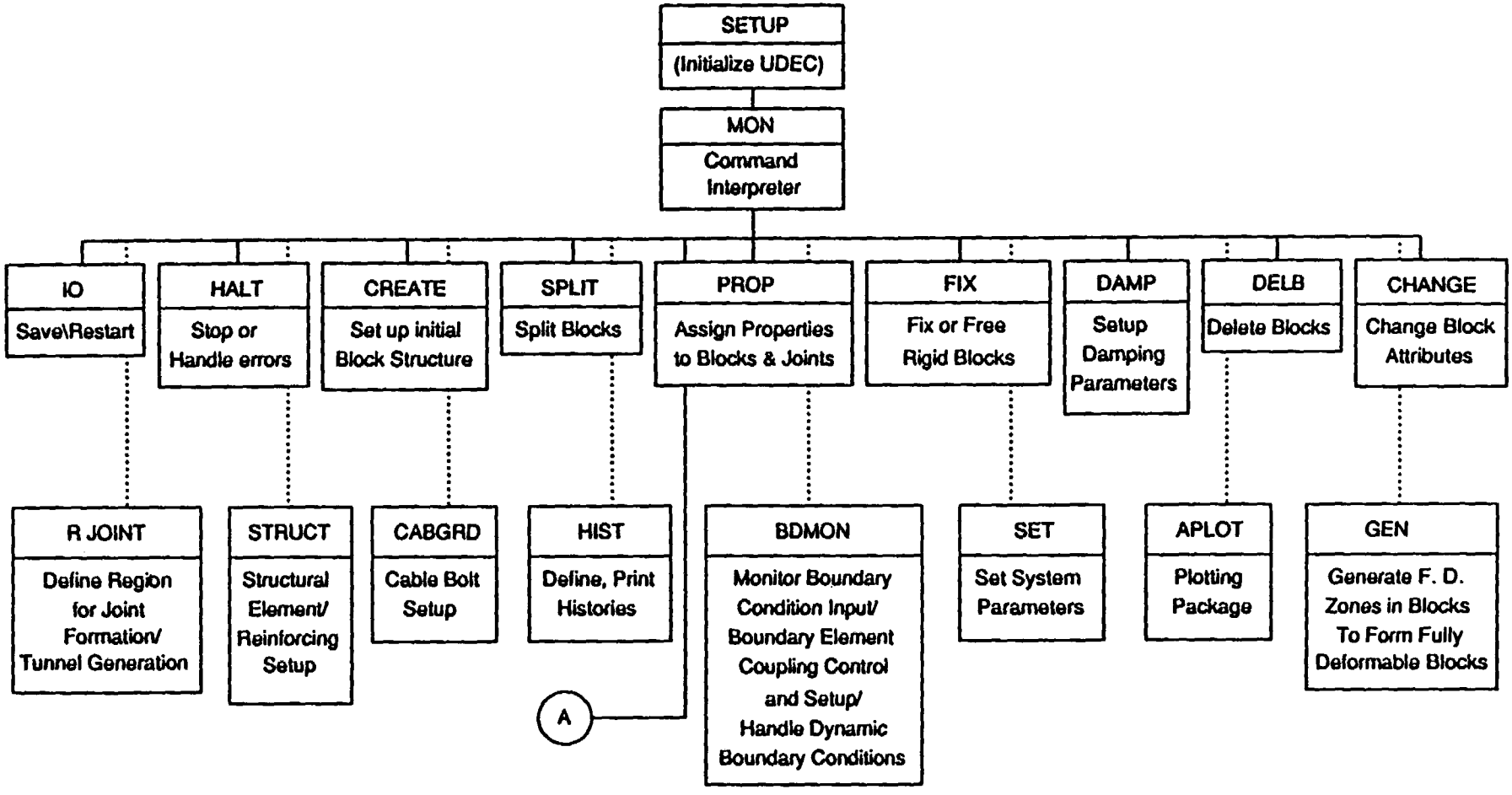

Fig. 1.2-6 Simplified Flow Chart of the Overall Functions of the UDEC Code

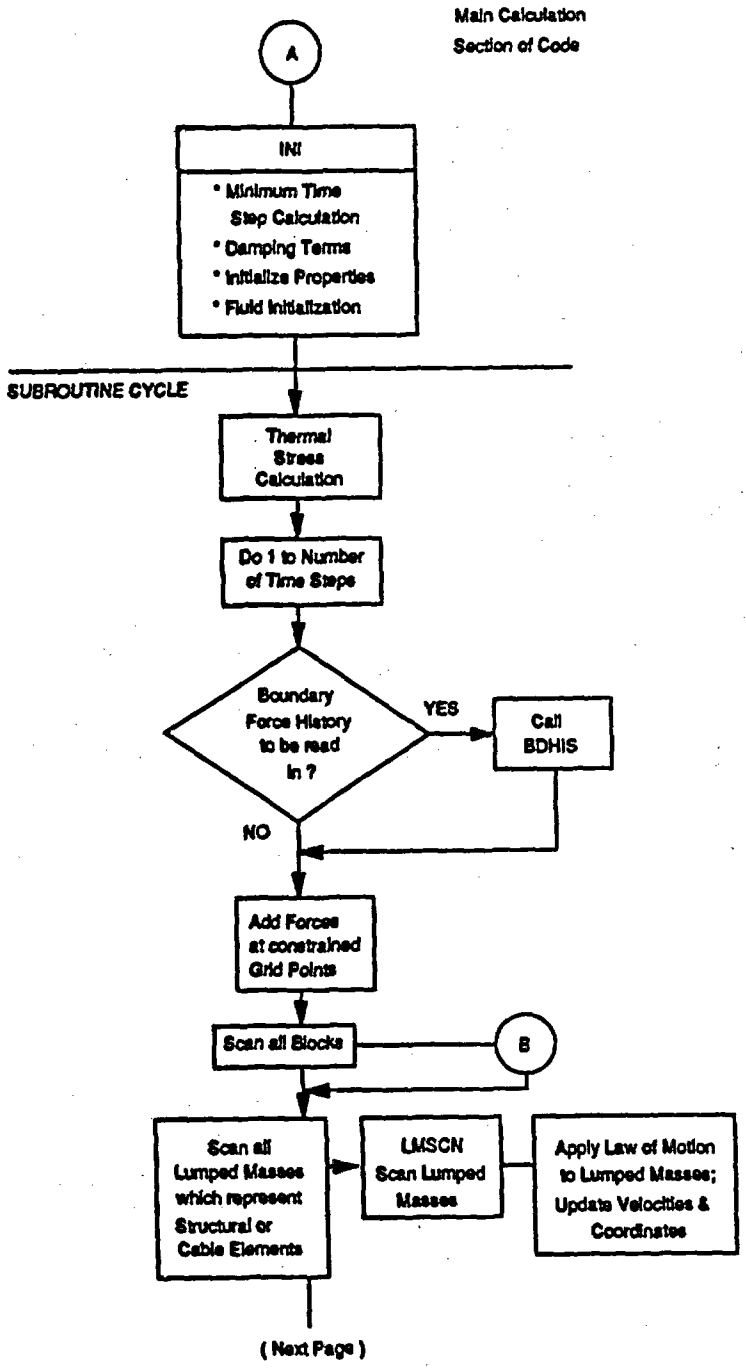

Fig. 1.2-7 Main Calculation Section of the UDEC Code

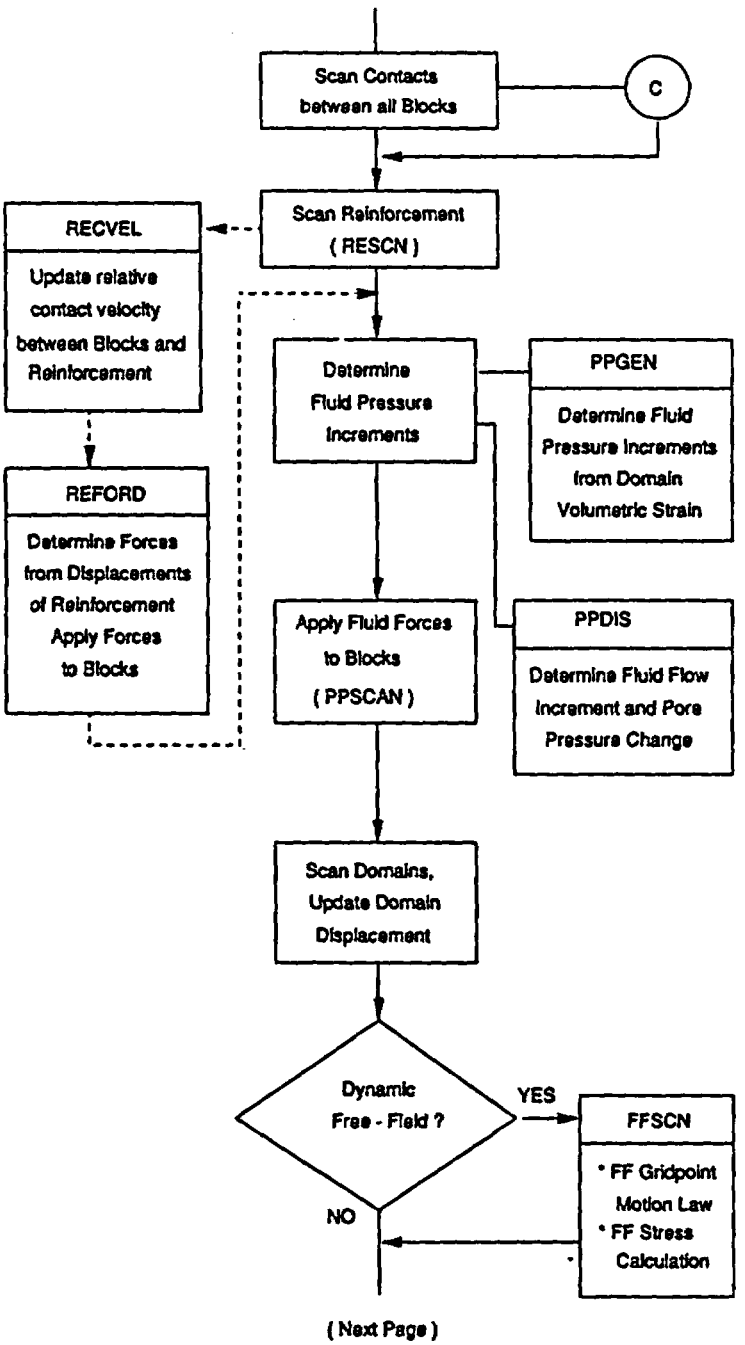

Fig. 1.2-8 Main Calculation Section of the UDEC Code (continued)

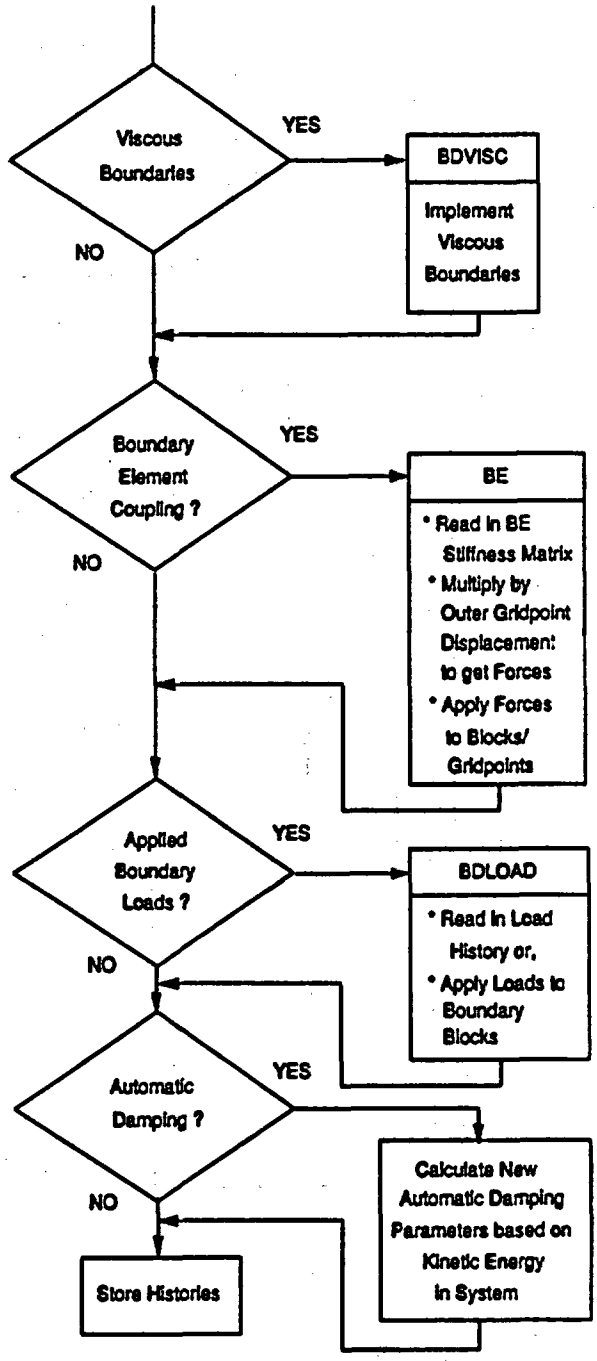

Fig. 1.2-9 Main Calculation Section of the UDEC Code (concluded)

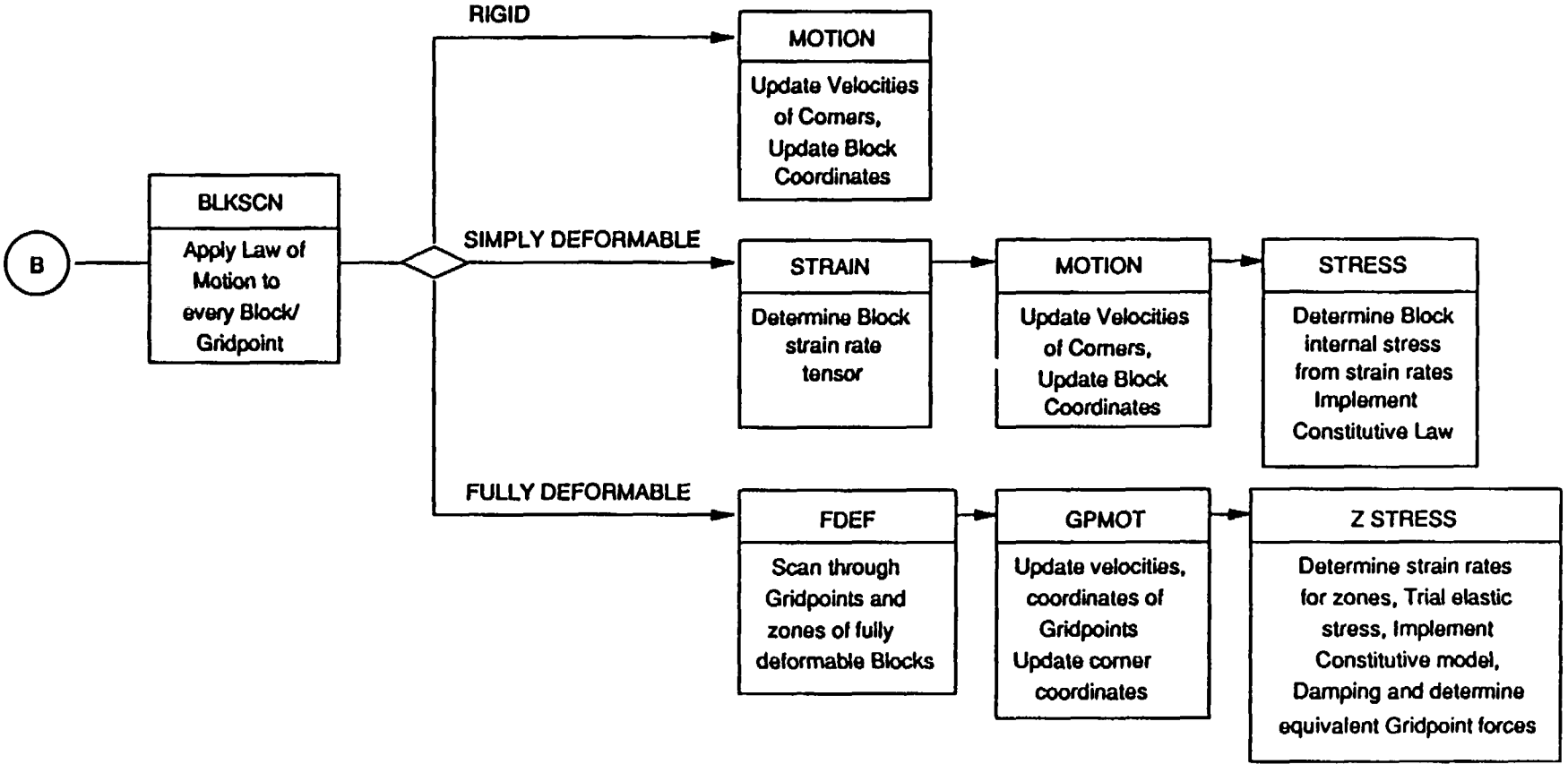

Fig. 1.2-10 Implementation of the Law of Motion

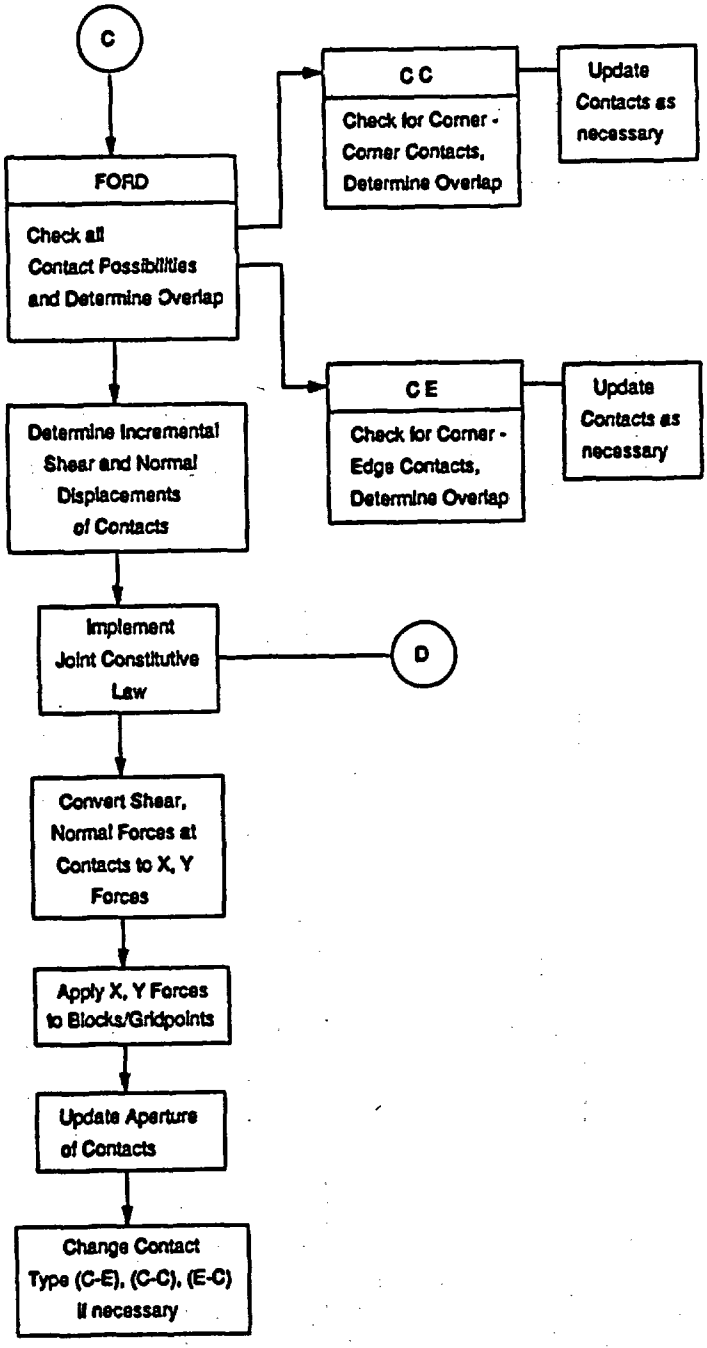

Fig. 1.2-11 Contact Detection Logic

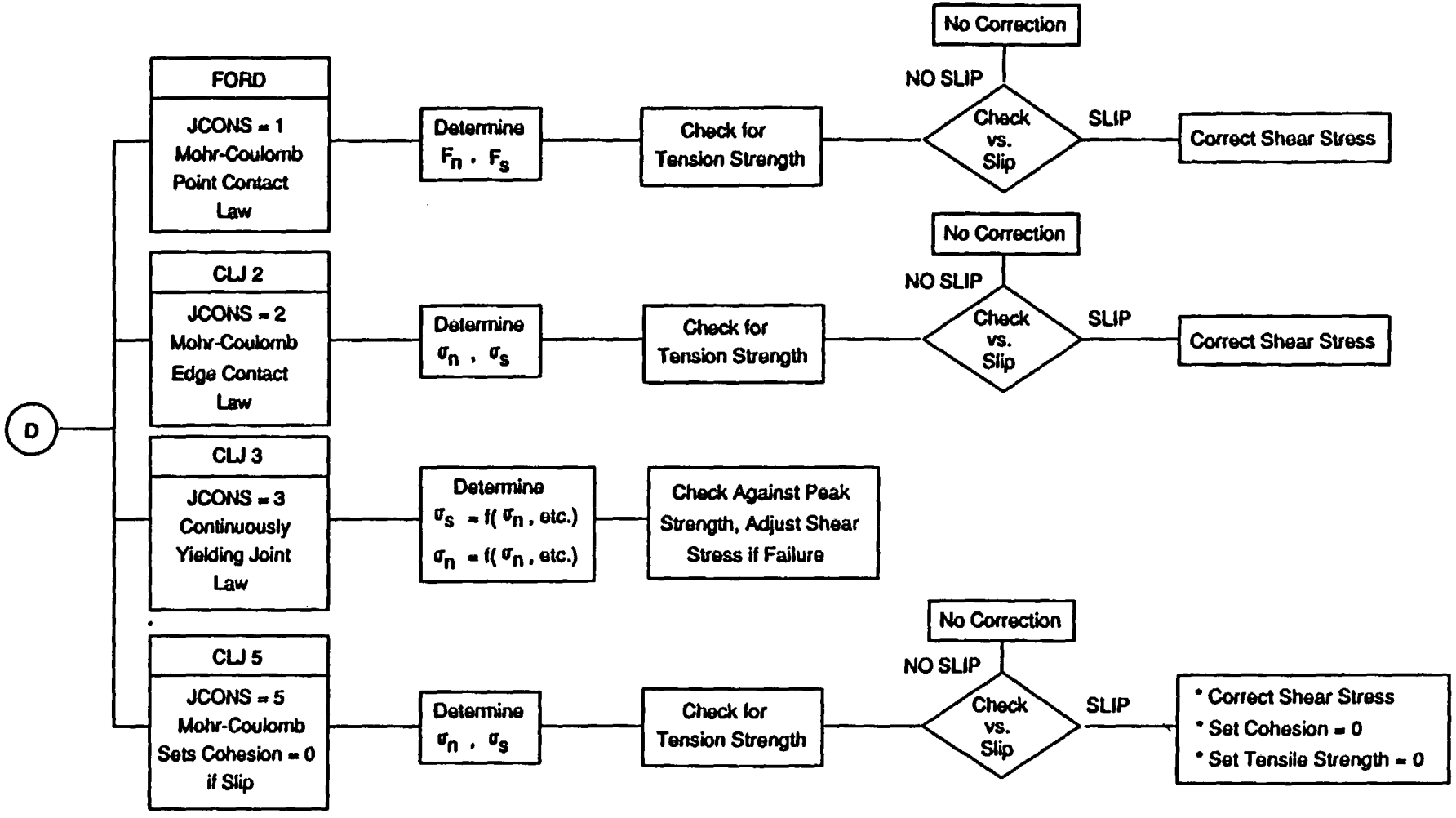

Fig. 1.2-12 Implementation of Joint Constitutive Laws

1.3 GENERAL NUMERICAL PROCEDURE

1.3.1 Introduction

This section presents the basic mathematical formulations and solution methodologies employed in UDEC. Discussions are given on the basic algorithms for detecting and defining the mechanical interactions between blocks, the explicit solution procedure employed, damping to obtain the quasi-static solution, dynamic analysis methods and numerical stability requirements.

1.3.2 Terminology

The distinct element method employed in UDEC requires that the body first be divided into a number of blocks which are separated from one another by joints (also termed fractures or interfaces) (see Fig. 1.3-1). The geometry of the blocks are defined by their corners and edges. Blocks may be defined as rigid (no internal deformation allowed), simply deformable (limited possible internal deformation modes), and fully deformable (complete definition of stress and strain tensors). For fully deformable blocks, the interior of the blocks is discretized into triangular finite difference zones (i.e., elements). Each zone is defined by the grid points which lie at its three vertices.

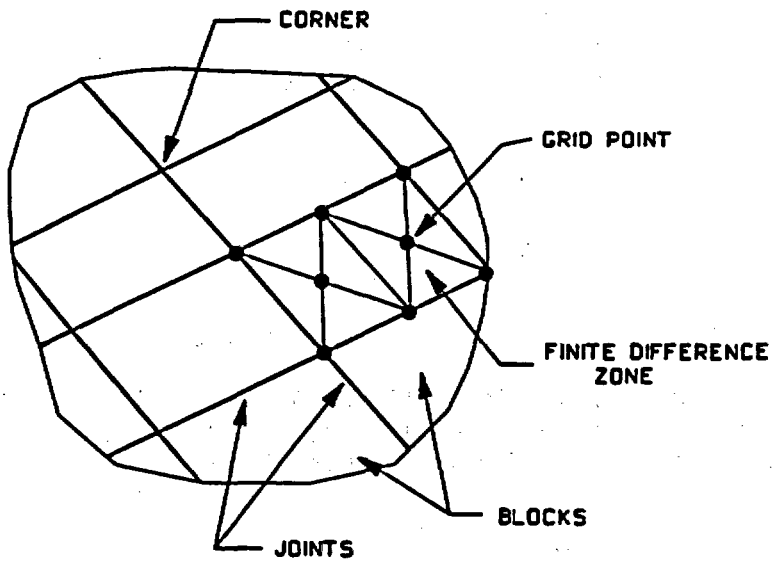

Fig. 1.3-1 Illustration of Geometry Terminology

When blocks contact one another in two dimensions, three potential modes of contact are possible: edge-to-edge, corner-to-edge, and corner-to-corner. For rigid and simply deformable blocks, where no internal discretization is performed, the contact locations are determined by the block corners. For fully deformable blocks, internal discretization may result in several grid points lying on the boundary of the block (e.g., Fig. 1.3-1). These boundary grid points are treated as new corners and are used to provide a more accurate determination of the stress state along an edge.

1.3.3 Basis for the Distinct Element Method

1.3.3.1 Introduction

The following discussion regarding the implementation of the distinct element method used in UDEC is taken from Lemos (1987). Additional information on distinct element methods may be found in Cundall (1980), Cundall and Hart (1984) and Cundall (1987).

1.3.3.2 Contact Between Blocks

When two blocks come into contact, a force develops between them which can be resolved into normal and shear components [Fig. 1.3-2a]. The simplest model of mechanical interaction is to assume that the blocks are connected by normal and shear elastic springs, i.e., interaction forces are proportional to the relative displacement between the two blocks (Fig. 1.3-3). This relation is expressed more conveniently in incremental form.

$$\begin{aligned} \Delta F_n &= K_n \, \Delta u_n \\ \Delta F_s &= K_s \, \Delta u_s \end{aligned} \qquad (1.3\text{-}1)$$

where K_n and K_s are the contact normal and shear stiffnesses.

Contact between two block edges [Fig. 1.3-2(b)] can be represented by two corner-edge contacts. The contact length, ℓ, allows contact stresses to be calculated as

$$\begin{aligned} \sigma_n &= F_n \, / \, \ell \\ \sigma_s &= F_s \, / \, \ell \end{aligned} \qquad (1.3\text{-}2)$$

and stress increments to be expressed in terms of the usual joint stiffnesses k_n and k_s [stress/length] as

$$\Delta\sigma_n = k_n \Delta u_n$$
$$\Delta\sigma_s = k_s \Delta u_s \qquad (1.3\text{-}3)$$

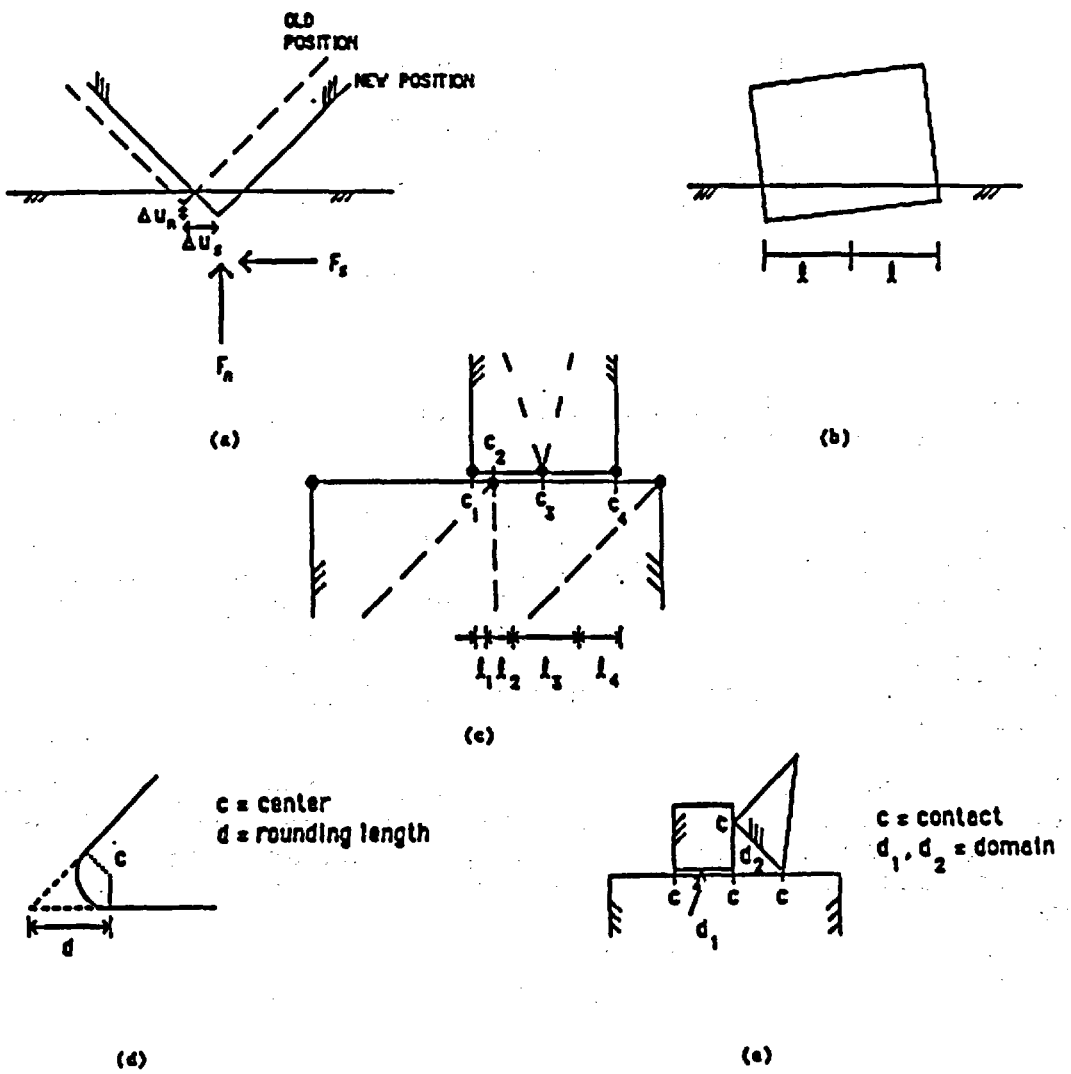

Fig. 1.3-2 Block Contact Geometry: (a) corner-edge contact; (b) edge-edge contact; (c) contact lengths for fully-deformable blocks; (d) rounded corner; and (e) domains

When blocks are discretized into a fine internal mesh (fully-deformable), gridpoints may be placed along the original edges [Fig. 1.3-2(c)]. These gridpoints are treated as new corners, since the edge is now able to deform into a polygonal line. The same expressions (1.3-3) are used, with contact lengths defined as shown in Fig. 1.3-2c.

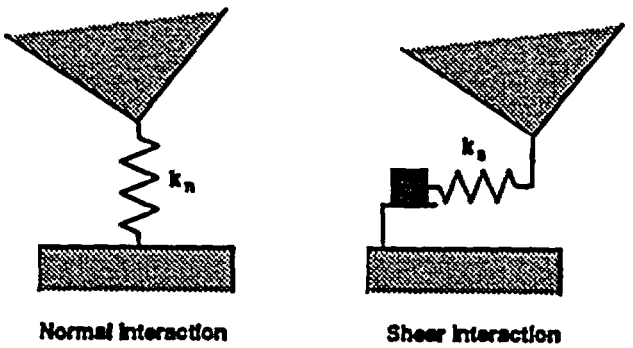

Fig. 1.3-3 Mechanical Representation of Interfaces in Distinct Element Method

The overlaps in Figs. 1.3-2(a) and (b) represent only a mathematically convenient way of measuring relative normal displacements. In finite element or displacement discontinuity models, joints are similarly assigned a zero thickness, with overlapping indicating compressive joint stresses and separation indicating tension. If normal joint stiffnesses are increased, overlaps can be made as small as desired.

At each timestep, the incremental stresses calculated by expressions (1.3-3) are added to the existing stresses, and the constitutive criteria are checked. In the simplest model, no tensile stresses are allowed—i.e., defining tensile stresses as positive,

$$\sigma_n \leq 0 \qquad (1.3\text{-}4)$$

and the shear stresses are limited by a Mohr-Coulomb friction law

$$|\sigma_s| \leq c - \sigma_n \tan \phi \qquad (1.3\text{-}5)$$

where c and ϕ are the joint cohesion and friction angle. In general, the joint constitutive relations must provide the stress increments as a function of the displacement increments, current stresses and possibly other state parameters.

$$\Delta\sigma_n, \Delta\sigma_s = f(\Delta u_n, \Delta u_s, \sigma_n, \sigma_s \ldots) \qquad (1.3\text{-}6)$$

One such model, the continuously-yielding joint model, is described in Section 1.4, - Component Models.

In principal, an interaction logic based on corner-edge contacts is sufficient, even for complex geometries. However, particular problems may arise, for instance, when the contact point approaches one of the edge endpoints. Then, the determination of which edge and corner are in contact may become ambiguous. Also, the contact normal may not be uniquely defined, or it may experience sudden jumps as the blocks rotate with respect to each other. It is important that the contact normal varies in a smooth way for any relative motion between blocks, so that the normal and shear components of the interaction force are physically meaningful. These problems are overcome in UDEC by assuming that the block corners are rounded, for the purpose of analyzing the interaction mechanics. A corner is approximated by an arc of a circle tangent to the two adjacent edges [Fig. 1.3-2(d)]. The distance between the tangency points and the actual corner, the rounding length d, is prescribed by the user and is the same for all corners (i.e., circle radii vary according to the corner angle). This scheme permits corner-corner contacts to be handled without ambiguity. The contact normal is defined by the line connecting the centers of the rounded corner circles. A smooth transition between corner-edge and corner-corner contacts is also achieved.

Rounded corners have the added advantage of eliminating the problem of closely-packed systems being "locked" by very small corner-corner overlaps. In a real situation, such sharp corners would probably be crushed. Rounded corners may thus provide a better approximation of the physical reality. The rounding length, if kept small (typically around a few percent of the average edge length), has no practical influence on the results

of the analysis. Since distinct element codes allow large block motion, elaborate procedures are required in order to update the contact structure, detecting new contacts and deleting others. The main difficulty is to make such updates computationally efficient, since checking all possible interactions would be impractical. UDEC takes advantage of the network of "domains" created by a 2-D block assembly. Domains are the regions of space between blocks which are defined by the contact points, as d_1 and d_2 in Fig. 1.3-2(e). During a small time increment, new contacts can only be formed between corners and edges within the same domain, so local updates can be executed efficiently whenever some prescribed measure of motion within the domain is attained. The contact updating procedure is further facilitated by a linked list data structure which follows closely the physical arrangement of corners and contacts. Details of the linked list structure can be found in the UDEC User's Manual, Volume 2 of this document.

1.3.3.3 Block Deformability

Blocks may be rigid, simply or fully deformable in the distinct element method. The basic formulation for rigid blocks is given by Cundall et al. (1978). Details of the formulation are given in Cundall (1971) and elsewhere. This formulation represents the medium as a set of distinct blocks which do not change their geometry as a result of applied loading. Consequently, the formulation is most applicable to problems in which the behavior of the system is dominated by discontinuities and where the material elastic properties may be ignored. Such conditions arise in low-stress environments and/or where the material possesses high strength and low deformability.

For many applications, the deformation of individual blocks cannot be reasonably ignored — i.e., blocks cannot be assumed to be rigid. Two approaches have been developed. In one approach, termed "simply deformable", each block is allowed three degrees of freedom to deform internally. In the second approach, termed "fully deformable", arbitrary deformation of blocks is permitted through internal discretization of blocks into finite difference zones. Both the simply-deformable and fully-deformable algorithms are used in UDEC and are described by Cundall et al. (1978).

Simply-deformable blocks use three modes of internal deformation corresponding to the three strains in two dimensions—i.e., ε_{11}, ε_{22}, and $\varepsilon_{12} + \varepsilon_{21}$. These modes are shown in Fig. 1.3-4. In addition to these modes, there remain the three rigid-body modes considered by rigid blocks (two translational and one rotational degrees of freedom), making six degrees of freedom per block in total.

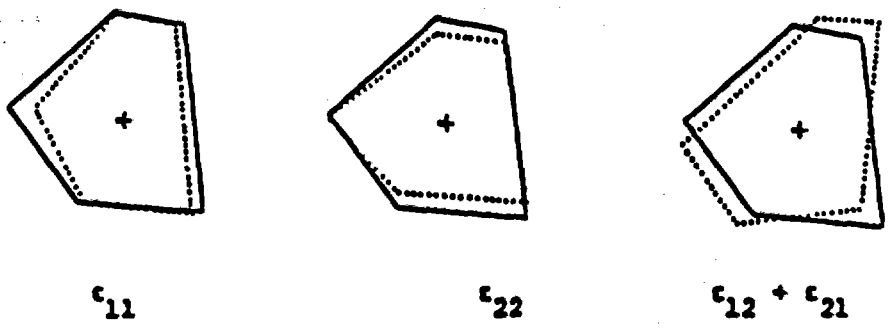

Fig. 1.3-4 Three Independent Modes of Deformation Used In Simply-Deformable Blocks

However, some deformation modes, such as those shown in Fig. 1.3-5, cannot be represented by simply-deformable blocks. A more detailed description of the limitations of SDEF blocks is given by Williams and Mustoe (1987).

To overcome inherent limitations of SDEF blocks it is often possible to substitute fully-deformable blocks with a minimum number of internal finite difference zones. For quadrilateral blocks with two zones per block, the increased storage and computing time is minimal when compared to simply-deformable blocks. For this reason, simply-deformable blocks are not discussed in detail beyond this point.

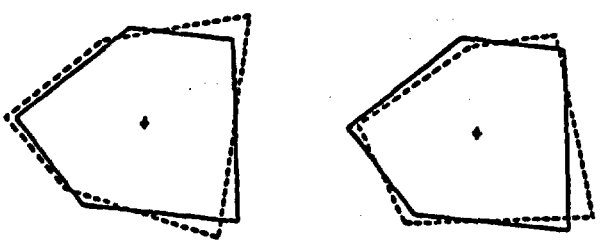

Fig. 1.3-5 Deformation Modes Not Possible With SDEF Blocks

Each fully deformable block is independently discretized into an internal finite-difference mesh. An explicit, large deformation, Lagrangian formulation with constant strain triangles is used. Plane strain conditions are assumed. Since the displacment field has a linear variation within each zone, the block boundary is always defined by a polygonal line, allowing the block interaction logic previously described to be used for any degree of mesh refinement. General constitutive relations can be assumed for the block material. At present, elastic and elasto-plastic models are included in this version of UDEC.

The code UDEC possesses an automatic mesh generator which performs the internal discretization for arbitrarily shaped blocks. The user only specifies the maximum zone edge length (m.z.e.l.) desired. The generation procedure starts by placing gridpoints at all block corners (the gridpoints become zone vertices). Then, edges longer than the m.z.e.l. are subdivided, until a relatively uniform distribution of edge lengths is achieved. A triangulation of the block is then performed by connecting the boundary gridpoints. Links are always established between the closest points. In a second stage, the mesh is refined. The largest zone side is halved, and the adjacent zones are subdivided. This process is repeated until all zone sides are smaller than the m.z.e.l. Finally, the internal gridpoints are iteratively relocated, until they coincide with the average of the coordinates of the surrounding gridpoints.

UDEC also has two special mesh generators. The manual mesh generator allows the user to specify grid point locations within blocks. The other special zone generator works only for quadrilateral blocks. The generator for quadrilateral blocks produces internal grid points with either four or eight neighboring zones. The resultant mesh consists of "crossed" grid lines which improves behavior when modelling plastic flow as explained later.

The deformability of fully-deformable blocks is governed by the assigned constitutive (i.e., stress-strain) relation. During each timestep, zonal strain rates are related to nodal (i.e., gridpoint) velocities in the usual fashion:

$$\dot{\varepsilon}_{ij} = \frac{1}{2} \left(\dot{u}_{i,j} + \dot{u}_{j,i} \right) \qquad (1.3\text{-}7)$$

Zone rotations are also calculated as:

$$\dot{\omega}_{ij} = \frac{1}{2} (\dot{u}_{i,j} - \dot{u}_{j,i}) \qquad (1.3\text{-}8)$$

These rotations produce changes in stress components referred to a fixed frame of reference. Rotations are used to adjust zone stresses to account for rotation (c.f. Eq. 1.4-114)

Notice that, due to the incremental treatment, Eq. (1.3-7) does not imply a restriction to small strains. Incremental strains are obtained from strain rates through multiplication by the time step.

The constitutive relations for deformable blocks are used in an incremental form, so that implementation of non-linear problems can be accomplished easily. The actual form of the equations is:

$$\Delta\tau^{e}_{ij} = \lambda\, \Delta\varepsilon_{v}\delta_{ij} + 2\,\mu\Delta\varepsilon_{ij} \qquad (1.3\text{-}9)$$

where λ,μ are the Lame constants,

$\Delta\tau^{e}_{ij}$ are the elastic increments of the stress tensor,

$\Delta\varepsilon_{ij}$ are the incremental strains,

$\Delta\varepsilon_{v} = \Delta\varepsilon_{11} + \Delta\varepsilon_{22}$ is the increment of volumetric strain, and

δ_{ij} = Kronecker delta function.

Non-linear and post-peak strength models are readily incorporated into the code in a direct way without recourse to devices such as equivalent stiffnesses or initial strains, which need to be introduced into matrix-oriented programs to preserve linearity dictated by the matrix formulation. In an explicit program, however, the process is relatively simple — after each timestep, the strain state of each zone is known. The program then needs to know the stress in each zone in order to proceed to the next timestep. The stress is uniquely defined by the stress-strain model whether it is a linearly-elastic relation or a complex, non-linear and post-peak strength model.

UDEC provides two constitutive models for fully-deformable blocks: an isotropic elastic model and Mohr-Coulomb plasticity model with non-associated flow rule. These models are described further in Section 1.4.

1.3.3.4 Equations of Motion

1.3.3.4.1 Equations of Motion For Rigid Blocks

The motion of an individual rigid block is determined by the magnitude and direction of resultant out-of-balance moments and forces acting on it. In this section, the equations of motion which describe translation and rotation of the block about its centroid are developed. Mass damping terms, which may be introduced into the equations of motion, have been omitted from this section for clarity. Consider the motion of a single mass acted on by a varying force, F(t). Newton's second law of motion can be written in the form

$$\frac{\partial \dot{u}}{\partial t} = \frac{F(t)}{m} \qquad (1.3\text{-}10)$$

The central difference scheme for the left-hand side of Eq. (1.3-10) at time t can be written as

$$\frac{\partial \dot{u}}{\partial t} = \frac{\dot{u}^{(t + \Delta t/2)} - \dot{u}^{(t - \Delta t/2)}}{\Delta t} \qquad (1.3\text{-}11)$$

Substituting Eq. (1.3-11) in Eq. (1.3-10) and re-arranging yields

$$\dot{u}^{(t + \Delta t/2)} = \dot{u}^{(t - \Delta t/2)} + \frac{F(t)}{m} \Delta t \qquad (1.3\text{-}12)$$

With velocities stored at the half-timestep point, it is possible to express displacement as

$$u(t + \Delta t) = u(t) + \dot{u}^{(t + \Delta t/2)} \Delta t \qquad (1.3\text{-}13)$$

Because the force depends on displacement, the force/displacement calculation is done at one time instant. Figure 1.3-6 illustrates the central difference scheme with the order of calculation indicated by the arrows.

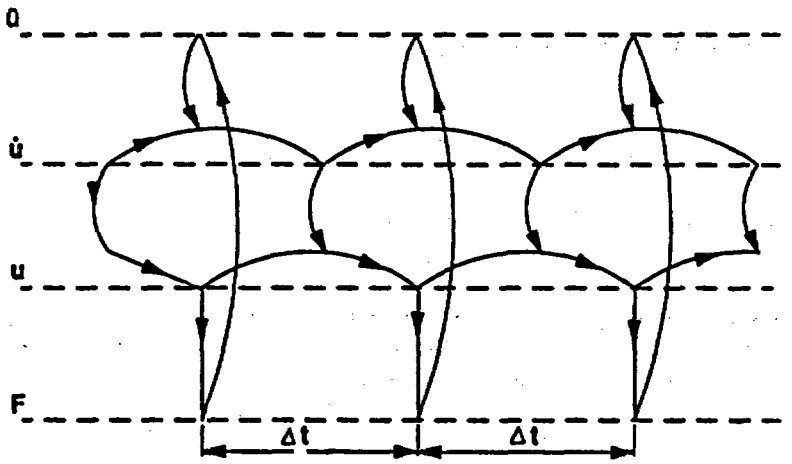

Fig. 1.3-6 Interlaced Nature of Calculation Cycle Used in Distinct Element Formulation

For blocks which are acted upon by several forces as well as gravity, the velocity equations become:

$$\dot{u}_i(t + \Delta t/2) = \dot{u}_i(t - \Delta t/2) + \left(\frac{\Sigma F_i(t)}{m} + g_i\right)\Delta t \qquad (1.3\text{-}14)$$

$$\dot{\theta}(t + \Delta t/2) = \dot{\theta}(t - \Delta t/2) + \frac{\Sigma M(t)}{I}\Delta t$$

where $\dot{\theta}$ = angular velocity of block about centroid,

I = moment of inertia of block,

$\dot{u}_i$ = velocity components of block centroid,

ΣM = the sum of moments; and

ΣF_i = the sum of applied forces.

The new velocities in Eq. (1.3-14) are used to determine the new block location according to

$$\dot{x}_i(t + \Delta t/2) = x_i(t) + \dot{u}(t + \Delta t/2)\ \Delta t$$

$$\theta_i(t + \Delta t/2) = \theta_i(t) + \dot{\theta}\ (t + \Delta t/2)\ \Delta t \qquad (1.3\text{-}15)$$

where θ_i = rotation of block about centroid, and

x_i = coordinates of block centroid.

Thus, each iteration produces new block positions which generate new contact forces. Resultant forces and moments are used to calculate linear and angular accelerations of each block. Block velocities and displacements are determined by integration over incremental timesteps. The procedure is repeated until a satisfactory state of equilibrium or mode of failure results.

1.3.3.4.2 Equations of Motion For Gridpoints

The equations of motion for gridpoints of zones in fully-deformable blocks are identical to those for centroids of rigid blocks, except that rotational terms are neglected for gridpoints. In determining the forces acting on a gridpoint, the stresses in surrounding zones are accounted for by integrating over a surface, S, enclosing the gridpoint:

$$F_i^z = \int_S \sigma_{ij} n_j \, dS \qquad (1.3\text{-}16)$$

where S is the surface enclosing the mass of surrounding elements lumped at the gridpoint, and

n_j is the unit normal to S.

The total force acting on a grid point is the resultant of all external forces applied to the grid point (from block contacts or

otherwise), plus the contribution from surrounding zones, F_i^z. Contact forces acting directly at a grid point are applied directly to the grid point. Contact forces applied to a zone edge between two grid points are distributed to the two grid points by linear interpolation.

1.3.3.5 Calculation Procedure

The distinct element algorithm is based on two sets of computations performed at each time step. First, kinematic quantities are updated. Then, the application of constitutive models provides the forces and stresses. The procedure for fully-deformable blocks can be summarized in the following steps.

1. New gridpoint velocities, $\dot{u}_i$, are obtained from the equations of motion.

2. Displacement increments are calculated as $\Delta u_i = \dot{u}_i \, \Delta t$.

3. The location of the block boundary is updated, and contact displacement increments are calculated.

4. Application of the joint constitutive relations provides the new contact stresses and forces.

5. Zone strain increments are calculated as (c.f., 1.3-7)

$$\Delta \varepsilon_{ij} = \frac{1}{2} \left(\frac{\partial u_i}{\partial x_j} + \frac{\partial u_j}{\partial x_i} \right) \Delta t$$

6. The application of the block material constitutive relations gives the new zone stresses.

7. Contact forces, zone stresses and external loads are assembled into the new force vector F_i, for the next time step.

For rigid blocks, the procedure above is based on block centroid velocities and zonal stresses and strains are not computed.

1.3.4 Damping

1.3.4.1 Introduction

As described in the previous section, UDEC uses a dynamic algorithm for problem solution. Natural dynamic systems contain some degree of damping of the vibrational energy within the system. Otherwise, the system would oscillate indefinitely when subjected to driving forces. Damping is, in part, due to energy loss as a result of slippage along contacts of blocks within the system, internal friction loss in the intact material, and any resistance caused by air or fluids surrounding the structure. UDEC is used to solve two general classes of mechanical problems: quasi-static and dynamic. Damping is used to solve both classes of problems. Quasi-static problems involve use of more damping than dynamic problems. Two types of damping, mass-proportional and stiffness-proportional damping are available in UDEC. Mass-proportional damping or viscous damping, applies a force which is proportional to (mass) velocity, but in the opposite direction. Stiffness proportional damping applies a force to contacts or stresses in zones which are proportional to the incremental force or stress and in the same sense. In UDEC, either form of damping may be used separately or in combination. The use of both forms of damping in combination is termed Rayleigh damping (Bathe and Wilson, 1976; Zienkiewicz, 1977). For solution of quasi-static problems using finite difference schemes, mass-proportional or viscous damping is generally used (Otter et al., 1966). UDEC allows use of an automatic "adaptive" viscous damping scheme developed by Cundall (1982) for solution of quasi-static problems. Damping for static analysis is discussed in Section 1.3.4.3. For dynamic analyses, either mass-proportional or stiffness-proportional, or both (i.e., Rayleigh) forms of damping may be used as described in Section 1.3.4.4.

1.3.4.2 Mass and Stiffness Damping

In continuum analysis of structures, proportional Rayleigh damping is typically used to damp the natural frequencies of the system. In dynamic finite element analysis, a damping matrix, C, is formed with components proportional to the mass (M) and stiffness (K) matrices:

$$C = \alpha M + \beta K \qquad (1.3\text{-}17)$$

In the above equation, α and β are the mass and stiffness proportional damping constants. For a multiple degree-of-freedom system, choice of the α and β constants cannot be performed with certainty. However, the critical damping ratio, ξ_i, at any natural frequency of the system, ω_i can be found from (Bathe and Wilson, 1976):

$$\alpha + \beta\omega_i^2 = 2\omega_i \xi_i$$

or

$$\xi_i = \frac{1}{2} \left(\frac{\alpha}{\omega_i} + \beta\omega_i \right) \qquad (1.3\text{-}18)$$

Figure 1.3-7 shows the variation of the normalized critical damping ratio, ξ_i, with angular frequency, ω_i. Three curves are given: mass and stiffness components only and the sum of both components. As shown, mass-proportional damping is dominant at lower angular frequency ranges while stiffness-proportional damping dominates at higher angular frequencies. The sum curve reaches a minimum at:

$$\xi_{min} = (\alpha\beta)^{1/2};$$

$$\omega_{min} = (\alpha/\beta)^{1/2} \text{ and} \qquad (1.3\text{-}19)$$

$$f_{min} = \omega_{min}/2\pi$$

where f_{min} can be termed the "fundamental frequency" of the system in cycles/sec at some proportion of critical damping, ξ_{min}.

The values of f_{min} and ξ_{min} are required by UDEC as input if the automatic damping option is not selected. Mass proportional damping is analogous to immersing the system in viscous fluid - the absolute motion of the blocks and/or gridpoints will be damped based on the viscosity of the fluid. The viscosity of the fluid can be increased by increasing ξ_{min} and/or ω_{min}.

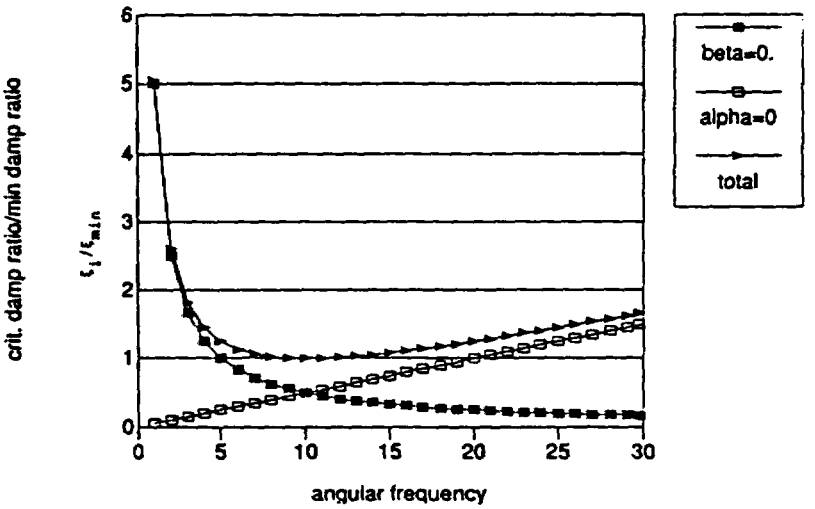

Fig. 1.3-7 Variation of Normalized Critical Damping Ratio with Angular Frequency

Mass-proportional damping is generally most appropriate for lower frequency applications, including static problems. Mass-proportional damping is included in the equation of motion for rigid block translation or grid point motion as follows:

$$\frac{\partial \dot{u}_i}{\partial t} = \frac{F_i}{m} - \alpha \dot{u}_i + g_i \qquad (1.3\text{-}20)$$

where α is the damping constant described above. The difference equation in time is written as:

$$\dot{u}_i(t + \Delta t/2) = \{\dot{u}_i(t-\Delta t/2)\ (1 - \frac{\alpha \Delta t}{2}) + (\frac{F_i}{m} + g_i)\Delta t\} / (1 + \frac{\alpha \Delta t}{2}) \qquad (1.3\text{-}21)$$

Rigid block rotations are damped in the same manner.

Stiffness proportional damping is physically equivalent to dashpots across contacts and zones and serves to damp relative block motion. Stiffness proportional damping can be increased by increasing ξ_{min} or by decreasing ω_{min}. The following viscous terms are thus added to the contact forces and element stresses:

$$F_i^v = \beta \, \Delta F_i^e \, / \, \Delta t$$
$$\sigma_{ij}^v = \beta \, \Delta \sigma_{ij}^e \, / \, \Delta t \qquad (1.3\text{-}22)$$

where ΔF_i^e and $\Delta \sigma_{ij}^e$ are the elastic force and stress increments.

When a contact is sliding, the viscous term is dropped since friction already provides energy dissipation.

1.3.4.3 Damping For Quasi-Static Analysis

For quasi-static problems, only mass-proportional damping is generally used. UDEC provides an automated damping option within the code as described here. For static problems, the timestep does not signify real time and is only an iterative device for reaching the steady state solution. Here, the user wishes to obtain the equilibrium or steady-state of the body by using the minimum number of timesteps (or, also called "cycles") of calculation. UDEC provides an automated scheme which does not require user specification of damping constants. Figure 1.3-8 shows three potential damping modes for reaching the steady state equilibrium displacement of a mass on a spring in free vibration subjected to viscous damping. The potential modes are: overdamped, underdamped and critically damped. In overdamping, the viscosity is very large, and the equilibrium is approached as time approaches infinity with non-oscillatory behavior. Underdamped systems oscillate, approaching the equilibrium state with increasing time. Critical damping again is non-oscillatory and, at most, can have one passage through the equilibrium position. The automatic damping in UDEC provides a slightly underdamped solution to elastic problems and a nearly critically-damped solution to problems in which energy loss by joint slip or intact material failure occurs.

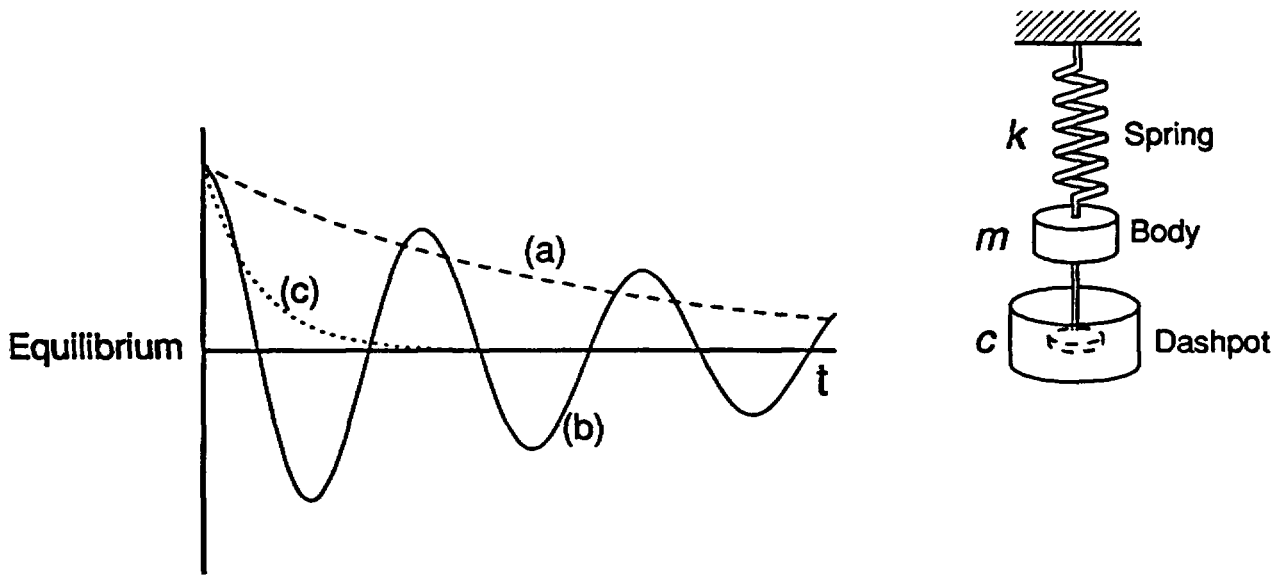

Fig. 1.3-8 Damping Modes for Damped Mass on an Elastic Spring. (a) overdamping; (b) underdamped (oscillatory); and (c) critical damping.

The automatic or "adaptive" damping scheme in UDEC adjusts the mass damping constant, α, (Eq. 1.3-17) to the conditions which occur during solution of any particular problem (Cundall, 1982). As was discussed in the previous section, a general method for selection of an optimum value of α prior to running the problem is not generally possible. The algorithm used here monitors the rate of energy change in the body as cycling continues. A parameter, R, is calculated at every other cycle, where R is given by:

$$R = \frac{\text{rate of energy dissipation due to mass damping}}{\text{rate of change of kinetic energy}} \qquad (1.3\text{-}23)$$

The value of α is adjusted to keep R within prescribed limits found by experiment. If R is kept close to 0.5, a damping effect similar to critical damping is achieved. The algorithm is similar to a servo-mechanism in which an output system control parameter is continuously adjusted based on the measured system response. Lorig (1984) examined the variation in α with the number of cycles for a typical quasi-static problem (Fig. 1.3-9), in which most blocks surround a tunnel reach zero-velocity equilibrium although some fall by gravity. The oscillation of α beyond 1500 cycles results from increases in total kinetic energy as some blocks fall from the tunnel crown.

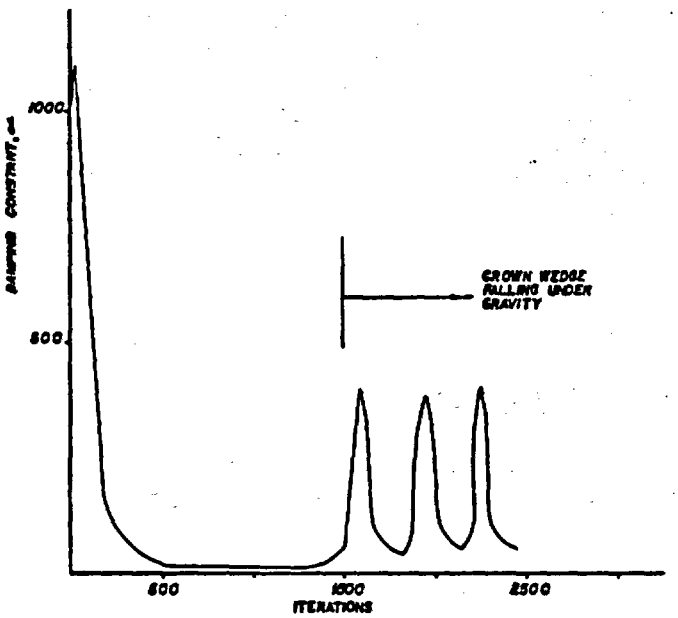

Fig. 1.3-9 Variation in α for a Typical Tunneling Problem Obtained in UDEC (α is automatically adjusted to speed convergence for quasi-static problems. The cyclic change in α after 1500 timesteps (iterations) is a result of wedges falling from the crown of the tunnel.) [Lorig (1984)].

1.3.4.4 Damping For Dynamic Analysis

For dynamic problems, some combination of mass and stiffness damping or stiffness damping alone is generally required. For simple continuous elastic systems, the eigenfrequencies are known and therefore the choice of f_{min} and ξ_{min} is fairly well defined.

For example, with analysis of structural systems, a fraction of critical damping of 2% to 10% is generally used (e.g., Biggs, 1964). For discontinuous systems, in which slip and separation between blocks may occur, the overall oscillatory behavior is not well known. The result is that either experience or experimentation with the model to determine the damping is necessary. The objectives are to determine the fundamental frequency of the body and the fraction of critical damping to provide sufficient damping without resulting in instability or inaccurate temporal solutions. Several methods of defining the damping parameters are possible for dynamic analysis. The fundamental frequency of a system can be determined simply by using no damping and applying the dynamic loading while monitoring the system response (i.e., velocity, displacement, etc.). Since no damping is used, the system will oscillate, and the fundamental or lowest frequency can be obtained from a temporal plot of the system oscillation. Once the frequency is known, the fraction of critical damping is set by trial and error. Suggested values for block rock systems are in the order of 0.5 to 1%.

1.3.5 Mechanical Timestep Determination and Numerical Stability

1.3.5.1 Timestep Calculation

Explicit methods are only conditionally stable. For a linear elastic system the mechanical timestep must be less than

$$\Delta t_{stab} = 2 \; / \; \omega_{max} \qquad (1.3\text{-}24)$$

where ω_{max} is the highest eigenfrequency of the system.

As distinct element systems can be rather complex and change considerably during the course of the analysis, the timestep required for numerical stability is calculated only approximately. Two estimates are obtained, one based on the stability of the internal mesh calculations, the other accounting for the contact stiffness. The minimum of the two is taken.

The explicit finite difference solution procedure used for the fully-deformable blocks is based on the assumption that no information is transmitted from a gridpoint to its neighbor within one timestep. Therefore, the timestep required for the stability of the zone computations is estimated as

$$\Delta t^z = 2 \min_i \left[\frac{m_{(i)}}{k_{(i)}} \right]^{1/2} \qquad (1.3\text{-}25)$$

where m_i is the mass of node i, and

k_i is a measure of the stiffness of the elements surrounding the node.

The minimum value of the ratio for any nodal point is used.

In a distinct element model, k_i must account for the stiffness of the intact rock, as well as the stiffness of the discontinuities. It can be calculated as the sum of two terms

$$k_i = \Sigma k_{zi} + k_{ji} \qquad (1.3\text{-}26)$$

The first term represents the sum of the contributions of the stiffness of all the elements connected to node i, which are estimated as

$$k_{zi} = \frac{8}{3} \left[K + \frac{4}{3} G \right] \frac{b_{max}}{h_{min}} \qquad (1.3\text{-}27)$$

where K and G are the bulk and shear elastic moduli of the block material, respectively,

b_{max} is the largest edge, and

h_{min} the minimum height of the triangular element.

The joint stiffness term, k_{ji}, exists only for nodes located on the block boundary, and is taken as the product of the normal or shear joint stiffnesses (whichever is larger) and the sum of the lengths of the two block edge segments adjacent to node i.

For rigid blocks, the time step is calculated, by analogy to a single degree of freedom system, as

$$\Delta t^b = \text{FRAC}*2 \ (M_{min}/K_{max})^{1/2} \qquad (1.3\text{-}28)$$

where M_{min} is the mass of the smallest block in the system, and

K_{max} is the maximum contact stiffness.

FRAC is supplied by the user in order to account for the fact that a block is in contact with several blocks.

In UDEC, K_{max} is taken as

$$K_{max} = \max (K_{n,s} , k_{n,s} * l_{typ}) \qquad (1.3\text{-}29)$$

where $K_{n,s}$ is the contact normal or shear stiffness (whichever is higher), $k_{n,s}$ the joint stiffness and l_{typ} the typical contact length. FRAC is typically 0.1. The timestep is finally chosen as

$$\Delta t = \min (\Delta t^z, \Delta t^b) \qquad (1.3\text{-}30)$$

When stiffness-proportional damping is used, this timestep may not guarantee stability and may have to be reduced by a user-supplied factor. Belytschko (1983) gives the following formula for adjusting the timestep:

$$\Delta t = \frac{2}{\omega_{max}} \left[[(1 + \xi^2)]^{1/2} - \xi \right] \qquad (1.3\text{-}31)$$

where ω_{max} is the highest eigenfrequency of the system, and

ξ is the fraction of damping at this frequency.

1.3.5.2 Density Scaling

For quasi-static problems, UDEC allows use of a simple procedure for improving efficiency termed mass density scaling. As long as inertial forces remain small compared with the other forces in the system, inertial masses may be modified without affecting the solution. Therefore, block densities or individual zone densities used in the calculation of inertial gridpoint masses may be scaled to achieve larger timesteps. Improved convergence is obtained when all inertial masses are set to the same value.

The equation of motion may be written (excluding damping terms) in terms of inertial (m_i) and gravitational (m_g) masses as:

$$m_i \ddot{u} = \Sigma F + m_g g \qquad (1.3\text{-}32)$$

For the usual case in which inertial and gravitational masses are identical, this equation reverts to the familiar form:

$$\ddot{u} = \frac{\Sigma F}{m_i} + g \qquad (1.3\text{-}33)$$

However, if the inertial and gravitational masses are different, as in the case of density scaling, then Eq. (1.3-32) may be re-written as:

$$\ddot{u} = \frac{\Sigma F}{m_i} + \frac{m_g}{m_i} g \qquad (1.3\text{-}34)$$

This has no effect on the gravitational masses and the block weights are all correct, but all blocks will accelerate equally under equal forces. Mass density scaling is provided as an option in UDEC.

1.3.6 Dynamic Analysis*

1.3.6.1 Introduction

Stress waves propagating in a jointed rock mass can induce episodes of slip or separation on the discontinuities. Time domain techniques are required for the analysis of these nonlinear dynamic problems. The explicit time integration algorithm of the distinct element method makes the method an appropriate tool for these analyses. Most dynamic geomechanical studies (e.g., seismic analysis of rock foundations) are based on continuum models. Few reported studies have taken into account the effects of the discontinuities. Dowding et al. (1983a; 1983b) analyzed the transient dynamic behavior of caverns in jointed rock using a hybrid rigid block-finite element model. The region around the opening was modeled with rigid blocks, and embedded in a continuum discretized with finite elements, where the dynamic excitation was applied. The present distinct element model with deformable blocks makes it possible for the whole region of study to be accurately modeled with distinct elements.

The numerical representation of dynamic systems in geomechanics with a mesh of finite extent requires the use of boundary conditions which allow for adequate energy radiation and do not reflect outgoing waves back into the model. In order to satisfy this requirement, non-reflecting boundaries were implemented in UDEC, as described in the next section. Examples of dynamic problems are presented in Volume 3 of this report.

Earthquake analysis of surface structures normally involves the consideration of an upward propagating stress wave, which is applied at the base of the model. In the lateral direction, at some distance from the structure, free-field conditions will be established. In order to avoid an unacceptably large model, a technique has been developed to provide adequate lateral boundary conditions at a closer distance. The free-field model is coupled to the blocky system by viscous dashpots which provide non-reflecting boundary conditions.

---

*This discussion is modified from Lemos (1987).

1.3.6.2 Non-Reflecting Boundaries

1.3.6.2.1 Dynamic modeling of unbounded media

The modeling of geomechanics problems involves media, which, at the scale of the analysis, are better represented as unbounded. Deep underground excavations are normally assumed to be surrounded by an infinite medium, while surface and near-surface structures are assumed to lie on a half-space. Numerical methods relying on the discretization of a finite region of space require that appropriate conditions be enforced at the artificial numerical boundaries. In static analyses, fixed or elastic boundaries (e.g., represented by boundary element techniques) can be realistically placed at some distance from the region of interest. In dynamic problems, however, such boundary conditions cause the reflection of outward propagating waves back into the model, and do not allow the necessary energy radiation. The use of a larger model can minimize the problem, since material damping will absorb most of the energy in the waves reflected from distant boundaries. However, this solution leads to large computational costs. The alternative is to use non-reflecting (or absorbing) boundaries. Several formulations have been proposed. The viscous boundary developed by Lysmer and Kuhlemeyer (1969) was selected for the present distinct element model. It is based on the use of independent dashpots, and is nearly totally effective for body waves approaching the boundary at angles off incidence above 30°. For lower angles of incidence or surface waves, the energy absorption is only approximate. However, it has the advantage of being an inexpensive technique which can be used in time domain analyses. Its effectiveness has been demonstrated in both finite element and finite difference models (Kunar et al., 1977). A variation of this technique proposed by White et al. (1977) is also widely used.

More efficient energy absorption, for example in the case of Rayleigh waves, requires the use of frequency-dependent dashpots, which can only be used in frequency domain analyses (e.g., Lysmer and Waas, 1972). These are usually designated as consistent boundaries, and involve the calculation of dynamic stiffness matrices coupling all the boundary degrees of freedom. Boundary element methods may be used to derive these matrices (e.g., Wolf, 1985). A comparative study of the performance of different types of elementary, viscous and consistent boundaries was reported by Roesset and Ettouney (1977).

A different procedure to obtain efficient absorbing boundaries for use in time domain studies was proposed by Cundall et al. (1978). It is based on the superposition of solutions with stress and velocity boundaries in such a way that reflections are canceled. In practice, it requires the use of two parallel, overlapping grids in a narrow region adjacent to the boundary, whose results are added. This method has been shown to provide effective energy absorption, but it is of difficult implementation for a blocky system of complex geometry.

1.3.6.2.2 Numerical Implementation

The viscous boundaries proposed by Lysmer and Kuhlemeyer (1969) consist of independent dashpots attached to the boundary in the normal and shear directions. They provide viscous normal and shear tractions given by

$$t_n = - \rho \, c_p \, v_n$$
$$t_s = - \rho \, c_s \, v_s \qquad (1.3\text{-}35)$$

where v_n and v_s are the normal and shear components of the velocity at the boundary, ρ is the mass density, and c_p and c_s are the P- and S-wave velocities.

The viscous terms can be introduced directly into the equations of motion of the gridpoints lying on the boundary. A different approach, however, was implemented in UDEC, in which the tractions t_n and t_s are calculated and applied at every timestep in the same way as the boundary loads. This alternative scheme allows the viscous boundaries to be used also with rigid and simply-deformable blocks. Tests have shown that this implementation is equally effective. In the practical analyses executed, no reduction of timestep was required by the use of the non-reflecting boundaries. Timestep restrictions demanded by high joint stiffnesses or small zones are usually more important.

In seismic analysis, the dynamic input is often a vertically propagating plane wave, which has to be applied at the base of the model. This boundary should also be a non-reflecting boundary so

that the waves propagating downwards from the free-surface are absorbed. A motion with velocity v° and stress σ_s° can be induced at a non-reflecting boundary by applying a stress

$$\sigma_s = \sigma_s^\circ - \rho c_s (v - v^\circ) \qquad (1.3\text{-}36)$$

For a plane harmonic shear wave $\sigma_s^\circ = \rho c_s v^\circ$. Therefore,

$$\sigma_s = 2\sigma_s^\circ - \rho c_s v \qquad (1.3\text{-}37)$$

—i.e., a standard non-reflecting boundary can be used, provided that twice the shear stress corresponding to the forcing motion is applied. Example problems in Volume 3 of this report illustrate the use of non-reflecting boundaries.

1.3.6.3 Dynamic Free-Field

1.3.6.3.1 Boundary Conditions for Seismic Analysis

Seismic analysis of surface and embedded structures by numerical techniques requires the discretization of a region of the soil or rock adjacent to the foundation. The seismic input is normally represented by a plane wave propagating upwards (Fig. 1.3-10). This dynamic excitation can be applied as a stress wave at the base of the model (AC), which is a non-reflecting boundary, as explained in the previous section. The boundary conditions at the sides AB and CD must account for the free-field motion which would exist in the absence of the structure. A simple solution is to extend the model laterally so that free-field conditions are achieved. For soils with high material damping, this condition can be obtained within a relatively small distance (Seed et al., 1975). When the material damping is low, the required distance may lead to an impractical model. An alternative procedure is to "enforce" the free-field motion in such a way that boundaries AB and CD retain their non-reflecting properties—i.e., outward waves originating from the structure are properly absorbed. This approach was used in the continuum finite-difference code NESSI (Cundall et al., 1980). A technique of this type was developed for the present distinct element model. It involves the execution of a one-dimensional free-field calculation in parallel with the blocky system analysis. The lateral boundaries AB and CD are coupled to the free-field grid by viscous dashpots (Fig. 1.3-11).

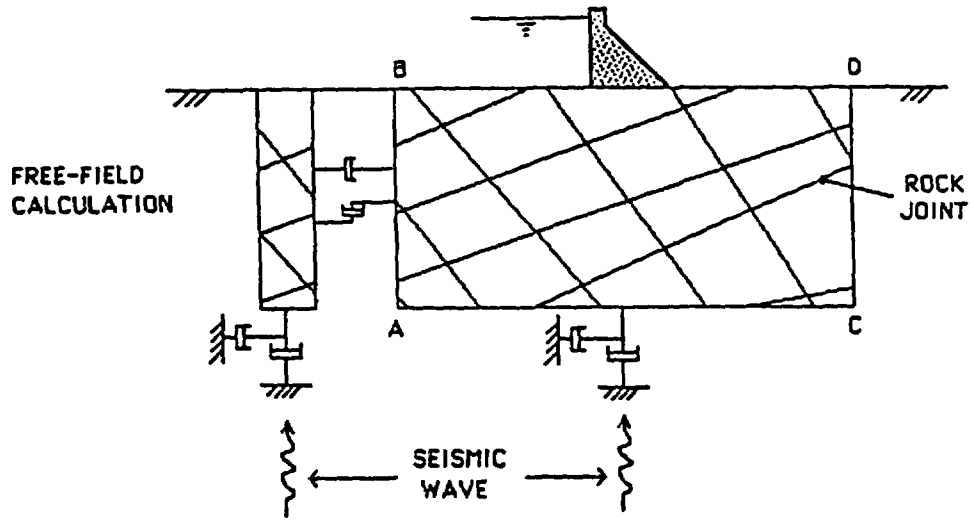

Fig. 1.3-10 Model for Seismic Analysis of Surface Structures: Block Assembly and Free-Field Mesh [Lemos, 1987]

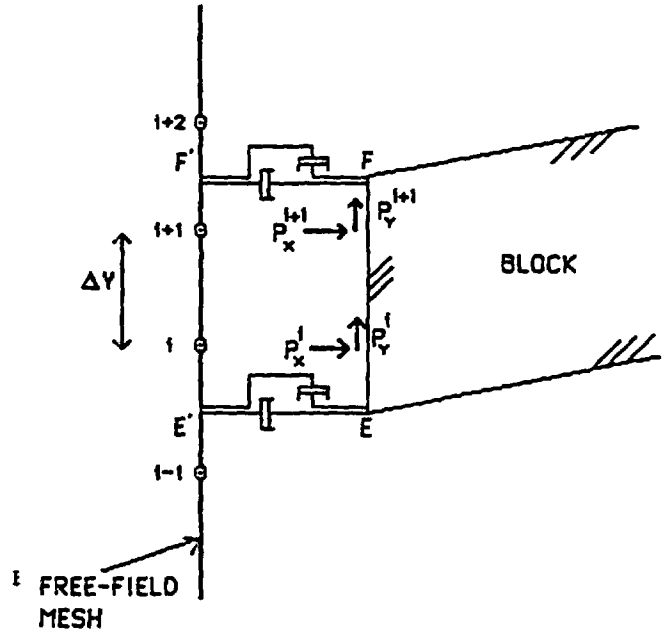

Fig. 1.3-11 Coupling of Block Model and Free-Field Mesh [Lemos (1987)]

1.3.6.3.2 Free-Field Representation

The free-field model consists of a one-dimensional "column" of unit width, simulating the behavior of the extended jointed medium. An explicit finite-difference method was selected for the model. The height of the free-field equals the length of the lateral boundaries of the blocky system. It is discretized into n elements of equal length Δy. Element masses are lumped at the n+1 gridpoints. A linear variation of the displacement field is assumed within each element, which is therefore in a state of uniform strain (and stress). Since all quantities are independent of the horizontal coordinate x, the element deformations are given by

$$\varepsilon_{xx} = 0, \ \varepsilon_{yy} = \frac{\partial u_y}{\partial y} \text{ and } \gamma_{xy} = \frac{\partial u_x}{\partial y}, \qquad (1.3\text{-}38)$$

Finite difference approximations to these expressions are

$$\varepsilon_{yy}^{i} = \frac{u_y^{i+1} - u_y^{i}}{\Delta y} \text{ and } \gamma_{xy}^{i} = \frac{u_x^{i+1} - u_x^{i}}{\Delta y} \qquad (1.3\text{-}39)$$

where element i lies between gridpoints i and i+1.

Stresses are calculated by application of the constitutive relations described in Section 1.4 - Component Models. Gridpoint forces are assembled from the element stresses as

$$F_x^{i} = \sigma_{xy}^{i} + \sigma_{xy}^{i-1} \text{ and } F_y^{i} = \sigma_{yy}^{i} + \sigma_{yy}^{i-1} \qquad (1.3\text{-}40)$$

The time integration uses the same central-difference scheme described in Section 1.3.3.4. Damping and numerical stability are handled in a similar fashion.

At the gridpoint at the base of the free-field, shear and normal dashpots provide the absorbing boundary conditions, and the dynamic input is applied in the form of a stress record.

1.3.6.3.3 Coupling with the blocks

The free-field calculation provides gridpoint velocities v_x^f and v_y^f, and element stresses σ_{xx}^f and σ_{xy}^f. In order to achieve the required boundary conditions along the l.h.s. AB, the following stresses must be applied

$$\sigma_{xx} = \sigma_{xx}^f + \rho c_p \ (v_x - v_x^f)$$
$$\sigma_{xy} = \sigma_{xy}^f + \rho c_s \ (v_y - v_y^f) \qquad (1.3\text{-}41)$$

where v_x and v_y are the components of the block gridpoint velocity. Along the r.h.s. CD, the sign of the second term must be reversed.

Figure 1.3-11 illustrates how the coupling of the free-field mesh with a block edge EF is executed. The contribution from the free-field stresses in Eqs. (1.3-41) is applied in the form of concentrated forces at discrete points on the block edge, at the same y-coordinate of the free-field gridpoints. For example, at point i, the following forces are applied

$$P_x^i = \frac{1}{2} \left[(\sigma_{xx}^f)^{i-1} + (\sigma_{xx}^f)^i \right] \Delta y$$
$$P_y^i = \frac{1}{2} \left[(\sigma_{xy}^f)^{i-1} + (\sigma_{xy}^f)^i \right] \Delta y \qquad (1.3\text{-}42)$$

For the r.h.s. boundary, the negative of these expressions is applied. The second term of Eqs. (1.3-41) is applied at the block corners (gridpoints) E and F. For example, at E, the forces to be applied are

$$R_x = - \rho c_p \ (v_x^E - v_x^{fE}) \ \ell$$
$$R_y = - \rho c_s \ (v_y^E - v_y^{fE}) \ \ell \qquad (1.3\text{-}43)$$

where ℓ is the block edge half-length.

The free-field velocities v_x^{fE} and v_y^{fE}, at point E', are obtained by linear interpolation between the adjacent gridpoint velocities (in this case, i-1 and i). The free-field mesh should be fine enough to guarantee an adequate number of support points for the blocks, otherwise excessive slip may occur at some boundary joints.

Normally, the dynamic loading follows a static calculation corresponding to the in-situ conditions. In this case, the in-situ free-field stresses are subtracted from σ_{xx}^f and σ_{xy}^f before the forces P_x^i and P_y^i are calculated. At the same time, the reaction forces (and external loads) along the lateral boundaries which provided equilibrium to the block system in the in-situ state must be stored, so that they are applied to the blocks in addition to the free-field forces during the dynamic loading.

1.3.6.4 Limitations of Dynamic Analysis

Experience with numerous dynamic analyses has shown that, for good accuracy with the distinct element method, the wave length of the highest frequency of interest in the model should be at least 8 times the width of the largest finite-difference zone. The appropriate relation for specifying the mesh is determined by the frequency of the input record and the elastic properties of the medium. For example, assume that a maximum frequency of 100 Hz is to be propagated through a rock column with a bulk modulus of 1 GPa, a shear modulus of 0.15 GPa, and a density of 2610 kg/m^3. The compressional wave speed would be 664 m/sec, and the wavelength at 100 Hz would be 6.64 m. If eight zones per wavelength are required, then the maximum zone size would be 0.83 m.

For dynamic input with a high peak velocity and short rise-time, this requirement may necessitate a very fine spatial mesh and correspondingly fine integration time mesh. The effect is compounded in discontinuum codes because the wave propagation across discontinuities can produce higher frequency components than are provided in the input wave. The consequence is that reasonable analyses may be prohibitively time and memory consuming. In such cases, it may be possible to adjust the input by recognizing that most of the power for the input history is composed of lower frequency components. By filtering the history and removing high frequency components, a coarser mesh may be used without significantly affecting the results.

The filtering procedure can be accomplished with a low-pass filter routine such as the Fast Fourier Transform technique. For example, the unfiltered velocity record shown in Fig. 1.3-12 represents a typical waveform containing a very high frequency spike. The highest frequency of this input exceeds 50 Hz but, as shown by the power spectral density plot of Fourier amplitude versus frequency (Fig. 1.3-13), most of the power (approximately 99%) is made up of components of frequency 15 Hz or lower. It can be inferred, therefore, that by filtering this velocity history with a 15 Hz low-pass filter, less than 1% of the power is lost. The input filtered at 15 Hz is shown in Fig. 1.3-14(a), and the Fourier amplitudes are plotted in Fig. 1.3-14(b). The difference in power between unfiltered and filtered input is less than 1%, while the peak velocity is reduced 38% and the rise time is shifted from 0.035 sec to 0.09 sec. Analyses should be performed with input at different levels of filtering to evaluate the influence of the filter on model results.

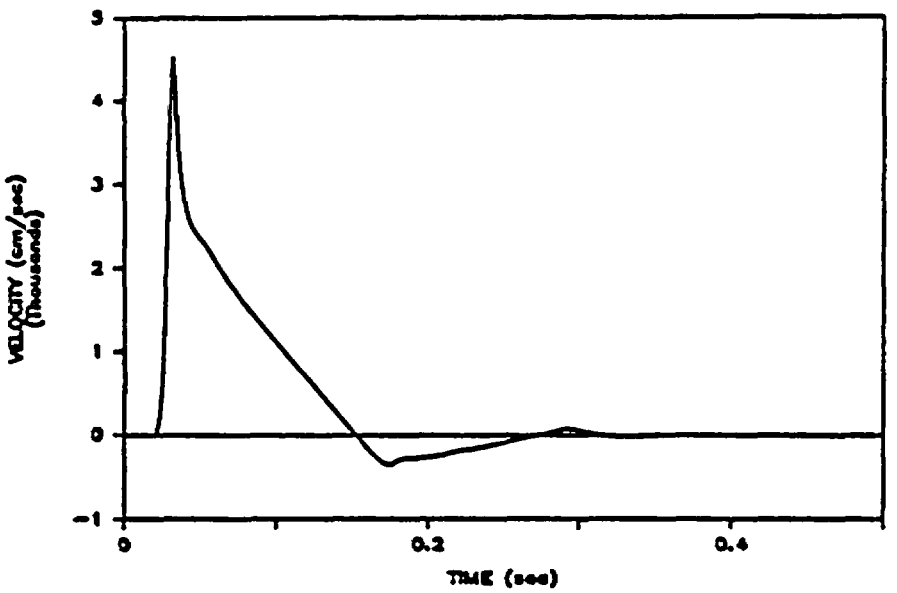

Fig. 1.3-12 Unfiltered Velocity History

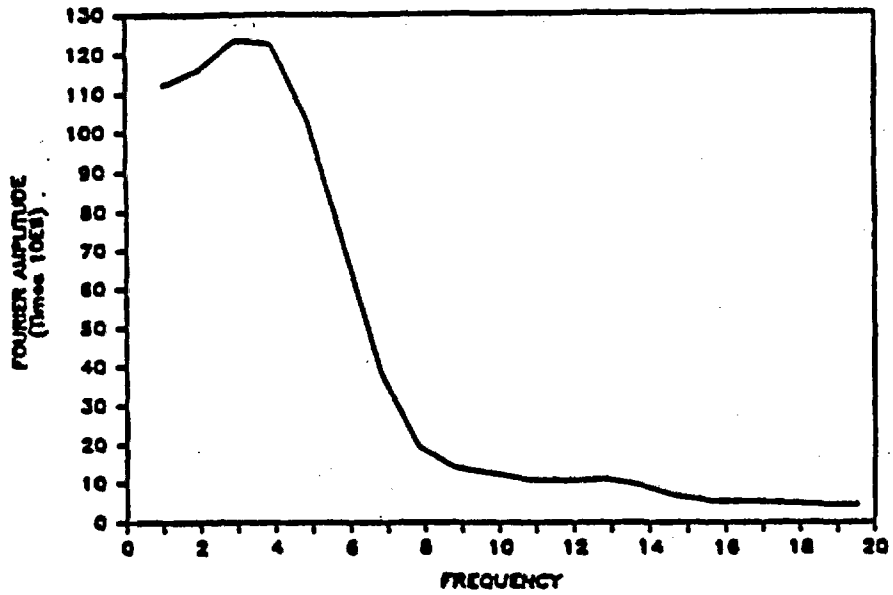

Fig. 1.3-13 Unfiltered Power Spectral Density Plot

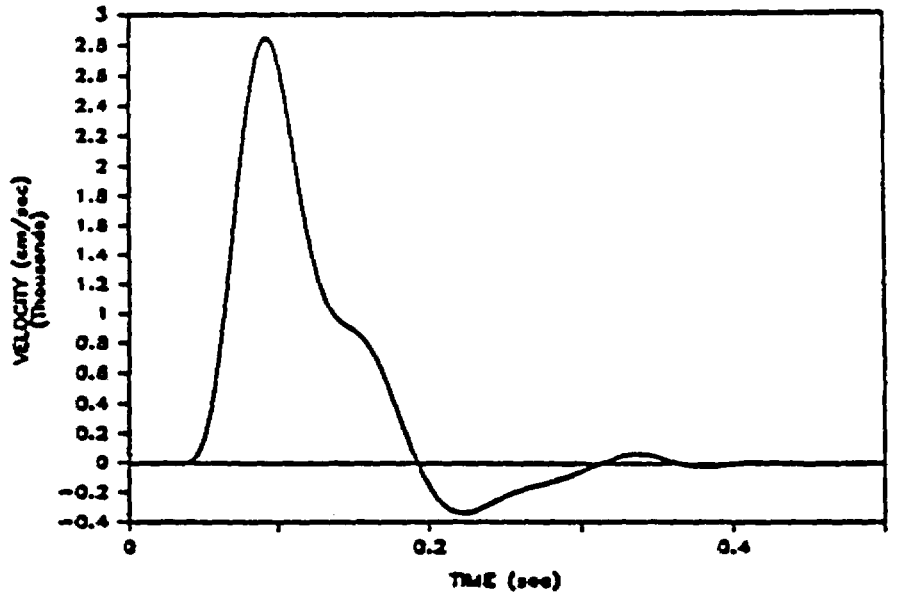

Fig. 1.3-14(a) Filtered Velocity History at 15 Hz

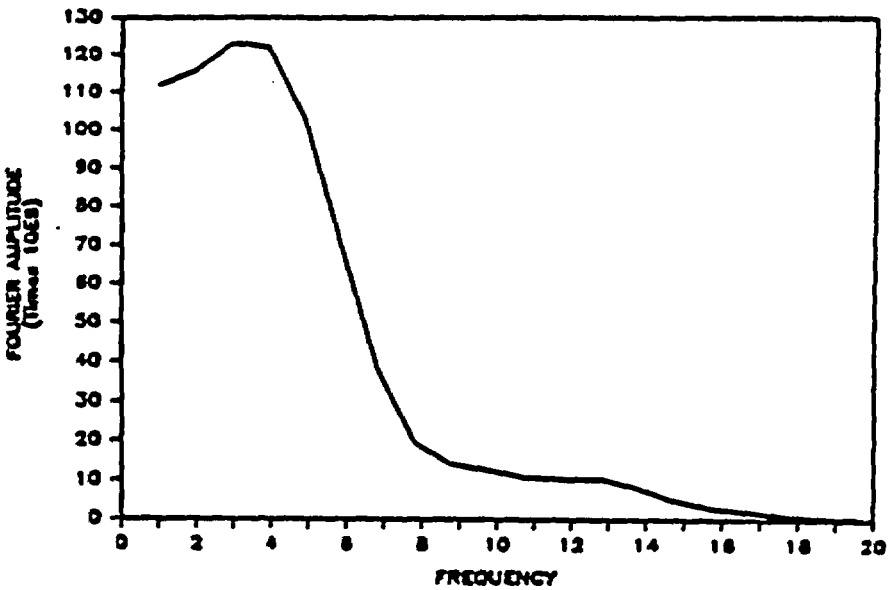

Fig. 1.3-14(b) Results of Filtering at 15 Hz

1.4 COMPONENT MODELS

1.4.1 Introduction

In this section, the major optional features of the UDEC code are discussed in detail. These include provisions for:

(1) fluid flow along fractures;

(2) heat transfer and thermal stress analysis;

(3) rock support and reinforcement logic;

(4) boundary element coupling of the far field; and

(5) intact rock and joint constitutive models.

Prior to describing each of these features, some discussion on the method which the code uses for storage and handling of variables and constants is necessary. A detailed description of the code structure can be found in Volume 2, User's Manual and Program Guide, Chapter 6. Variables in UDEC are stored in "Linked Lists" which are a series of one-dimensional arrays containing information on the blocks, and their contacts, the finite difference zones and gridpoints (if fully-deformable blocks are used), the boundary conditions and the structural elements. The positions of variables within these arrays are defined by an address which points to the first memory location for a particular block or contact, and an integer offset from this location to the item of interest (e.g., contact forces for a particular contact). As contacts between blocks are created or destroyed and no longer exist, the number of locations of contacts within the array may grow or decrease. All of these individual "linked list" arrays are combined into one single dimensional real array (and its integer equivalent) in the program for convenience.

The numerical values of the offsets (always denoted by an integer beginning with the letter k) to specific variables within the linked lists are defined in the main common block "UDECOM". Therefore, in the following discussion, certain variables used in calculation are not given specific variable names, but defined by their offset designation within the linked list. UDEC allows multiple material types in which the constitutive models and/or properties may vary from location to location within the modeled region. Properties are stored in a series of small arrays which are also held in "UDECOM". This common block is included in all major subroutines and is used for passing global constants such as material properties.

1.4.2 Fluid Flow

1.4.2.1 Purpose

The purpose of this component model is to provide for calculation of the flow of fluid through the fractures in a jointed, fully saturated rock mass. This calculation may be useful in determination of fluid flow from injection or withdrawal wells, flow under a dam or other surface structures, or flow of non-Newtonian fluids such as grout from an injection point.

1.4.2.2 Assumptions and Limitations

The model here assumes that fluid flow only occurs in fractures; the intact blocks of material are assumed to be impermeable. The model used in UDEC is two-dimensional, there is no thermal coupling to the fluid flow, and the joint is assumed to be fully saturated. The UDEC code can be very inefficient for solving transient fluid flow problems. The explicit solution procedure used may result in very small fluid timesteps, requiring exceedingly large solution times. Arbitrary domain volumes at joint intersections can lead to inaccuracies in transient analyses. Finally, fluid flow calculations are restricted to fully-deformable blocks. Fluid flow is governed by a parallel plate analogy, and thus the fractures themselves are assumed to be planar (along any block edge) with parallel sides. Flow along the fractures is assumed to be laminar and governed by the "cubic law". Experiments conducted by Louis (1969) showed that this law is essentially valid for laminar flow in rock joints. Louis proposed an empirical correction factor for the above expression in order to account for fracture roughness. Witherspoon et al. (1979) tested both open and closed joints. They reported that the cubic law is still valid for the latter, provided that the actual mechanical aperture is used. Due to the effects of roughness and tortuosity of flow, the fracture conductivity in their experiments was reduced by a factor between 1.04 and 1.65. Barton et al. (1985) proposed an empirical formula which gives the hydraulic aperture (to be used in the cubic law) as a function of the mechanical aperture and the joint roughness coefficient (JRC).

1.4.2.3 Notation

Table 1.4-1 provides offsets and main common block variable names for pertinent fluid flow variables. Table 1.4-2 provides program control notations pertinent to the fluid flow logic.

Table 1.4-1

FLUID FLOW VARIABLE NOTATION

Variable Notation		Comments	Where Found
Algebraic	Computer		
a	KCAP	Offset to mean joint aperture	Contact data array
q	KCQ	Offset to flow-rate across joint or contact	Contact data array
l	KCL	Offset to length associated with joint	Contact data array
p	KPP	Offset to domain pore pressure	Domain data array
P_o	KPPO	Offset to old domain pore pressure	Domain data array
A	KDAR	Offset to domain area	Domain data array
P	KBDPP	Offset to pore pressure at a boundary corner	Boundary corner array
k_j	PERMJ(I)	Joint permeability factor, material number I	In main common UDECOM
k_c	PERMC(I)	Contact permeability factor, material number I	"
ρ_w	RHOW	Fluid density	"
K_w	BULKW	Fluid bulk modulus	"
	COHW	Fluid yield stress for Bingham-type fluid	"

Table 1.4-2

FLUID FLOW PROGRAM CONTROL NOTATION

Variable Notation	Comments	Where Found
FRACW	Fraction of fluid flow timestep	Main Common UDECOM
SSFLAG	Steady flow calculation flag	"
PTOL	Tolerance for steady flow calculations	"
NSFDT	Number of fluid flow calculation cycles between mechanical cycles (for coupling purposes)	"

1.4.2.4 Derivation

As stated previously, UDEC assumes that the blocks themselves are impermeable, and therefore the fluid flow is restricted to the joints. Louis (1969) studied fluid flow in an open concrete joint for laminar and turbulent conditions for varying roughnesses of the joint. It was found that, for laminar conditions, the assumption of flow between parallel plates was applicable. The mean flow velocity for viscous laminar flow between parallel plates is given by:

$$V = k_f J \qquad (1.4\text{-}1)$$

J is the hydraulic gradient given by $\Delta P/l$, where ΔP is the pressure drop over a fracture of length, l. The joint hydraulic conductivity is denoted by k_f, where

$$k_f = \frac{a^2 g}{12\ \nu} \qquad (1.4\text{-}2)$$

where a = fracture width (aperture),

ν = kinematic viscosity of the fluid, and

g = acceleration of gravity.

The flow per unit width can be expressed as

$$q = Va = \frac{a^3 g}{12\nu} J \qquad (1.4\text{-}3)$$

which is usually referred to as the cubic law (e.g., Witherspoon et al., 1979). This relation is shown in Fig. 1.4-1. Note that the cubic law assumes the constant b=1 and α=3 in this figure. The above derivation refers to Newtonian fluids such as water in which flow is not shear stress dependent.

Another general class of fluids in which the initiation of flow is governed by the shearing stress exerted on the fluid is termed a Bingham substance. Bingham materials, such as a cement grout or thixotropic drilling fluids, exhibit viscoplastic behavior. The viscoplastic fluid exhibits similar flow behavior to the Newtonian fluid (i.e., flow linearly related to pressure gradient) with the exception that no flow occurs until a threshold gradient, J_0 is exceeded. The stresses applied to an element of fluid between parallel plates are shown in Fig. 1.4-2. Summing the forces on this element, one obtains:

$$J_0 = \frac{2\tau_y}{a} \qquad (1.4\text{-}4)$$

which gives the threshold gradient, J_0, at which flow occurs (see Fig. 1.4-3).

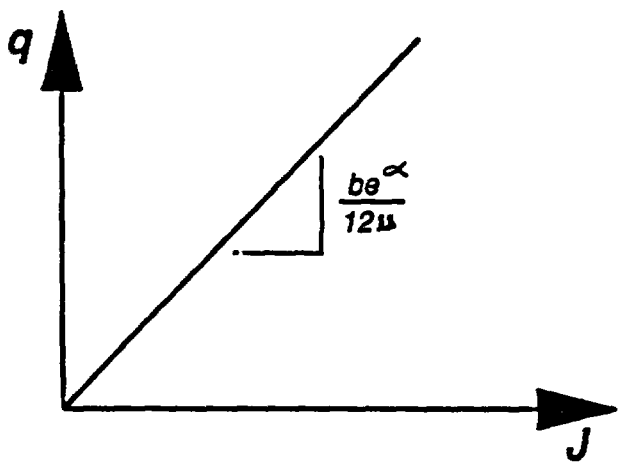

Fig. 1.4-1 Flow-Gradient Relation for Newtonian Fluid in UDEC

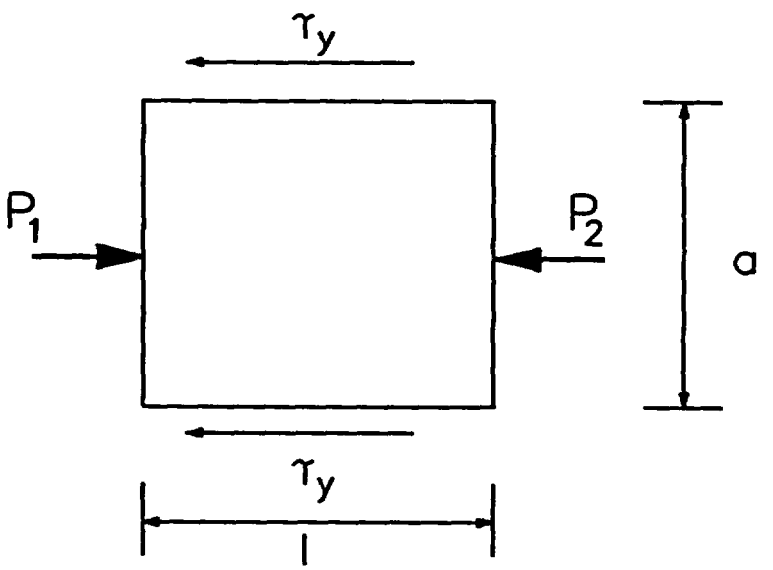

Fig. 1.4-2 Force Equilibrium for Fluid Volume Element

The expression for the threshold gradient can also be obtained by considering the equation for steady laminar flow of a Bingham plastic in a circular pipe. This equation is known as Buckingham's equation (Wilkinson, 1960):

$$Q = \frac{\pi\, a^4\, \Delta P}{8L\, \mu_p} \left[1 - \frac{4}{3} \left[\frac{2L\tau_y}{a\, \Delta P} \right] + \frac{1}{3} \left[\frac{2L\tau_y}{a\, \Delta P} \right]^4 \right] \qquad (1.4\text{-}5)$$

where Q = volume rate of flow,

a = pipe radius,

μ_p = Bingham plastic viscosity,

$\Delta P/L$ = pressure gradient = J, and

τ_y = yield stress.

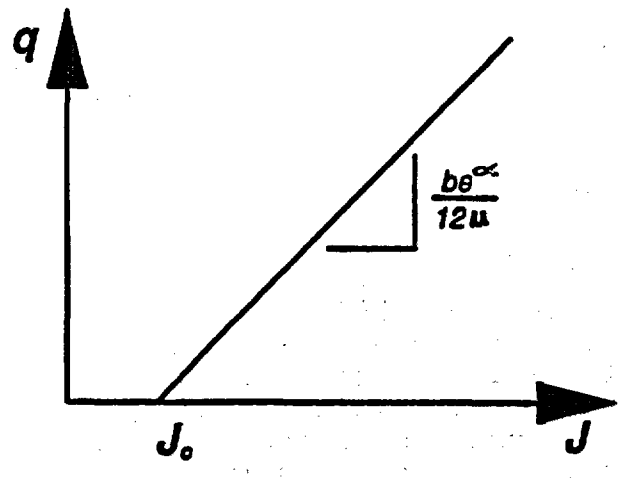

Fig. 1.4-3 Flow-Gradient Relation for Bingham Fluid in UDEC

From this expression, it can be seen that no flow occurs if the pressure gradient J is zero or equals $2\tau_y/a$. It is not clear from the equation what occurs at pressure gradients between zero and $2\tau_y/a$, but it is reasonable to assume that no steady flow occurs within this range. Therefore, the threshold gradient, J_o, the gradient at which steady flow is possible, is given by

$$J_o = \frac{2\tau_y}{a} \qquad (1.4\text{-}6)$$

1.4.2.5 Application

The fluid flow logic is applicable to examination of fluid flow through jointed rock in which the porous flow through the intact material is considered negligible in comparison. Since thermal buoyancy effects are not considered, isothermal flow is assumed. The Newtonian fluid logic can be used for calculations of water flow, whereas the Bingham (visco-plastic) fluid can be any material which exhibits Newtonian flow after a threshold gradient has been achieved. A large class of fluids used in geotechnical applications (grout, drilling mud, well treatment fluids) may be applicable to this model.

1.4.2.6 Numerical Method Type

The fluid flow logic uses the same finite difference approach for solution of the fluid equations. No new or unique numerical methods are required in the problem solution.

1.4.2.7 Derivation of the Numerical Model

A fully-coupled mechanical-hydraulic analysis is performed, where fracture conductivity is dependent on mechanical deformation and, conversely, joint water pressures affect the mechanical computations. The numerical implementation makes use of the domain structure shown in Fig. 1.3-2(e). For a closely- packed system, there exists a network of domains, each of which is assumed to be filled with fluid at uniform pressure and which communicates with its neighbors through contacts. Fully-saturated conditions are assumed. When gravitational loading is present, the effects of the hydrostatic pressure are simulated by applying buoyancy forces to the blocks. In this case, domain pressures equal the total water pressure minus the hydrostatic pressure.

When a pressure differential exists between adjacent domains, flow will take place. The flow rate is calculated in two different ways depending on the type of contact. For a point contact (i.e., corner-edge or corner-corner), the flow rate is

$$q = - k_c \Delta p \qquad (1.4\text{-}7)$$

where k_c is a contact permeability parameter.

When the contact possesses a length (i.e., an edge-edge contact), a more realistic calculation is possible, based on the cubic law of flow in fractures. The flow rate is then given by

$$q = - k_j a^3 \Delta p / l \qquad (1.4\text{-}8)$$

where k_j is a joint permeability factor,

a is the contact hydraulic aperture, and

l is the contact length.

The hydraulic aperture is given, in general, by

$$a = a_o + \Delta a \qquad (1.4\text{-}9)$$

where a_o is the aperture at zero normal stress, and

Δa is the mechanical change in aperture due to the contact normal displacement.

A minimum value, a_{res}, is assumed for the aperture, beyond which mechanical closure does not affect the contact permeability.

At every time step, flow rates through all the contacts are calculated based on these formulae. Then, domain pressures are updated, taking into account the net flow into the domain and possible changes in domain area due to the motion of the surrounding blocks. The new domain pressure is

$$p = p_o + K_w \, Q \, \Delta t/A - K_w \, \Delta A/A_m \qquad (1.4\text{-}10)$$

where p_o is the old domain pressure,

Q is the sum of flow rates into the domain from all surrounding contacts,

K_w is the bulk modulus of fluid, and

$\Delta A = A - A_o$, $A_m = (A + A_o)/2.$

where A and A_o are, respectively, the new and old domain areas.

The new domain pressures are then added to the forces to be applied to the surrounding block edges. This process results in effective normal stresses in all contacts and total stresses inside the impermeable blocks.

1.4.2.8 Location

The fluid flow logic is called from subroutine CYCLE. Fluid pressure increments from domain volumetric strain is determined in PPGEN, and fluid flow and pore pressure dissipation found in PPDIS.

1.4.2.9 Numerical Stability and Accuracy

The numerical stability of the fluid flow algorithm, for slowly varying domain areas, requires that the timestep be limited to

$$\Delta t^f = \min \left[A_i \, / \, (K_w \, \Sigma \, k_i) \right] \qquad (1.4\text{-}11)$$

where the sum of k_i is extended to all contacts surrounding the domain, A_i, with

$$k_i = \max (k_c , k_j \, a^3 / l) \qquad (1.4\text{-}12)$$

The minimum value of Δt^f for any domain is taken and, if less than the mechanical timestep, is used in the analysis. For joint contacts (edge-edge), the domain area is the product of joint length and aperture. Because the minimum joint aperture is a_{res}, the domain area is always positive, even if the blocks are overlapping. A minimum domain area can be set for computational efficiency. Large contact permeabilities or very small domain areas require very small timesteps. In addition, the fluid filling a joint increases the apparent stiffness by K_w/a. If a is small, this may be much larger than the joint mechanical stiffness and require the adjustment of the timestep. There are several ways of reducing the run times of fluid flow analyses. The use of density scaling of the blocks or the scaling of the bulk modulus of the fluid can improve efficiency by producing mechanical and hydraulic time steps of the same order of magnitude. In many cases, only the final steady-state condition is of interest. This condition does not depend on domain areas, and an equal area can be used for all domains, which leads to faster convergence. This scheme also eliminates the problem of the fluid stiffness affecting the mechanical time step.

Problems containing joints of very different apertures generally require a large number of timesteps for the steady-state condition to be reached. In many cases, the domain pressures change very slowly, and their mechanical effects are only felt after several timesteps. A procedure to be used in such cases was developed in which several fluid flow timesteps are executed between mechanical timesteps. It is based on an adaptive procedure which "triggers" an update of the mechanical quantities whenever the maximum increment of pressure in any domain exceeds some prescribed tolerance (PTOL, see Table 1.4-2).

1.4.2.10 Alternatives

No other fluid flow models exist within the UDEC code. The explicit solution algorithm is sufficiently general to allow inclusion of other non-Newtonian fluid flow mechanisms.

1.4.3 Heat Transfer and Thermal Stress Analysis

1.4.3.1 Purpose

The heat transfer and thermal stress coupling in UDEC was developed to allow examination of design and performance assessment problems in underground nuclear waste repositories. As such, the logic provides for application of exponentially-decaying flux and volumetric heat sources as well as convective and radiative boundary conditions. The logic is general, however, allowing a variety of problems to be examined not strictly associated with nuclear waste disposal.

The heat transfer logic may be coupled to the stress analysis portion of the code to allow calculation of thermoelastic stresses in the intact blocks. Since the body being modeled may consist of intact blocks and fractures, the overall response of the body may be non-linear depending on the failure properties of the fractures.

1.4.3.2 Assumptions and Limitations

The following are the assumptions and limitations of the heat transfer and stress-coupling logic in UDEC.

1. Heat flow within the body is modeled by conduction only. The joints themselves have no effect on heat transfer.

2. Heat flow may be isotropic or transversely isotropic.

3. There is no coupling between the fluid flow and heat transfer models.

4. The coupling of heat transfer and stress is in one direction only, i.e., heat transfer properties are not strain or pressure dependent, nor are the mechanical properties or failure characteristics temperature dependent. There is no energy change in the body as a function of strain or inertia. Since UDEC runs in large deformation mode, the geometry of the blocks (and the finite difference zones of which they are composed) is updated automatically. There is, therefore, a possible small geometric effect on heat transfer which can be modeled by the code. This potential effect is considered to be very minor.

5. Convective and radiative heat transfer mechanisms are restricted to the surfaces and boundaries of the problem.

The limitation that joints do not factor into the heat transfer is not felt to be restrictive for geomechanical problems. Numerous field experiments (e.g., Zimmerman et al., 1986) have shown that jointing has little influence on the heat transfer properties of rock, and that in-situ thermal diffusivity varies, generally, by less than 10% of the laboratory-determined values. Some uncertainty is also obviously associated with the choice of the thermal and mechanical properties for the material. The thermal model requires definition of the thermal conductivity (isotropic or directional), specific heat, density and thermal expansion coefficient. The required mechanical properties vary depending upon the constitutive law used. Uncertainty occurs in the definition of these properties, particularly the in-situ Young's modulus.

Although the blocks are considered to be elastic in most coupled thermal analyses, the Mohr-Coulomb plasticity model may be used to allow yield in the intact material. The manner in which coupling of the heat transfer and thermal logic is performed may affect the accuracy of following non-linear material behavior. Thermomechanical calculations are restricted to fully-deformable blocks due to the need to calculate block expansions.

Finally, there is no thermal coupling in terms of energy change due to mechanical deformations or mechanical accelerations due to heating. In other words, the acceleration and resultant stress changes of the body due to heating are negligible, as are the temperature changes resulting from straining or acceleration of the body.

1.4.3.3 Notation

Table 1.4-3 provides offsets and main common block variables for properties and variables specific to the heat transfer logic. Table 1.4-4 provides boundary and initial conditions variables and control notation pertinent to the heat transfer logic.

Table 1.4-3

HEAT TRANSFER THROUGH MODEL NOTATION

Variable Notation		Comments	Where Found
Algebraic	Computer		
For Rigid or Simply Deformable Blocks			
T_i	KBTEM	Offset in block data array to to block centroid temperature	Block data array/UDECOM
ΔT_i	KBDT1	Offset in block data array to block centroid temperature change over preceding timestep	"
$\frac{1}{C_p m}$	KBTHM	Offset in block data array to block centroid "thermal mass"	"
$\Sigma \Delta T_i$	KBDTEM	Offset in block data array to accumulate block centroid temperature change	"
For Fully-Deformable Blocks			
T_i	KGTEMP	Offset in gridpoint data array for gridpoint temperature	Gridpoint data array/ UDECOM
ΔT_i	KGDTEM1	Offset in gridpoint data array array for gridpoint temperature change over preceding timestep	"
$\frac{1}{C_p m}$	KTHMG	Offset in gridpoint data array for gridpoint thermal mass	"

Table 1.4-3
(continued)

Variable Notation		Comments	Where Found
Algebraic	Computer		
For Fully-Deformable Blocks			
$\Sigma\Delta Ti$	KGDTEM	Offset in gridpoint data array for accumulated gridpoint temperature change	Gridpoint data array UDECOM
C_p	SPEC(i)	Specific heat	"
k_x	XCOND(i)	X-direction thermal conductivity	"
k_y	YCOND(i)	Y-direction thermal conductivity	"
α	THEXP(i)	Linear thermal expansion coefficient	"
Δt	DELT	Thermal timestep	"
Ti	KTEMP	Offset in corner data array to corner temperature	"
ΔTi	KDTEM1	Offset in corner data array to corner temperature change in one cycle	"
$\frac{1}{C_{pm}}$	KTHMA	Offset in corner data array to corner thermal mass	"
$\Sigma\Delta Ti$	KDTEM	Offset in corner data array to accumulated temperature change	"

Table 1.4-4

HEAT TRANSFER MODEL CONTROL AND BOUNDARY CONDITION NOTATION

Variable Notation	Comment	Where Found
KBFIX	Flag for fixed block temperature	Block data array UDECOM
KTHGF	Flag for fixed gridpoint temperature	Gridpoint data array UDECOM
KTHPF	Flag for fixed corner temperature	Corner data array UDECOM
NTHER	Number of thermal cycles executed before switching to mechanical cycles	UDECOM
NMECH	Number of mechanical cycles executed when called from thermal cycles	UDECOM

1.4.3.4 Derivation

The heat transfer in UDEC is based on conductive transfer within the medium with the provision for temperature, flux, convective or radiative boundaries. The standard equations for transient heat conduction can be found in many texts, such as Karlekar and Desmond (1982), and are reviewed here. The basic equation of conduction heat transfer is Fourier's law, which can be written in one dimension as

$$Q_x = - k_x \frac{\partial T}{\partial x} \qquad (1.4\text{-}13)$$

where Q_x = flux in the x-direction (W/m^2), and

k_x = thermal conductivity in the x-direction ($W/m\ ^\circ C$).

A similar equation can be written for Q_y. Also, for any mass, the change in temperature can be written as

$$\frac{\partial T}{\partial t} = \frac{Q_{net}}{C_p M} \qquad (1.4\text{-}14)$$

where Q_{net} = net heat flow into mass (M),

C_p = specific heat ($J/kg^\circ C$), and

M = mass (kg).

These two equations form the basis of the thermal logic in UDEC. Equation (1.4-14) can be written as

$$\frac{\partial T}{\partial t} = \frac{1}{C_p \rho} \left[\frac{\partial Q_x}{\partial x} + \frac{\partial Q_y}{\partial y} \right] \qquad (1.4\text{-}15)$$

where ρ is the mass density.

Combining this with Eq. (1.4-13),

$$\frac{\partial T}{\partial t} = \frac{1}{C_p \rho} \frac{\partial}{\partial x} \left[k_x \frac{\partial T}{\partial x} \right] + \frac{\partial}{\partial y} \left[k_y \frac{\partial T}{\partial y} \right]$$

$$= \frac{1}{\rho C_p} \left[k_x \frac{\partial^2 T}{\partial x^2} + k_y \frac{\partial^2 T}{\partial y^2} \right] \qquad (1.4\text{-}16)$$

if k_x and k_y are constant. This is the standard two-dimensional diffusion equation.

Temperature changes cause stress changes for fully-deformable blocks according to the equation

$$\Delta\sigma_{ij} = - \delta_{ij} K \beta \Delta T \qquad (1.4\text{-}17)$$

where $\Delta\sigma_{ij}$ = change in ij stress component,

δ_{ij} = Kronecker delta function,

$$\begin{bmatrix} 1 & 0 \\ 0 & 1 \end{bmatrix}$$

K = bulk modulus,

β = volumetric thermal expansion coefficient β, and

ΔT = temperature change.

Note that $\beta = 3\alpha$, where α = linear thermal expansion coefficient.

The mechanical changes can also cause temperature changes as energy is dissipated in the system.

1.4.3.5 Application

This model is applicable to any general two-dimensional heat transfer problem in which the assumptions and limitations apply. Although the UDEC code considers the material to be a discontinuum, the joints may be bonded, and the model will behave essentially as a continuum with the given constitutive law for thermomechanical simulations. The present version of the code does not provide temperature dependency of the thermal or mechanical properties, or time-dependent mechanical models.

1.4.3.6 Numerical Method Type

The model uses a standard finite difference approach to discretization of the two-dimensional diffusion equation. No new or unique numerical techniques are used.

1.4.3.7 Derivation of Numerical Method

As described in previous sections, UDEC allows the user the option of using rigid, simply-deformable or fully-deformable blocks. The difference in these methods (for heat transfer calculations) is the way in which the code treats internal block discretizations. The fully-deformable blocks are automatically discretized into a number of triangular finite difference zones for mechanical calculations, whereas the rigid and simply-deformable are not. When conducting thermal analyses, UDEC uses the existing triangular finite difference zones from fully-deformable blocks [Fig. 1.4-4(a)], or generates a thermal triangular zone mesh within the blocks for rigid or simply-deformable blocks [Fig. 1.4-4([b)]. It has been found that more accurate results are obtained when using fully-deformable blocks.

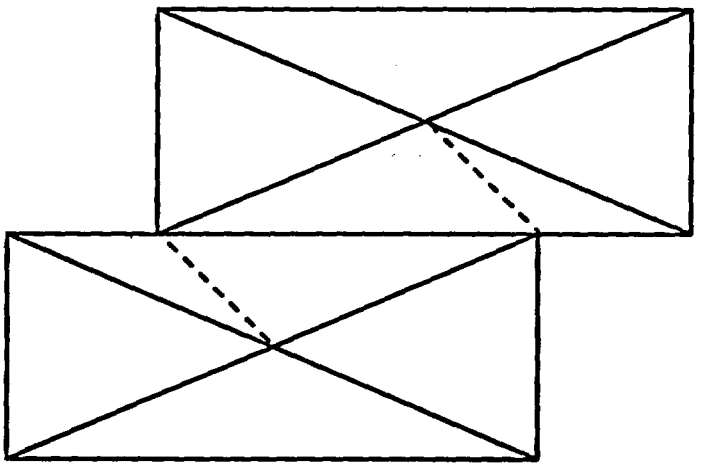

(a) fully-deformable blocks — extra triangular zones are formed using contact points

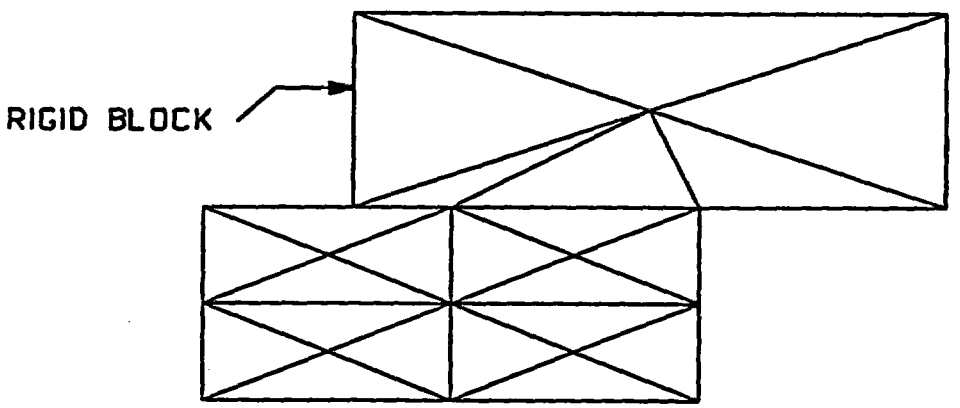

(b) block centroids are used for rigid blocks

Fig. 1.4-4 Block Discretization for Heat Transfer Analysis

Explicit Logic

At each timestep, Eqs. (1.4-13) and (1.4-14) are solved numerically, using the following scheme.

1. In each triangle, $(\partial T/\partial x)$ and $(\partial T/\partial y)$ are approximated using the equation

$$\frac{\partial T}{\partial x_i} = \frac{1}{A} \int T n_i \, ds$$

$$\equiv \frac{1}{A} \sum_{m=1}^{3} \bar{T}^m \varepsilon_{ij} \Delta x_j^m \qquad (1.4\text{-}18)$$

where A = area of the triangle,

n_i = i^{th} component of outward normal,

$\bar{T}^m$ = average temperature on side m,

Δx_j^m = difference in x_j between ends of side m, and

ε_{ij} = two-dimensional permutation tensor,

$$\varepsilon_{ij} = \begin{bmatrix} 0 & 1 \\ -1 & 0 \end{bmatrix} .$$

The heat flow into each gridpoint of the triangle is calculated from

$$F_i = A_j Q_i \qquad (1.4\text{-}19)$$

where A_j is the width of the line perpendicular to the component Q_i, as shown in Fig. 1.4-5:

$$F_{total} = F_x + F_y$$

$$= A_y Q_x + A_x Q_y \qquad (1.4\text{-}20)$$

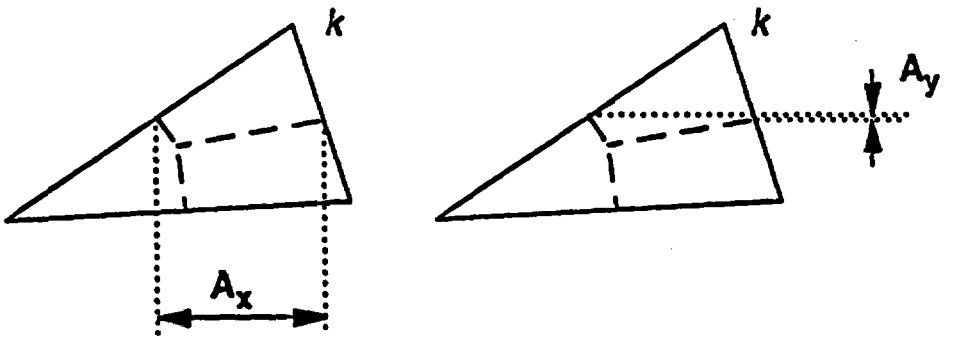

Fig. 1.4-5 Heat Flow Into Gridpoint k

2. For each gridpoint,

$$\Delta T = \frac{Q_{net}}{C_p M} \Delta t \qquad (1.4\text{-}21)$$

where Q_{net} is the sum of F_{total} from all zones affecting gridpoint i.

This scheme is explicit, so Δt is limited by numerical stability considerations. An implicit scheme is also available, and is described below.

Implicit Logic

The implicit thermal logic in UDEC uses the Crank-Nicholson method, and the set of equations is solved by an iterative scheme known as the Jacobi method. An implicit method is advantageous for solving linear problems such as heat conduction with constant conductivity, because it allows the use of much larger timesteps than those permitted by an explicit method, particularly at later times in a problem, when temperatures are changing slowly.

Theory

The usual one-dimensional explicit finite difference scheme for heat conduction can be written

$$\frac{\rho C_p}{k} \cdot \frac{T_i(t + \Delta t) - T_i(t)}{\Delta t} = \frac{T_{i+1}(t) - 2T_i(t) + T_{i-1}(t)}{(\Delta x)^2} \qquad (1.4\text{-}22)$$

An implicit method can be derived by replacing the right-hand side of Eq. (1.4-22) by the expression:

$$\frac{1}{2}\left[\frac{T_{i+1}(t+\Delta t) - 2T_i(t+\Delta t) + T_{i-1}(t+\Delta t)}{(\Delta x)^2} + \frac{T_{i-1}(t) - 2T_i(t) + T_{i-1}(t)}{(\Delta x)^2}\right] \qquad (1.4\text{-}23)$$

This method, known as the Crank-Nicholson method, has the advantage that it is stable for all values of Δt, but has the disadvantage of being implicit. This means that the temperature change at any point depends on the temperature change at other points. This can be seen by rewriting the implicit scheme as

$$\frac{\rho C_p}{k\Delta t}\Delta T_i = \left[\frac{T_{i+1} + \frac{1}{2}\Delta T_{i+1} - 2(T_i + \frac{1}{2}\Delta T_i) + T_{i-1} + \frac{1}{2}\Delta T_{i-1}}{(\Delta x)^2}\right] \qquad (1.4\text{-}24)$$

since $T_k(t + \Delta t) = T_k(t) + \Delta T_k$. (1.4-25)

The implicit method requires that a set of equations be solved at each timestep for the values of ΔT_i.

In matrix notation, the explicit method can be written as

$$\underline{\Delta T} = \underline{\underline{C}}\ \underline{T} \tag{1.4-26}$$

where $\underline{\underline{C}}$ is a coefficient matrix,

$\underline{T}$ is a vector of the temperatures, and

$\underline{\Delta T}$ is a vector of the temperature changes.

The implicit scheme can be written as

$$\underline{\Delta T} = \underline{\underline{C}}(\underline{T} + \tfrac{1}{2}\underline{\Delta T}) \tag{1.4-27}$$

which can be rewritten as

$$(\underline{\underline{I}} - \tfrac{1}{2}\underline{\underline{C}})\underline{\Delta T} = \underline{\underline{C}}\ \underline{T} \tag{1.4-28}$$

where $\underline{\underline{I}}$ is the identity matrix and we need to solve for $\underline{\Delta T}$ at each timestep.

The matrix

$$(\underline{\underline{I}} - \tfrac{1}{2}\ \underline{\underline{C}}) \tag{1.4-29}$$

is diagonally dominant and sparse, because only neighboring points contribute non-zero values to $\underline{\underline{C}}$.

This set of equations is thus efficiently solved by an iterative scheme. For ease of implementation as a simple extension of the explicit method, the Jacobi method is used. For the NxN system $\underline{A}\underline{x} = \underline{b}$, this can be written for the n^{th} iteration as

$$x_i(n+1) = \frac{b_i}{a_{ii}} - \sum_{\substack{j=1 \\ j\neq i}}^{N} \left[\frac{a_{ij}}{a_{ii}} x_j(n) \right] \qquad i = 1,2, \ldots N \tag{1.4-30}$$

that is,

$$x_i(n+1) = \frac{1}{a_{ii}} \left[b_i - \sum_{j=1}^{N} a_{ij}\, x_j(n) \right] + x_i(n) \tag{1.4-31}$$

In our case, this becomes,

$$\Delta T_i(n+1) = \frac{1}{(1-\frac{1}{2}C_{ii})} \left[\sum_{j=1}^{N} C_{ij}\, T_j - \sum_{j=1}^{N} (\delta_{ij} - \tfrac{1}{2}C_{ij}) \Delta T_j(n) \right] + \Delta T_i(n)$$

$$= \frac{1}{(1-\frac{1}{2}C_{ii})} \left[\sum_{j=1}^{N} C_{ij}\, T_j + \tfrac{1}{2} \sum_{j=1}^{N} C_{ij}\, \Delta T_j(n) - \Delta T_i(n) \right] + \Delta T_i(n) \tag{1.4-32}$$

This equation shows the analogy between the implicit scheme and the explicit scheme which can be written as

$$\Delta T_i = \sum_{j=1}^{N} C_{ij}\, T_j \tag{1.4-33}$$

The amount of calculation required for each timestep is approximately n + 1 times that required for one timestep in the explicit scheme, where n is the number of iterations per timestep. This extra calculation can be more than offset by the much larger timestep permitted by the implicit method. However, the implicit scheme can give poor accuracy because it assumes that the temperature change is a linear function of time in a single timestep, which may not be accurate, especially when temperatures are changing fast, as they generally do near the beginning of a run.

1.4.3.8 Location

The thermal calculations are initiated from subroutine MAIN. Thermal timesteps are controlled from THCYC, and thermal stresses calculated in TSTR. Thermal boundary conditions are handled in APPTH and initial conditions in INITEM. Thermomechanical coupling occurs in CYCLE.

1.4.3.9 Numerical Stability and Accuracy

Inaccuracy in the solution of coupled thermal and mechanical problems can enter in four areas.

1. The thermal and mechanical models are effectively decoupled, requiring the user to pre-define at what time coupling is to occur. How often this coupling is performed may determine the accuracy of the method in defining the mechanical state for non-linear material models.

2. The accuracy of the thermal problem as a result of discretization density.

3. Inaccuracies inherent in the boundary conditions.

4. Constraints of the numerical method (implicit vs explicit).

Coupling of the Thermal and Mechanical Models

The mechanical logic (the standard UDEC program) is used in the thermomechanical program to take "snapshots" of the mechanical state at appropriate intervals in the development of the transient thermal stresses. The procedure for coupling this logic with the thermal logic is outlined in Fig. 1.4-6.

1. SETUP

. define problem geometry
. define material properties
. define thermal properties
. set boundary conditions (thermal and mechanical)
. set initial conditions (thermal and mechanical)
. set any internal conditions, such as heat sources

2. CYCLE TO EQUILIBRATE MECHANICALLY

3. PERFORM ANY DESIRED ALTERATIONS such as excavations

4. CYCLE TO EQUILIBRATE MECHANICALLY

REPEAT steps 3 and 4 until "initial" mechanical state is reached for thermal analysis.

5. TAKE THERMAL TIMESTEPS until

(a) desired time is reached; or

(b) temperature increases cause "large" out-of-balance forces in blocks.

6. CYCLE TO EQUILIBRATE MECHANICALLY

REPEAT steps 5 and 6 until sufficient time has been simulated.

REPEAT steps 3 to 6 as necessary.

Fig. 1.4-6 General Solution Procedure for Thermal-Mechanical Analysis

A difficulty associated with implementing this scheme lies in determining the meaning of "large" in Step 5(b). An advantage of explicit schemes is that the solution is reached in a physically meaningful manner, which is important for non-linear constitutive laws. In order to accomplish this in thermal analyses, the out-of-balance force caused by the temperature changes should not be allowed to adversely affect the accuracy of the solution. If the analysis being performed is linear, no temperature increase will be too great, and UDEC need only equilibrate when the simulation time is such that a solution is required. For non-linear problems, experimentation is necessary to obtain a feel for what "large" means in the particular problem being solved. This is performed by trying different allowable temperature increases when running the program.

For example, if decaying heat sources are being used, it could be possible that the user should not attempt coupling until <u>after</u> yield has occurred. In this case, poor results could be obtained. The following is a suggested method for determination of coupling frequency.

1. Save the mechanical equilibrium state reached by UDEC (in case further trials are necessary).

2. Plot the stresses and shear displacements. If the stresses are near yield, the thermal stresses caused by the temperature changes should not be large. If the stresses are far from yield, larger stresses can be tolerated.

3. Run thermal steps until a particular temperature increase is reported by the program.

4. Cycle mechanically to attain equilibrium.

5. Again, plot the stresses and shear displacements. If the area where the stresses are at or near yield is not much larger than at step 2 and the shear displacements are not very different, the temperature increase allowed was acceptable. If the changes are judged to be too great, the run must be repeated with a smaller allowed temperature change.

An important point to note is that the same temperature increase is not necessarily acceptable for all times in a problem. While the system is far from yield, large temperature increases will be acceptable, but near yield only relatively small increases can be tolerated.

Inaccuracy due to Discretization

UDEC divides fully-deformable blocks into triangular zones for mechanical calculations. For thermal calculations, the same zoning is used, with the exception that the triangles are further divided where the block is in contact with a corner on another block [Fig. 1.4-4(a)].

Rigid and simply-deformable blocks are divided into triangles using the centroid as a common vertex of all the triangles, with the other vertices at the corner and at the contact with corners on other blocks [Fig. 1.4-4(b)].

If the schemes outlined above were used without modification, it would be possible for very narrow triangles (such as those shown in Fig. 1.4-7) to be formed.

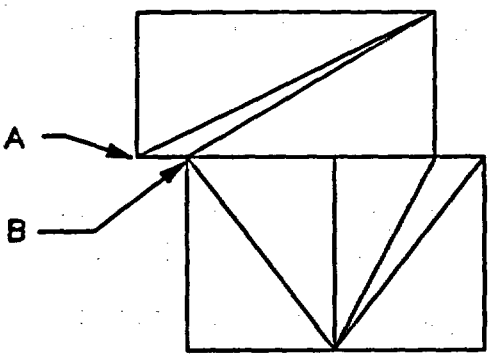

Fig. 1.4-7 Zones Which May Cause Inaccuracy

This causes inaccuracy and may also lead to extremely small thermal timesteps. To avoid this, it is important to not have blocks with small zones neighboring on blocks with large zones or large rigid blocks. The "thermal tolerance" option on the **RUN** command should also be used to force points such as A and B, in Fig. 1.4-7, to be treated as one for thermal calculations (see Vol. 2, UDEC User's Manual, for details).

Boundary Locations — When modeling an infinite region, it is necessary to truncate the UDEC grid far enough away from the region of interest that the boundaries do not affect the solution. To determine whether the boundaries are far enough away, the steps listed below should be followed.

1. Let the boundary representing infinity be insulated (the default boundary condition).

2. Solve the problem.

3. Examine the temperature changes on the boundary.

4. If the temperature changes are small, it is safe to assume the boundary has a negligible effect. If the temperature changes are not small, the boundary is probably too close. To confirm this, or disprove it, rerun the problem with the boundary temperatures fixed at their initial values. If the results are significantly different, the boundary was too close.

Use of the Implicit Scheme

The advantage of an implicit method is that the timestep is not restricted by numerical stability. The disadvantages are that:

(1) extra memory is required to use this method;

(2) a set of simultaneous equations must be solved at each timestep; and

(3) larger timesteps may introduce inaccuracy.

These disadvantages must be kept in mind when deciding which method to use. They are discussed below.

Memory Requirement

If an attempt is made to use the implicit method for too large a problem (based upon memory limitations of the computer hardware), an error message will be generated. The only way to avoid this is to run a smaller problem or use the explicit method.

Solving a Set of Equations

The set of equations to be solved at each timestep is solved iteratively. Each iteration of the solution takes about the same length of time as a single step of the explicit method. The number of iterations depends on the timestep chosen and the particular problem being solved, but it is always at least 4. Thus, the implicit scheme offers an advantage over the explicit scheme only if the timestep is much larger than that which the explicit scheme would use. On the other hand, the iterative scheme does introduce some restriction on the timestep. In general, a timestep between 100 and 10,000 times that used by the explicit scheme is satisfactory.

The program displays the iteration counter and a measure of convergence (the residual) to the left of the timestep counter while the implicit scheme is running. The user should check that the number of iterations being taken is such that the implicit scheme is indeed more efficient than the explicit scheme. If not, switch to the explicit scheme or change the timestep. This counter will also indicate if the method is not converging. If the residual is increasing with successive iterations, the method is not converging, and a smaller timestep must be used.

Inaccuracy Due to Large Timesteps

In the initial period of a solution, temperatures generally change much faster than they do later. It therefore is appropriate to use a smaller timestep or, more likely, the explicit method, initially, and then switch to the implicit method with larger timestep later in the solution. Convergence of the solution generally occurs in fewer iterations at later timesteps.

Selecting the Implicit Method — From the above discussion, it can be seen that the implicit method works best when used at late times in the solution period, and only if the timestep can be increased significantly over the one used by the explicit scheme.

1.4.3.10 Alternatives

Two alternative thermal solution methods were described: explicit or implicit logic. The disadvantages of each were given. One of the primary potential problems described was the possible allowance of a large temperature change prior to mechanical coupling. It is always possible to eliminate this problem by allowing very small temperature changes prior to coupling. The tradeoff here is that solution time will increase the more often coupling occurs.

1.4.4 Rock Support Models

1.4.4.1 Purpose

Rock support models are provided in UDEC to allow the user to simulate interior support systems (concrete arches, shotcrete, steel sets), as well as rock bolts or cable anchors (point anchorage or grouted), or local reinforcement applied only over joint surfaces. The bolts or cables may be fully or partially grouted, tensioned or non-tensioned. The code simulates the reinforcing effects of the support to the surrounding rock mass, allowing the user to determine the forces, moments and displacements of the components.

1.4.4.2 Assumptions and Limitations

The modeling of the interaction of structural elements with surrounding soil and rock is fairly well established (see, for example, Monsees, 1977). The modeling of point-anchor bolts and grouted cables and bolts is not as well developed theoretically. Primary contributors in this field include St. John and Van Dillen (1983); Donovan et al. (1984) and Lorig (1988). The behavior of bolts and cables is based primarily upon observations of pull-tests in the laboratory or field. There have been few successful programs of field instrumentation of bolts to determine full-scale in-situ response. Therefore, the reinforcement logic used in UDEC must be considered experimental in nature.

The three basic rock reinforcement types include interior supports, local rock reinforcement (bolts) which resist shear deformation at a discontinuity, as well as develop large axial forces, and grouted cable elements which primarily transmit axial forces. The assumptions of each model are described below.

Structural Elements for Interior Support

The interior support is modeled by connected beam elements which have three degrees of freedom (2 displacements, 1 moment) at each end node. An explicit solution scheme is used in which the mass of each element is "lumped" at nodal points. Local stiffness matrices are developed for each segment, and used to determine forces in the structure. This formulation is useful in that dynamic analysis of structures can be accomplished without significant additional difficulty. Also, a shear and normal stiffness interface can be placed between the structure and adjacent rock mass to provide for slipping or bonded contacts. The structural

elements are presently limited in the code to elastic behavior, thus failure of the supports cannot occur. The explicit procedure used, however, could allow non-linear models to be used through code modification without significant difficulty.

Rockbolt - Local Reinforcement Model

The local reinforcement model applies shear and normal stiffness across discontinuities only. Its limitation is that it neglects internal deformation of the blocks in calculation of forces in the bolts. It is therefore limited to circumstances in which the deformations in the body can reasonably be assumed to occur along its discontinuities. Reinforcement (i.e., rockbolts) has three-dimensional geometry. The two-dimensional model assumes that the bolts are infinitely long in the plane perpendicular to the modeled section. Thus, the reinforcing effect of the bolts is too great unless corrections are applied. In general, bolts are placed in a patterned manner, using a fixed bolt geometry for a given cross-section of a tunnel. The pattern is then spaced at a specified interval down the length of the tunnel. A simple method for accounting for this non-continuous nature of the bolting is to divide the material properties by the spacing, as described by Donovan et al. (1984). This strength reduction method does not apply well to spot or isolated bolting which is truly three-dimensional.

Cable Anchor Reinforcement Logic

This logic assumes that the reinforcing member has no lateral (shear) restraint. This is true for cables or long thin bars, in which the second moment of area is very small. The effects of grout surrounding the cables is taken into account along the entire length of the cable. This means that axial restoring forces developed in the cables and the shear forces in the grout are applied at internal gridpoint locations within the blocks themselves. Again, the primary assumption used is that the three-dimensional effect of the cable reinforcement can be obtained in a two-dimensional code by dividing all material properties by the spacing of the cables in the plane perpendicular to the model. As stated previously, the two-dimensional representation of bolting is limited to pattern bolting arrangements and is not particularly applicable to spot or isolated bolts.

1.4.4.3 Notation

Tables 1.4-5, -6 and -7 give the relevant offsets to variables and constants used in the structural element, local reinforcement and cable reinforcing logic.

Table 1.4-5

STRUCTURAL ELEMENT MODEL NOTATION

Notation		Comment	Where Found
Algebraic	Computer		
M_1	KXDC	Total moment, end 1 of element	Offsets in structural element array
M_2	KYDC	Total moment, end 2 of element	"
v	KCS	Total shear displacement	"
u	KCN	Total axial displacement	"
S	KCFS	Total shear force	"
T	KCFN	Total axial force	"
E	KCAP	Young's Modulus	"
I	KCQ	Second moment of area	"
L	KCL	Length	"
A	KGAM	Area	"

Table 1.4-5
(continued)

Notation		Comment	Where Found
Algebraic	Computer		
x	KX	X-coordinate of lumped mass	Offset in structural element lumped mass array
y	KY	Y-coordinate of lumped mass	"
$\dot{u}x$	KXD	X-velocity of lumped mass	"
$\dot{u}y$	KYD	Y-velocity of lumped mass	"
m	KBM	Mass	"
$\dot{\theta}$	KTD	Angular velocity of lumped mass	"
I	KBI	Dynamic moment of inertia of mass	"
ΣFx	KBFX	X-force sum	"
ΣFy	KBFY	Y-force sum	"
ΣM	KBFT	Moment sum	"
fx	KXL	Applied x-force to mass	"
fy	KYL	Applied y-force to mass	"

TABLE 1.4-6

LOCAL REINFORCEMENT MODEL NOTATION

Notation		Comment	Where Found
Algebraic	Computer		
x	KXC	X-coordinate of local reinforcement	Offset in local reinforcement array
y	KYC	Y-coordinate of local reinforcement	"
Us	KCS	Relative shear displacement of joint at reinforcement	"
			"
Un	KCN	Relative normal displacement of joint at reinforcement	"
θ	KCAP	Orientation of bolt relative to joint	"
Uaxial	KCQ	Total axial displacement of bolt	"
Fa	KCL	Axial force on bolt	"
Fs	KGAM	Shear force on bolt	"

Table 1.4-7

CABLE REINFORCING MODEL NOTATION

Notation		Comment	Where Found
Algebraic	Computer		
x	KX	X-coordinate of mass	Offset in lumped mass cable array
y	KY	Y-coordinate of mass	"
$\dot{u}x$	KXD	X-component of mass velocity	"
$\dot{u}y$	KYD	Y-coordinate of mass velocity	"
m	KBM	Mass	"
A	KAREA	Cross-sectional area of cable	"
ΣFx	KBFX	X-component force sum	"
ΣFy	KBFY	Y-component force sum	"
fx	KXL	Applied loads in x-direction	"
fy	KYL	Applied loads in y-direction	"
w1	KTD	Weighting factor #1	"
w2	KBI	Weighting factor #2	"
w3	KBFT	Weighting factor #3	"

Table 1.4-7
(continued)

Notation		Comment	Where Found
Algebraic	Computer		
	YIELD(I)	Tensile force yield of cable bolts	In main common block UDECOM
	YIELDC(I)	Compressive force yield of cable bolts	"
JKS JCOH	AKSJ(I)* COHJ(I)	Shear stiffness of grout on axial shear force for grout cable or grout-rock contact	"

*Note: The grout material is considered to be another material model, and values describing stiffness and strength are stored in material property arrays with other properties.

1.4.4.4 Derivation

Structural Elements

The structural element method is well documented in structural engineering texts. The use of beam elements in 2-D linear analysis of excavation support is reported by Dixon (1971), Brierley (1977), among others. Paul et al. (1983) presents analysis using beam elements which include non-linear behavior. Analysis of any support structure is initiated by discretization of the structure into a number of elements, the response of which to axial, transverse and flexural loads can be represented in matrix form. Two approaches to solution of the forces, displacements and moments in the structure are possible. First, the individual stiffness matrices for each beam element may be combined to form a global stiffness matrix which is then inverted using an implicit solution procedure. In the second approach (used in UDEC), the individual or "local" stiffness matrix of each element is maintained with the mass of each element "lumped" at its adjacent nodal points. The local stiffness matrix is used to derive the forces

and moments in the structure, whereas the equations of motion are used to define the displacement and rotation of each nodal mass. The lumped masses are connected to the surrounding rock mass by an interface with adjustable shear and normal stiffness (Fig. 1.4-8).

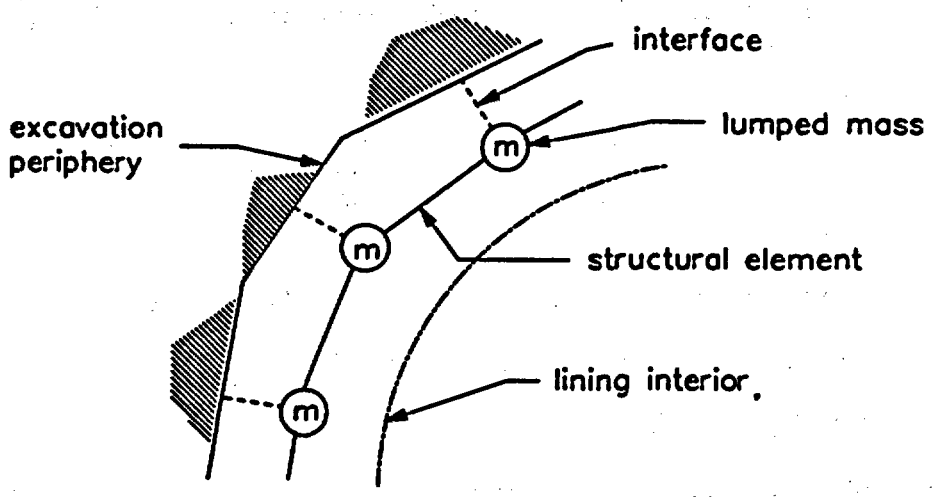

Fig. 1.4-8 Lumped Mass Representation of Structure Used in Explicit Formulation

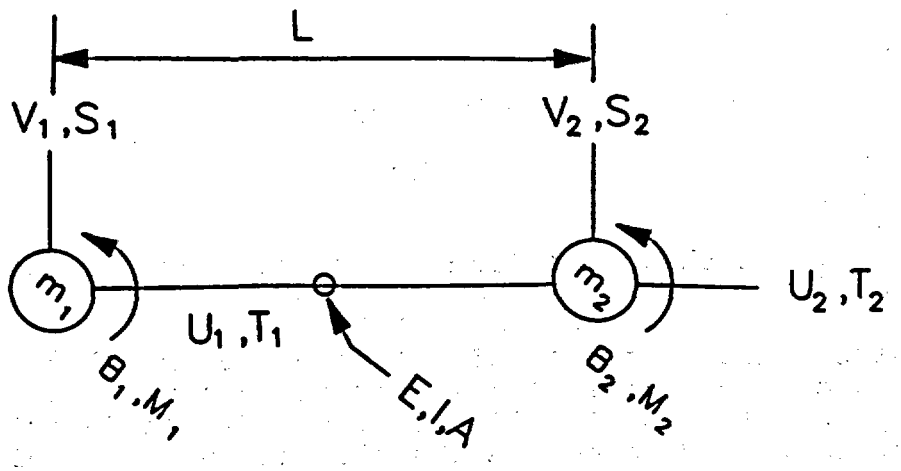

Fig. 1.4-9 Structural Element Sign Convention

Figure 1.4-9 shows a representation of the structural elements as used in UDEC. The mass of the elements (based on their density and geometric properties) is divided among the nodal points of the element. The structural and geometric properties of the beam itself are the Young's Modulus, E, the second moment of area (I), the cross-sectional area, A, and the length, L. The displacements and rotations of the masses are governed by the equation of motion:

$$\frac{\partial \dot{u}_i}{\partial t} + \alpha \dot{u}_i = \frac{F_i}{m} + g_i \qquad (1.4\text{-}34)$$

where $\dot{u}_i$ = velocity component of the mass (i = 1,2),

F_i = sum of the forces acting on the mass,

g_i = gravity acceleration,

m = mass of the node, and

α = viscous damping constant.

A similar expression can be obtained for the rotations of the mass (e.g., Eq. 1.3-14). The interaction of the mass with the surrounding rock mass is controlled by the stiffness of the contact between them:

$$\Delta F_n = K_n \Delta u_n$$
$$\Delta F_s = K_s \Delta u_s \qquad (1.4\text{-}35)$$

where K_n, K_s are the normal and shear stiffness of the contact.

The displacements of the nodal masses may be resolved into components normal and axial to the beam element as shown in the previous figure. The local stiffness matrix which describes the relation of force and moment in the element to the displacement and rotation of the nodes is given by:

$$\begin{bmatrix} T_1 \\ S_1 \\ M_1 \\ T_2 \\ S_2 \\ M_2 \end{bmatrix} = \frac{E}{L} \begin{bmatrix} A & & & & \text{SYM.} & \\ 0 & \frac{12I}{L^2} & & & & \\ 0 & \frac{6I}{L} & 4I & & & \\ -A & 0 & 0 & A & & \\ 0 & -\frac{12I}{L^2} & -\frac{6I}{L} & 0 & \frac{12I}{L^2} & \\ 0 & -\frac{6I}{L} & 2I & 0 & -\frac{6I}{L} & 4I \end{bmatrix} \begin{bmatrix} u_1 \\ v_1 \\ \theta_1 \\ u_2 \\ v_2 \\ \theta_2 \end{bmatrix}$$

where T_i are the thrust forces at each node,

S_i are the shear forces at each node,

M_i are the moments at each node,

u_i are the axial displacements at each node,

v_i are the shear displacements at each node, and

θ_i are the rotations at each node.

The solution methodology is discussed in Section 1.4.4.6.

Local Reinforcement

The reinforcement model presented here uses simple force-displacement relations to describe both shear and axial behavior of the reinforcement element. Large shear displacements are accounted for by assuming simple geometric changes develop locally in the reinforcement near a discontinuity. The resultant representation is most applicable to cases where deformation of individual rock blocks may be neglected in comparison with deformation of the reinforcing system. In such cases, attention may be focused reasonably on the effect of reinforcement near discontinuities.

Axial Behavior

Historically, testing of rock reinforcement has focused on pull-out tests for two reasons:

(1) ease of experimentation and interpretation or results; and

(2) provision of axial restraint (the main function of reinforcement in the prevailing conceptual models).

Consequently, a relatively good understanding of axial force-displacement relations has been achieved. The axial force-displacement relation used in the representation of rock reinforcement considered here is shown in Fig. 1.4-10.

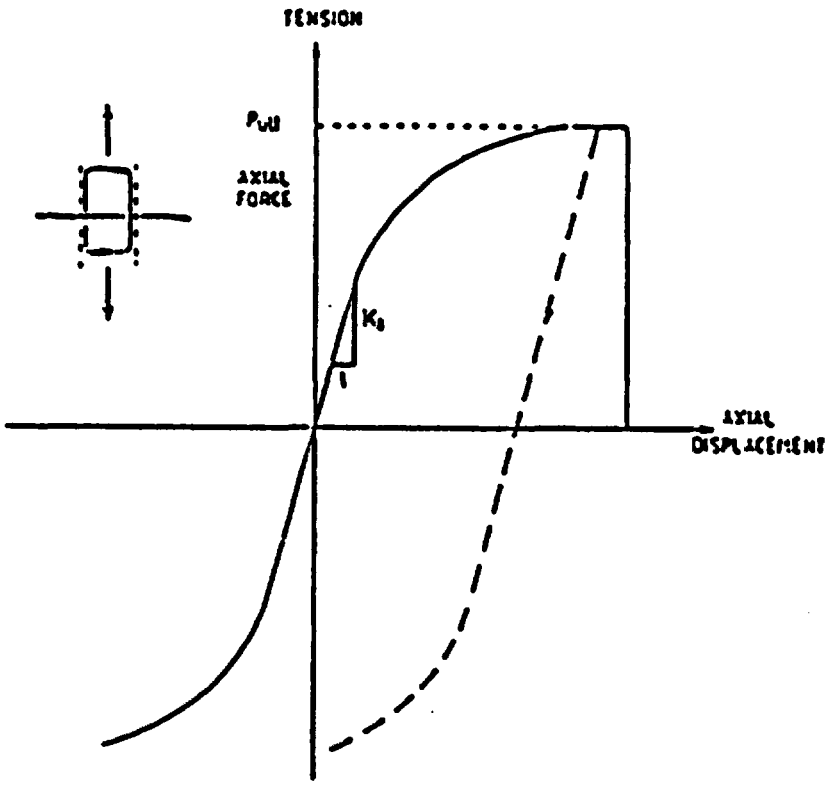

Fig. 1.4-10 Axial Behavior of Reinforcement System

Figure 1.4-10 indicates an identical response in tension and compression. This may not be the case for all reinforcing systems. The explicit formulation used in the distinct element method allows any force-displacement relation to be incorporated in the numerical scheme. In particular, for a specific reinforcement problem, the results of pull-out tests may be used to define the exact force-displacement relation to be used. If these results are not available, the force-displacement relation may be defined by a continuously-yielding model. The yield model used in the present study is a continuous, non-linear, force-displacement algorithm written in terms of the axial stiffness, the ultimate capacity, and a yield function. The yield function describes the force-displacement path followed in approaching the ultimate capacity.

The following theoretical expression given by Gerdeen et al. (1977) may be used to estimate the axial stiffness, K_a, for fully-bonded solid reinforcing elements:

$$K_a = \pi k d_1 \qquad (1.4\text{-}36)$$

where d_1 = reinforcement diameter,

$$k = [\frac{1}{2} G_g E_b / (d_2/d_1 - 1)]^{1/2},$$

G_g = grout shear modulus,

E_b = Young's modulus of reinforcement material, and

d_2 = hole diameter.

Comparisons with finite element analyses (Gerdeen et al., 1977), as well as limited comparisons with laboratory data for this investigation, indicate that Eq. (1.4-36) tends to slightly overestimate axial stiffnesses.

The ultimate axial capacity of the reinforcement depends on a number of factors, including strength of the reinforcing element, bond strength, hole roughness, grout strength, rock strength, and hole diameter. In the absence of results of physical tests, empirical relations may be used to estimate the ultimate anchorage

strength P_{ult}. One such relation for resin-grouted reinforcement is given by Littlejohn and Bruce (1975):

$$P_{ult} = 0.1\ \sigma_c\ \pi d_2\ L \qquad (1.4\text{-}37)$$

where σ_c = uniaxial compressive strength of the host rock material; and

L = bond length.

Shear Behavior

Recognition that reinforcement also acts to modify the shear stiffness and strength of discontinuities has led to laboratory shear testing of reinforced discontinuities.

Experimental results and theoretical investigations indicate that shearing along a discontinuity induces bending stresses in the reinforcement that decay very rapidly with distance into the rock from the shear surface. Typically, within one to two reinforcing element diameters, the bending stresses are insignificant.

The shear force-displacement relation used in the present study is shown in Fig. 1.4-11. The figure shows representative responses for reinforcement at various attitudes with respect to the traversed discontinuity and direction of shear. Each curve is characterized by a continuously-yielding model defined by a shear stiffness, an ultimate strength, and a yield function.

If the results of physical tests are not available, the shear stiffness, K_s, may be estimated using the following expression from Gerdeen et al. (1977):

$$K_s = E_b\ I\ \beta^3 \qquad (1.4\text{-}38)$$

where $\beta = [K/(4E_bI)]^{1/2}$,

$K = 2E_g/(d_2/d_1-1)$,

I = second moment of area of the reinforcement element, and

E_g = Young's modulus of the grout.

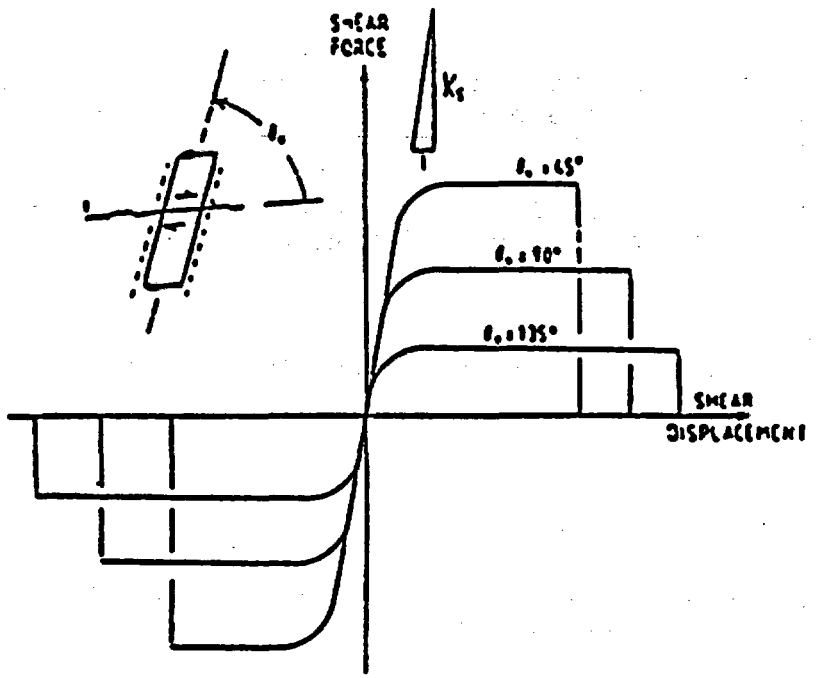

Fig. 1.4-11 Shear Behavior of Reinforcement System

Empirical relations can be used to estimate the maximum shear force, $F_{s,b}^{max}$, for a reinforcement element at various orientations with respect to a transgressed discontinuity and direction of shear. For example, Bjurstrom (1979) used the results of shear tests of ungrouted reinforcement perpendicular to a discontinuity in granite to develop the following expression:

$$F_{s,b}^{max} = 0.67\ d_1^2\ (\sigma_b \sigma_c)^{1/2} \qquad (1.4\text{-}39)$$

where σ_b = yield strength of reinforcement.

In their assessment of maximum shear resistance, St. John and Van Dillen (1983) apply the results of Azuar et al. (1979). The latter found that the maximum shear force was about half the product of the uniaxial tensile strength of the reinforcement and its cross-sectional area, for reinforcement perpendicular to the discontinuity. The force increased to 80-90% of that product for reinforcement inclined with the direction of shear. Shear displacements causing rupture were reported after approximately two reinforcement diameters for the perpendicular case and one diameter for the inclined case. St. John and Van Dillen interpret

differences between strength and amount of displacement before rupture in terms of the extent of crushing of rock around the reinforcement.

In the present formulation, the maximum shear force, $F_{s,b}^{max}$, for various orientations was calculated from the expression:

$$F_{s,b}^{max} = F_s^{max} \left[1 + [\text{sign}(\cos\theta_o, \Delta u_s) \cdot \cos(\theta_o)]\right]/2 \qquad (1.4\text{-}40)$$

where $F_s^{max} = \pi\, d_1^2\, \sigma_b/4$,

Δu_s = incremental change in shear displacement (see Fig. 1.4-12), and

$\text{sign}(\cos\theta_o, \Delta u_s)$ assigns the sign of Δu_s to $\cos(\theta_o)$.

It is seen that the maximum shear force, $F_{s,b}^{max}$, decreases from a maximum at

$$\theta_o = 0° \text{ to } 50\% \text{ of } F_s^{max} \text{ at } \theta_o = 90°$$

which is consistent with the results of Azuar et al. (1979).

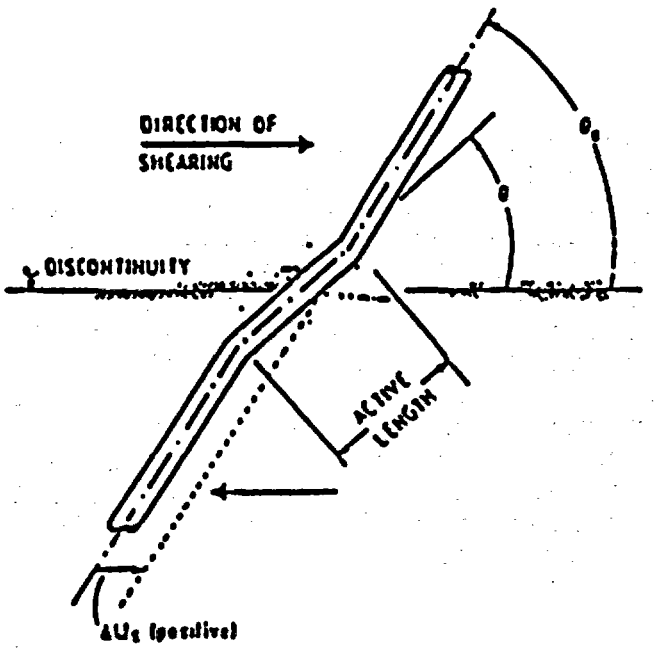

Fig. 1.4-12 Assumed Reinforcement Geometry After Shear Displacement, Δu_s

Cable Reinforcing Model

In assessing the support provided by rock reinforcement, it is often necessary to consider not only the local restraint provided by reinforcement where it crosses discontinuities but also restraint to intact rock which may experience inelastic deformation in the failed region surrounding an excavation. The model described in the previous section considers only the local restraint provided by the reinforcement at discontinuities. Such a formulation is most applicable to hard rock situations in which the bonding agent (e.g., epoxy resin) is capable of developing very large axial forces in the reinforcement over relatively short distances. However, in many instances, it is necessary to consider more than just the local effect of the reinforcement —its presence in resisting deformation must be accounted for along its entire length. Such situations arise in modeling inelastic deformations associated with failed rock and/or reinforcement systems (e.g., cable bolts) in which the bonding agent (grout) may fail in shear over some length of the reinforcement. The numerical formulation for rock reinforcement which accounts for inelastic deformation of the intact rock and shear behavior of the grout annulus is described here.

Axial Behavior

The axial behavior of conventional reinforcement systems may be assumed to be governed entirely by the reinforcing element itself. The reinforcing element is usually steel and may be either a bar or cable. Because the reinforcing element is slender, it offers little bending resistance (particularly in the case of cable), it is treated as a one-dimensional member subject to uniaxial tension or compression. A one-dimensional constitutive model is adequate for describing the axial behavior of the reinforcing element. In the present formulation, the axial stiffness is described in terms of the reinforcement cross-sectional area and Young's modulus, E. At present, the reinforcement has limited tensile and compressive capacity (Fig. 1.4-13). A more rigorous approach incorporating kinematic hardening is possible with little increase in computational effort.

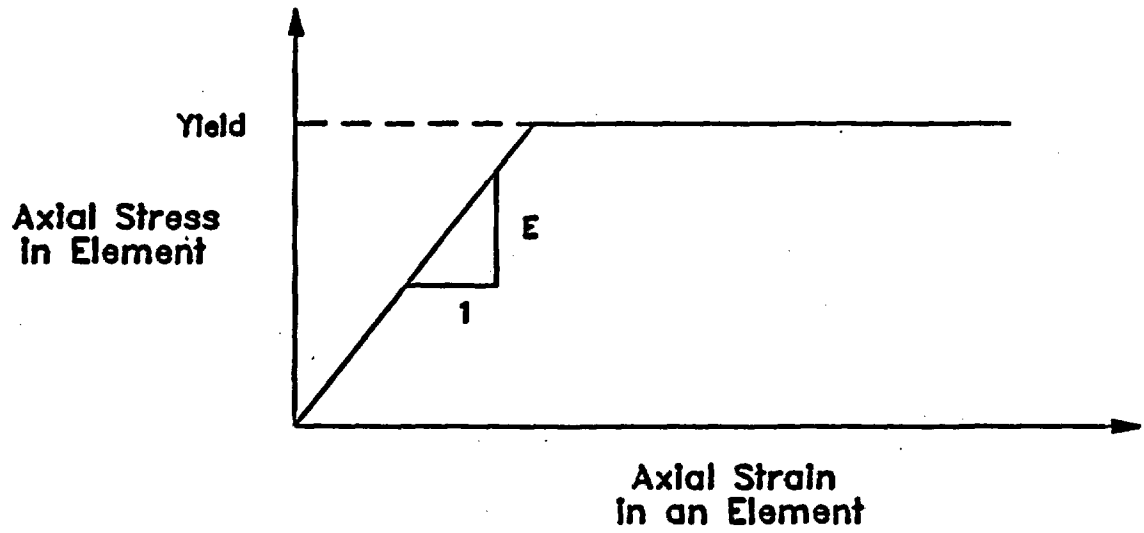

Fig. 1.4-13 Constitutive Behavior of the Reinforcing Element in Axial Tension

In evaluating the axial forces developed in the reinforcement, displacements are computed at nodal points along the axis of the reinforcement as shown in Fig. 1.4-14. Out-of-balance forces at each nodal point are computed from axial forces in the reinforcement as well as shear forces contributed through the grout annulus. Axial displacements are computed based on integration of Newton's Second Law of Motion using the computed out-of-balance axial force and a mass lumped at each nodal point.

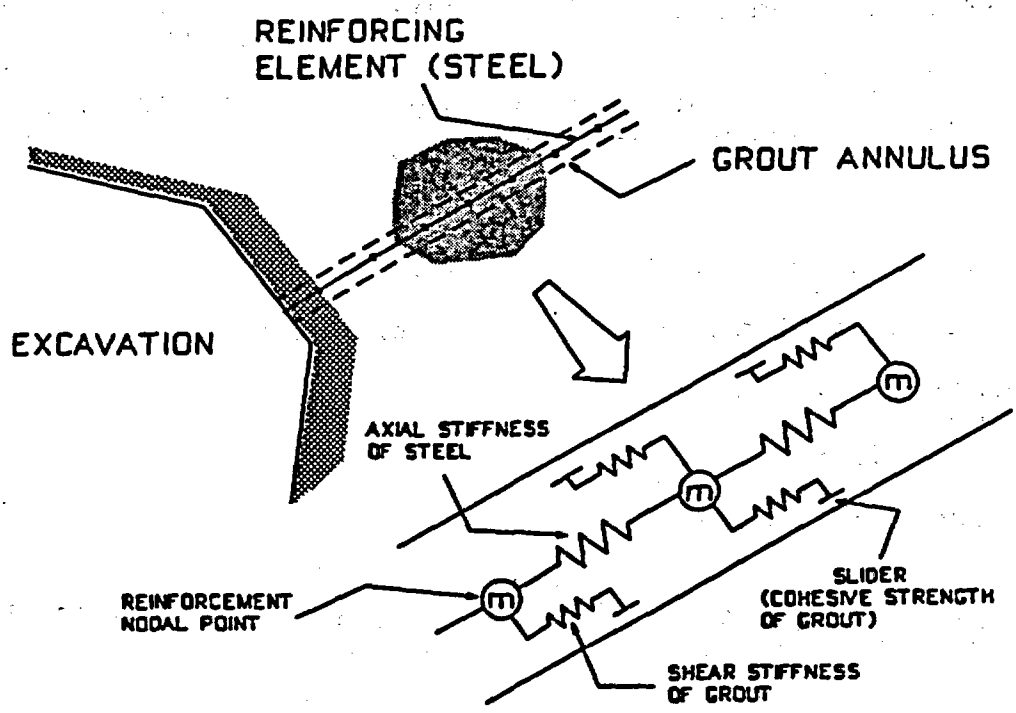

Fig. 1.4-14 Conceptual Mechanical Representation of Fully-Bonded Reinforcement Which Accounts For Shear Behavior of the Grout Annulus

Shear Behavior of Grout Annulus

The shear behavior of the grout annulus is represented at a spring slider system located at nodal points shown in Fig. 1.4-14. The shear behavior of the grout annulus during relative displacement between the reinforcing/grout interface and the grout/rock interface is described numerically by the grout shear stiffness. Figure 1.4-15 shows the assumed stress-strain behavior of bond of grout to its neighbors. A standard Mohr-Coulomb relation is used. Numerical estimates for this parameter can be derived from an equation describing the shear stress at the grout/rock interface (St. John and Van Dillen, 1983):

$$\tau_G = \frac{G_g}{(D/2+t)} \cdot \frac{u_b - u_r}{\ln(1+2t/D)} \qquad (1.4\text{-}41)$$

where u_b = axial displacement of the bolt,

u_r = axial displacement of the grout/rock interface,

G_g = grout shear modulus,

D = bolt diameter, and

t = annulus thickness.

Consequently, the required grout shear stiffness (JKS) per unit problem thickness is simply given by

$$JKS = \frac{2\pi\ G_g}{\ln\ (1+2t/D)} \qquad (1.4\text{-}42)$$

In the present formulation, the maximum amount of shear strength in the grout annulus is limited to a value τ_{peak}. The peak shear strength used may be estimated from the results of pull-out tests or, should such results not be available, the peak strength may be estimated as (St. John and Van Dillen, 1983):

$$\tau_{peak} = \pi\ (D+2t)\ \tau_I\ Q_B \qquad (1.4\text{-}43)$$

where τ_I is approximately one-half of the uniaxial strength of the weaker of the rock and grout, and

Q_B is the quality of the bond between the grout and rock (Q_B = 1 for perfect bonding).

The maximum shear force (JCOH) per unit problem thickness is, therefore, given by

$$JCOH = \pi\ (D+2t)\ \tau_{peak} \qquad (1.4\text{-}44)$$

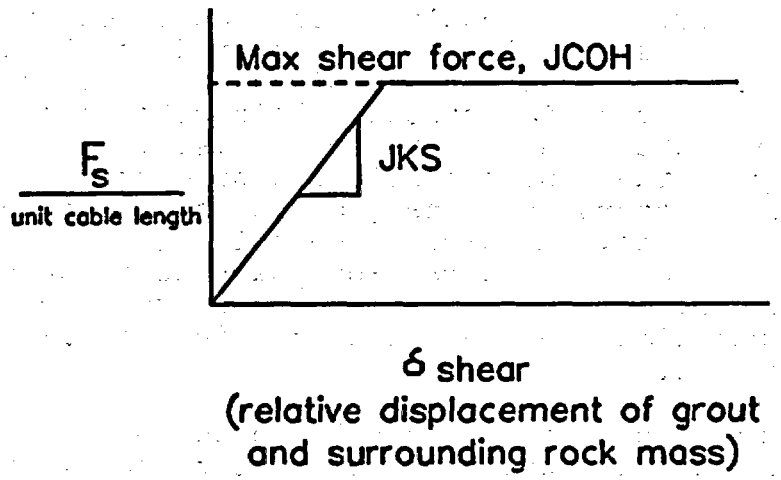

Fig. 1.4-15 Shear Behavior of the Grout Annulus

1.4.4.5 Application

The structural element logic is applicable whenever a continuous tunnel lining is used, e.g., concrete arch, shotcrete, regularly spaced steel sets, etc. The local reinforcing logic is applicable where rockbolts are used in hard rock where internal block deformations are minor, and displacement is localized on fracture planes. The cable reinforcing logic is best applied where long, thin bolts or cables are used which are grouted or end anchored, and/or where the internal deformations of the rock blocks may be significant. The cable reinforcing logic can only be used with the fully-deformable block option. There is no provision for thermal expansion or heat transfer by the structural supports.

1.4.4.6 Numerical Method Type

The structural logic uses the same explicit time-stepping algorithm as the basic mechanical logic in UDEC. No new or unique numerical methods are necessary.

1.4.4.7 Derivation of the Numerical Model

Structural Elements

The structural elements utilize the "lumped" mass approach described previously. As a result of this approach, the structural element nodes act essentially as any other free block in the body: each mass is subject to out-of-balance forces and moments relative to its neighboring masses. This methodology is simple in that it eliminates the need to solve systems of equations at each time step in the explicit solution procedure. The mass representing the structure is connected via shear and normal stiffness to the rock mass. A calculation point (which may be a grid point) is established at the rock boundary adjacent to the mass location. The following calculation steps are used during a typical explicit time step to define the interaction of the support and rock mass.

1. The displacement of the calculation point in the rock mass is determined relative to the motion of the mass (from the previous time step), as are the corresponding shear and normal forces (F_n, F_s) exerted from rock to the mass via the interface stiffnesses.

2. The axial (Fa) and shear (Fs) forces and moments (M) exerted on the mass by the structural elements themselves are determined based on the local stiffness matrix described previously:

$$\{F\} = [K]\{\delta\} \qquad (1.4\text{-}45)$$

where $\{F\} = \begin{bmatrix} T \\ S \\ M \end{bmatrix}$,

and $\{\delta\} = \begin{bmatrix} u \\ v \\ \theta \end{bmatrix}$.

3. A summation of forces and moments is performed at the mass and Newton's law of motion is applied to determine the velocity and rotation of the mass, and its new location for the given time step. In finite difference form, this is given by:

$$\dot{u}_i^{(t+\Delta t/2)} = \dot{u}_i^{(t-\Delta t/2)} + \left(\frac{\Sigma F_i(t)}{m} + g_i \right) \Delta t \qquad (1.4\text{-}46)$$

$$\dot{\theta}^{(t+\Delta t/2)} = \dot{\theta}^{(t-\Delta t/2)} + \frac{\Sigma M(t)}{I} \Delta t$$

where $\dot{u}_i$ = velocity components of mass,

$\dot{\theta}$ = angular velocity of mass,

Δt = time increment,

I = moment of inertia of mass, and

m = lumped mass.

The superscript terms in parentheses refer to times used in the central differencing scheme. Incremental block movements are determined by multiplying velocities in Eq. (1.4-46) by the time increment, Δt.

4. Steps 1 - 3 are repeated for each time step until equilibrium or the desired real time period has elapsed.

Local Reinforcement

Laboratory tests of fully-grouted untensioned reinforcement in good quality rocks with one discontinuity indicate that strains in the reinforcement are concentrated across the discontinuity [Bjurstrom (1979) and Pells (1974)]. This observation forms the basis of the numerical description of the behavior of rock reinforcement used here. The model assumes that, during shear displacement along a discontinuity, the reinforcement deforms as shown in Fig. 1.4-12. The short length of reinforcement which spans the discontinuity and changes of orientation during shear displacement is referred to as the active length. The assumed geometric changes were originally suggested in a derivation by Haas (1976) for conventional point-anchored reinforcement and adopted by Fuller and Cox (1978) in considering fully-grouted reinforcement.

In the model, it is assumed that the active length changes orientation only as a direct geometric result of shear and normal displacements at the discontinuity. Methods for estimating the active length are presented in the next section. The model may be considered to consist of two springs located at the discontinuity interface and oriented parallel and perpendicular to the reinforcement axis, as shown in Fig. 1.4-16(a). Following shear displacement, the axial spring is oriented parallel to the active length, while the shear spring remains perpendicular to the original orientation, as shown in Fig. 1.4-16(b). Similar geometric changes follow displacements normal to the discontinuity.

The force-displacement relations described previously are used to determine forces arising in the springs from incremental displacements of end points of the active length.

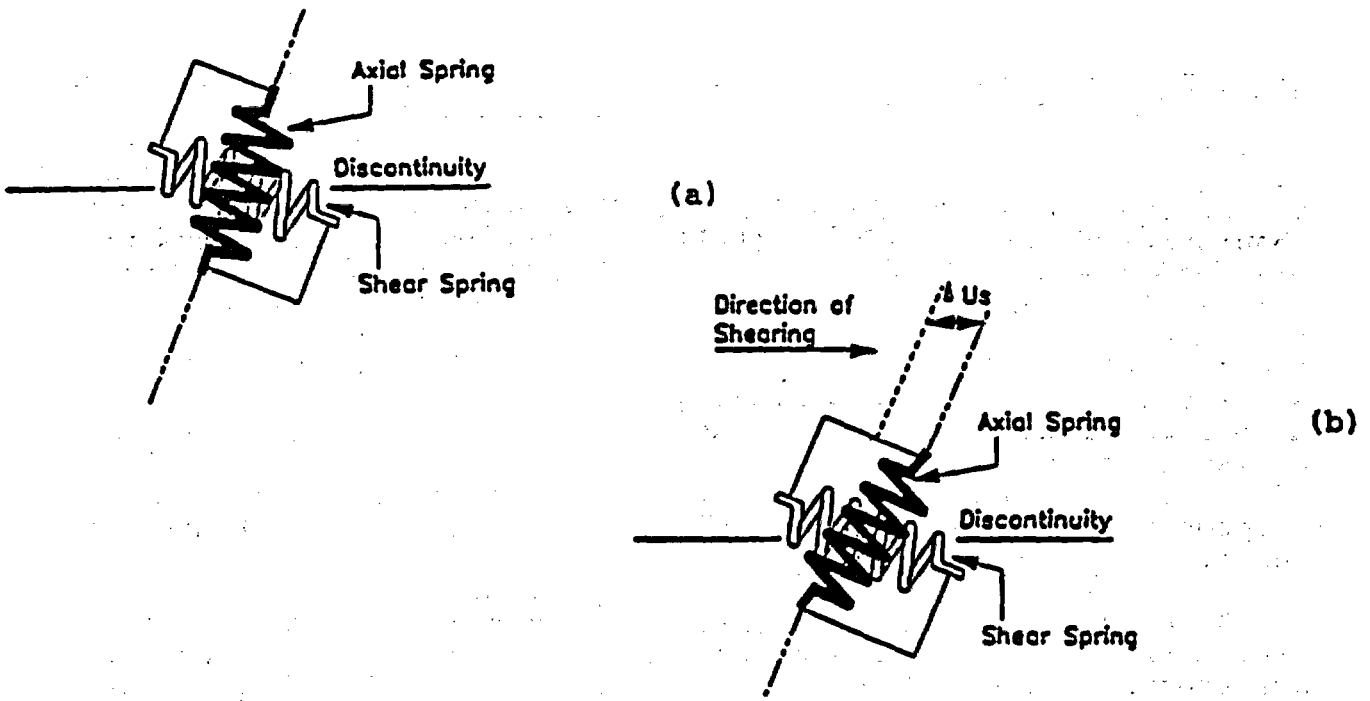

Fig. 1.4-16 Orientation of Shear and Axial Springs Representing Reinforcement Prior To and After Shear Displacement

In computing the incremental axial displacement of the active length, it is necessary to account for crushing of the grout and/or rock near the discontinuity as shear displacement causes the reinforcement to bear against one side of the hole. In the present model, a reduction factor, r_f, is applied to incremental axial displacements arising from changes in orientation of the active length to account for the crushing. The reduction factor is computed from the following expression:

$$r_f = |u_{axial}| \, (u_s^2 + u_n^2)^{-1/2} \qquad (1.4\text{-}47)$$

where u_{axial} = summation of axial displacement increments (i.e., discontinuity displacement increments resolved at each configuration in the direction of the active length),

u_s = total discontinuity shear displacement, and

u_n = total discontinuity normal displacement.

Note that no reduction (r_f = 1.0) is applied for cases in which there is no change in orientation of the active length.

Resultant shear and axial forces are resolved into components parallel and perpendicular to the discontinuity, as shown in Figs. 1.4-17(a) and (b). Forces are then applied to the neighboring blocks.

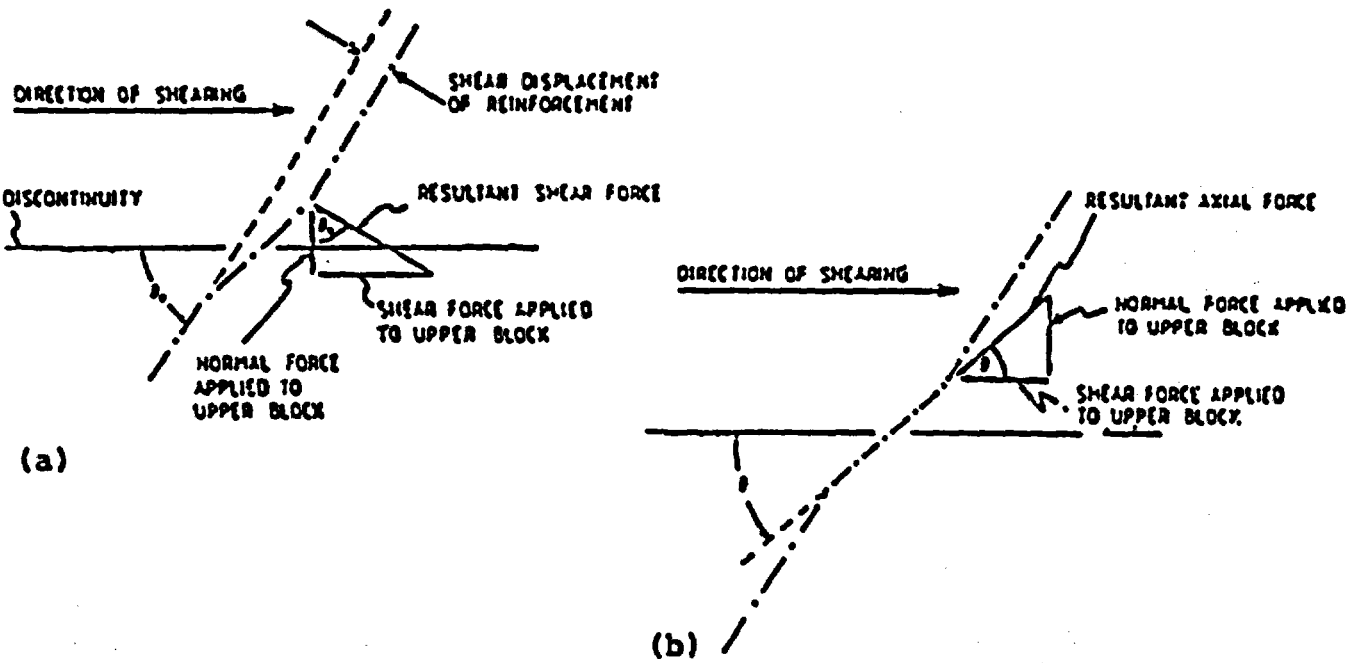

Fig. 1.4-17 Resolution of Reinforcement Shear and Axial Forces Into Components Parallel and Perpendicular to Discontinuity

Both shear and axial force-displacement relations employ a continuously-yielding model. The yield model for shear behavior is described in incremental form by the expression:

$$\Delta F_s = K_s \, |\Delta u_s| f(F_s) \qquad (1.4\text{-}48)$$

where ΔF_s is an incremental change in shear force,

Δu_s is an incremental change in shear displacement,

K_s is the shear stiffness, and

$f(F_s)$ is a function describing the path by which the shear force, F_s, approaches the ultimate or bounding shear force $F^{max}_{s,b}$.

In the present formulation, the function

$$f(F_s) = |F^{max}_{s,b} - F_s|(F^{max}_{s,b} - s)/(F^{max}_{s,b})^2 \qquad (1.4\text{-}49)$$

is used to represent the yield curve. From Eq. (1.4-48), the shear force "seeks" the bounding force in an asymptotic manner. An identical yield function involving axial forces is used to describe axial behavior.

Estimation of Active Length

An estimate of the active length is required to define the assumed local deformation illustrated in Fig. 1.4-12. It has been shown that the active length extends approximately one to two reinforcing element diameters either side of the discontinuity. In the absence of experimental data, results of theoretical analysis may be used to define the active length. For example, in defining the elastic shear stiffness, K_s, Gerdeen et al. (1977) also determine a quantity, ℓ, called the load transfer length, or "decay length". If ρ_{max} is the proportion of maximum deflection in the reinforcement, the relation between it and the load transfer length may be expressed by

$$e^{-\beta\ell} = \rho_{max} \qquad (1.4\text{-}50)$$

For example, the point at which the deflection decays to 5% of its maximum value is

$$e^{-\beta\ell} = 0.05$$

or

$$\ell = 3/\beta \qquad (1.4\text{-}51)$$

This approach was developed for reinforcement oriented perpendicular to the shear plane.

Dight (1982) presents a theoretical analysis for determining the distance from the shear plane to maximum moment which corresponds with the location of the plastic hinge in the reinforcement element. This approach places no restrictions on the orientation of the reinforcement with respect to the shear plane. A significant result of this analysis is that the distance of the plastic hinge from the shear plane does not appear to vary greatly with shear displacement, especially for displacements greater than 10 mm (0.4 in.) for typical reinforcement systems. This observation is in agreement with the assumed geometry changes described earlier.

Cable Reinforcement

As in the structural element logic, the mass of the cable elements is lumped at nodal points, and an explicit time stepping algorithm is used for problem solution. The primary difference here is that the masses representing the cables lie within the triangular finite difference zones which compose a block. Figure 1.4-18 shows a typical triangular constant-strain finite difference zone with the intersecting cable element represented by the mass lumped at the reinforcement nodal point. A set of weighting factors, W_1, W_2 and W_3 are used to linearly interpolate either the response at the finite difference gridpoints to the structural nodal points, or vice versa. The weighting factors are given by:

$$W_i = A_i/\Sigma A_i \qquad (1.4\text{-}52)$$

where A_i ($i = 1,2,3$) are the areas of the three subtriangles formed by connecting the finite difference gridpoints to the reinforcement nodal point. The calculation scheme is as follows:

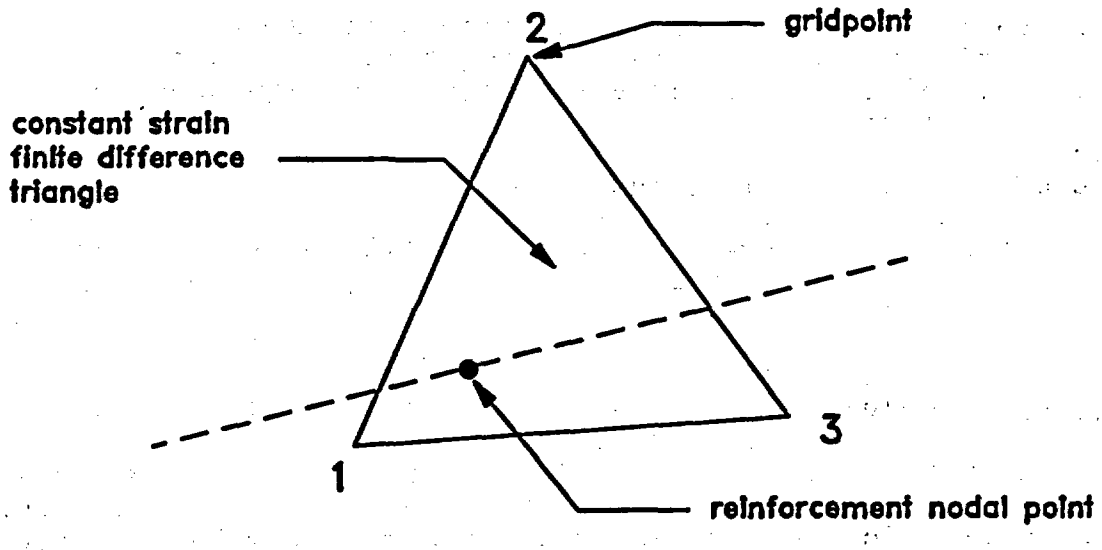

(a) typical reinforcing element passing through a triangular zone

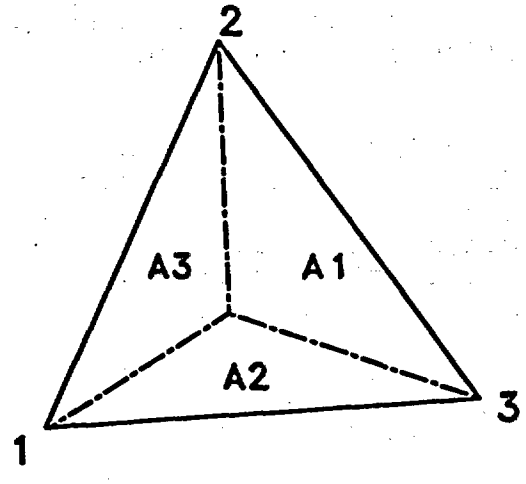

(b) areas used in determining weighting factors used to compute displacement of grout/rock interface

Fig. 1.4-18 Geometry of Triangular Finite Difference Zone and Transgressing Reinforcement Used in Distinct Element Formulation

1. Determine displacement components at the finite difference nodal points, and interpolate them to the reinforcement node location using equations of the form:

$$\overset{r}{\Delta u_j} = \sum_{i=1}^{3} W_i \overset{i}{\Delta u_j} i, \qquad j=1,2 \qquad (1.4\text{-}53)$$

where $\overset{r}{\Delta u_j}$ = j-displacement component at the reinforcement node,

$\overset{i}{\Delta u_j}$ = j-displacement component at the 3 surrounding finite difference points, and

W_i = the weighting factors.

Components $\overset{r}{\Delta u_j}$ are resolved to find the displacement parallel to the reinforcement.

2. The axial force induced in the bolt or cable is calculated from the shearing forces exerted on the grout from the surrounding rock. As shown in the previous section, the shear stress at the grout/rock interface is given by:

$$\tau_G = \frac{G_y}{(D/2+t)} \cdot \frac{u_b - u_r}{\ln(1+2t/D)} \qquad (1.4\text{-}54)$$

where u_b is the bolt axial displacement from the previous time step. The relative rock displacement is interpolated from the surrounding gridpoints as shown above. The shear stress, τ_G is limited to a peak strength, τ_{peak}, where τ_{peak} is estimated from:

$$\tau_{peak} = \pi(D + 2t)\tau_I \, Q_B \qquad (1.4\text{-}55)$$

as shown in Section 1.4.3.4. τ_G is forced to lie along the value of τpeak if, at any time, the value of τ_G attempts to be greater than τpeak.

3. The total axial forces in the reinforcing bar are determined by summing the grout shear component with that determined from the application of the law of motion to the mass lumped at the nodal point:

$$\Delta F_a = \frac{\Delta u_b \, AE}{L} \qquad (1.4\text{-}56)$$

where ΔF_a = incremental axial force in the bolt,

Δu_b = bolt displacement form previous time-step,

A = cross-sectional area of bolt,

E = Young's modulus of bolt, and

L = length of the bolt element.

The sum of forces will be used at the end of the calculation cycle to determine the displacement of the reinforcing node by integration of the law of motion.

4. The forces generated at the grout rock interface are applied back to the surrounding finite difference gridpoints using the interpolation formulae:

$$F_{i1} = W_1 \cdot F_{ip} \qquad i = 1,2$$

$$F_{i2} = W_2 \cdot F_{ip} \qquad (1.4\text{-}57)$$

$$F_{i3} = W_3 \cdot F_{ip}$$

where F_{ip} = force component generated at the grout-rock interface at node, and

W_j = weighting functions.

5. Continue timestepping.

1.4.4.8 Location

The calculation of support-structure interaction is called from subroutine CYCLE. The law of motion for the lumped masses is found in routine LMTION. The structural and cable force and moment determination are called from RESCN. The relative velocities of blocks and reinforcement are found in RECVEL and RVELCB. The force displacement calculations occur in REFORD and RVELCB. The actual structural element stiffness formulation is controlled by STRUCT, the local stiffness constitutive model in CLJ6 and the cable bolt formulation in RVELCB.

1.4.4.9 Numerical Stability and Accuracy

Since the structural element and reinforcement logic use the same basic explicit logic as the remainder of the code, the properties and geometry of the elements enters into the determination of the timestep required for numerical stability. The stable timestep for the structural elements is found from the following.

1. The structural element timestep is determined by calculating the minimum of the structural mass and interface stiffness timesteps as follows:

$$\Delta t^s = 2.0*frac*\ (m_{min}/akemax)^{1/2} \qquad (1.4\text{-}58)$$

where Δt^s = structural element timestep,

frac = user-definable fraction of critical timestep,

m_{min} = minimum structure lumped mass, and

akemax = maximum stiffness of the structure determined from maximum of (akax, akes)

where: $akax = \frac{AE}{L}$ = axial stiffness,

$$akes = \frac{12EI}{L^3} = \text{bending stiffness,}$$

$$\Delta t^i = 2.0 * frac * (m_{min}/akimax) \qquad (1.4\text{-}59)$$

where akimax = minimum of the normal and shear stiffness of the structure.

2. Local Reinforcement Model

The maximum local reinforcement stiffness is considered a block interface stiffness and is used in the block and zone time step calculations described in Section 1.3.

3. Cable Reinforcement

The cable reinforcement uses the same logic for calculation of minimum time step as the structural elements given above with two exceptions. The bending stiffness is not taken into account since the cables are assumed to have no lateral rigidity, and the shear stiffness of the grout is used rather than the interface stiffness in determination of maximum stiffness.

1.4.4.10 Alternatives

No specific alternative models for rock support exist within the UDEC code.

1.4.5 Boundary Element Far-Field Coupling

1.4.5.1 Purpose

Many problems in geomechanics involve the examination of underground excavations of surface structures in which boundaries of the problems must be considered infinite. Figure 1.4-19 illustrates the infinite boundaries for typical surface and underground problems.

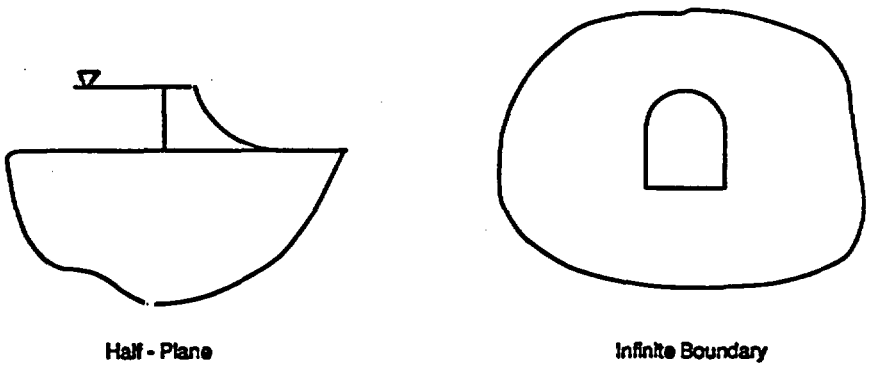

Fig. 1.4-19 Typical Geotechnical Problems in Which Infinite Boundaries Occur.

To accurately model infinite boundaries, UDEC (as well as most finite element or finite difference codes) requires that the boundaries of the model be placed at sufficient distance from the excavation or point of load application to eliminate boundary effects. This is generally accepted to be on the order of 7 to 10 radii of the excavation or disturbance. Unfortunately, representation of infinite boundaries requires a significant number of elements, resulting in additional solution time. To reduce the need for additional elements to represent infinity, UDEC allows boundary elements to be coupled to the outer boundaries of the distinct element blocks to represent the infinite elastic region. This can significantly reduce the required solution time.

1.4.5.2 Assumptions and Limitations

The boundary element coupling requires the following assumptions and limitations.

1. The far field rock mass response is isotropic-elastic.
2. The radius of boundary elements from excavations must be beyond the zone of yield of intact rock or joint slip. If not, accurate solution of failure cannot be ensured.
3. The problem to be analyzed must involve a free surface (half-plane) or an infinite region in all directions.
4. Boundary elements are restricted to the exterior of the grid only.

1.4.5.3 Notation

The boundary element control information and parameters are found in several locations in the code: (1) boundary corner array, which is combined with other linked lists to form the main program array; (2) main program common block UDECOM; and (3) the boundary element common block BECOM. The boundary corner offsets are given in Table 1.4-8 and the parameters from the common blocks in Table 1.4-9.

Table 1.4-8

NOTATION FOR BOUNDARY ELEMENT COUPLING — OFFSETS IN BOUNDARY CORNER LINKED LIST NOTATION

Offset	Command	Where Found
KBDX (=2)	Type of boundary in x	UDECOM
KBDY (=2)	Type of boundary in y	UDECOM
KBEN	Pointer to boundary element node 1	UDECOM
KBEN2	Pointer to boundary element node 2	UDECOM

Table 1.4-9

NOTATION FOR BOUNDARY ELEMENT COUPLING PARAMETERS FOUND IN COMMON BLOCKS

Notation		Comment	Where Found
Algebraic	Computer		
	NBEN	Number of BE nodes	UDECOM - Main Common
	LKPNT	Pointer to BE stiffness matrix	UDECOM - Main Common
	NPOIN	Number of BE nodes	BECOM - BE Common
	NDOFN	Number of BE degrees of freedom	"
	NBELM	Number of BE	"
	NGAUS	Number of interpolation points	"
	IHALF	Half-plane solution indicator	"
	IBEFIX	Fixed point indicator	"
	XFIX1	Fixed point coordinates	"
	YFIX1	Fixed point coordinates	"
	XFIX2	Fixed point coordinates	"
	YFIX2	Fixed point coordinates	"
	AYFIX	Fixed point translation	"
	AXFIX	Fixed point translation	"
E	EMOD	Young's modulus of far field	"

Table 1. 1.4-9
(continued)

Notation		Comment	Where Found
Algebraic	Computer		
υ	NU	Poisson's ratio of far field	BECOM - BE Common
P_{xx}	PXX	Initial stresses	"
P_{yy}	PYY	Initial stresses	"
P_{xy}	PXY	Initial stresses	"
	GPF(5)	Gauss interpolation parameters	"
	RWF(5)	Gauss interpolation parameters	"
	SGPF(5)	Gauss interpolation parameters	"
	SHF(5)	Gauss interpolation parameters	"

1.4.5.4 Derivation

Boundary Element Method*

The boundary element method is an integral method of analysis which is often used to compute the distribution of total stresses and induced displacements around underground excavations. A characteristic of integral methods is that the problem is specified and solved exclusively in terms of surface values of problem parameters of traction and displacement. Thus, the size of the numerical problem is related to the surface area of excavations resulting in a significant advantage in computational efficiency, compared with differential methods. Since discretization errors in this method are confined to the boundaries and fully continuous variation of stress and displacement in the problem domain are assured, the accuracy is potentially greater than that of differential methods. In addition, since the outer boundary of the problem domain is defined arbitrarily in differential methods, the boundary element method is better suited for problems involving infinite or semi-infinite regions. On the other hand, boundary element formulations exploit the principle of superposition and thus they are applicable to only linear elastic or at least piece-wise linear elastic material behavior. Differential formulations are better adapted to deal with material non-linearities.

Boundary element formulations for two- and three-dimensional elastodynamics have been presented by numerous authors (Crouch, 1976; Lachat and Watson, 1976; Brady and Bray, 1978; Brady, 1979; Watson, 1979; Crouch and Starfield, 1983). The literature appears to be equally divided between two alternative formulations, indirect and direct. Both formulations use known fundamental solutions that satisfy the governing equations of the domain. Indirect formulations solve first for unknown intensity of singularities that satisfy specified boundary conditions. The unspecified boundary parameters are then computed from the singular solutions. Direct formulations use the reciprocal theorem to develop a system of boundary integral equations which directly relate specified boundary parameters to unspecified boundary parameters. Consequently, the unknowns in the system are the actual displacements or tractions at the boundary. The following description of the boundary element formulation is based on that by Brady and Wassyng (1981).

---

*This discussion is taken from Lorig (1984).

Betti's Reciprocal Theorem

Direct boundary integral formulations in elastostatics are based on a theorem in linear elasticity known as Betti's reciprocal work theorem. (See for example, Love (1944) or Sokolnikoff (1956)). This theorem combines the solutions to two different boundary value problems shown in Fig. 1.4-20. In the first problem (a), the surface S is subject to induced tractions t_x, t_y, and induced displacements, u_x and u_y at any point on S. This problem represents the problem to be solved. In the second problem (b), an x-directional unit load is applied at point i on the surface S, inducing tractions T_x^{xi} T_y^{xi} and displacements U_x^{xi}, U_y^{xi} at a specific point on S. In this problem, T_x^{xi}, etc. represent known solutions to the problem of concentrated force applied to the interior of an elastic body and are referred to as fundamental solutions or kernel functions.

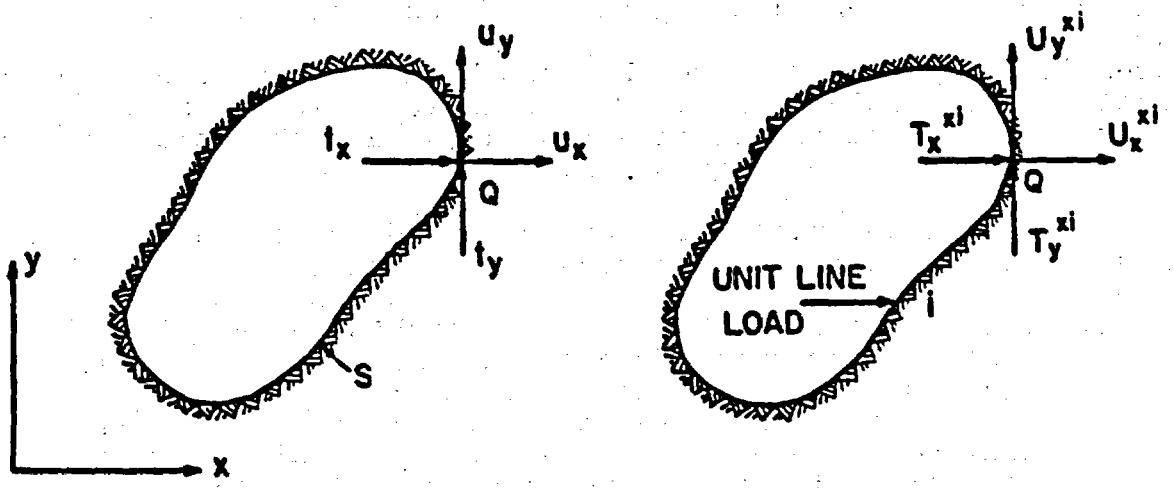

(a) LOAD CASE I *(b) LOAD CASE II*

Fig. 1.4-20 Load Cases Used in Boundary Element Formulation Using Betti's Reciprocal Work Theorem

The reciprocal theorem states that the work done by the first set of tractions (t_x, t_y) in acting through the second set of displacements (U_x^{xi} and U_y^{xi}) is equal to the work done by the second set of tractions (T_x^{xi} and T_y^{xi}) in moving through the first set of displacements (u_x, u_y). Mathematically, this can be written as

$$\int_S (T_x^{xi}\, u_x + T_y^{xi}\, u_y)\, dS = \int_S (t_x\, U_x^{xi} + t_y\, U_y^{xi})\, dS \qquad (1.4\text{-}60)$$

where the integrals are evaluated over the surface S. It should be noted that the integral of the left hand side is improper and will be discussed further later.

Fundamental Solutions

In two-dimensional elastostatics, boundary integral methods employ solutions to the problem of a concentrated force applied to the interior of infinite planes or half planes. These fundamental solutions give the displacements at any point in the body due to the applied loads and the displacement fields given by these solutions satisfy the Cauchy-Navier equations of equilibrium.

Expressions for stresses are obtained by differentiating the expressions for displacements. Tractions T_x^{xi}, etc. can be expressed in terms of the components of stress (σ_{ij}) and the unit outward normal of the surface in question.

Two fundamental solutions are commonly used in boundary element formulations written for underground excavation analysis.

1. For problems remote from the earth's surface in which the traction free surface may be reasonably ignored, the two-dimensional Kelvin's solution for a unit force in an infinite linear isotropic elastic, homogeneous medium is used. The displacements for this solution are reproduced in Section 1.4.5.4.1.

2. For near-surface problems, a half plane solution that automatically gives a traction free surface at the surface of the half plane is used. The displacements for this solution are given by Telles and Brebbia (1981) and are reproduced in Section 1.4.5.4.2.

All of the solutions for displacements have logarithmic singularities for the case where the displacements are to be determined at the load point. Expressions for tractions involve singularities (1/r) since they are obtained from differentiating the displacement components. These singularities require special treatment in boundary integral formulations, as described later. The elastic properties used in the boundary element formulation for the hybrid method are the equivalent elastic continuum properties for a jointed medium [see, for example, Goodman (1980)].

Linear Isoparametric Representation of Element Geometry and Functional Variation

Division of S in Fig. 1.4-20 into n segments allows Eq. (1.4-60) to be written as

$$\sum_{j=1}^{n} \int_{S_e} (T_x^{xi}\, u_x + T_y^{xi}\, u_y)\, dS = \sum_{j=1}^{n} \int_{S_e} (t_x\, U_x^{xi} + t_y\, U_y^{xi})\, dS \qquad (1.4\text{-}61)$$

Figure 1.4-21 shows a representative element of surface S together with the intrinsic coordinate, ξ, for the element. Displacements u_x and u_y and tractions t_x and t_y at any point on an element are expressed as functions of the nodal values of these variables.

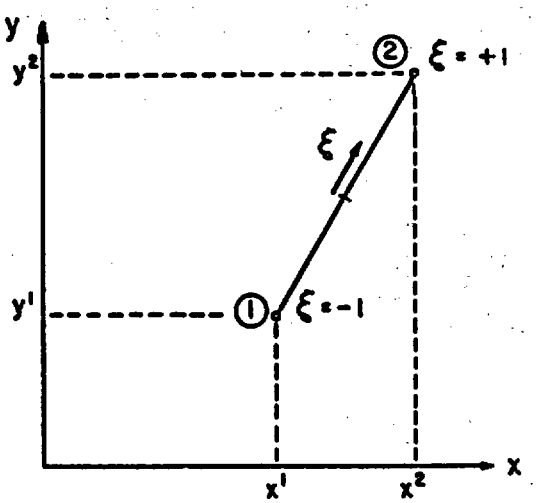

Fig. 1.4-21 Element Geometry Used in Linear Isoparametric Boundary Element Formulation

Linear representation of element geometry and functional variation with respect to element intrinsic coordinates is defined by

$$x(\xi) = N^1(\xi)x^1 + N^2(\xi)x^2$$

$$t_x(\xi) = N^1(\xi)t_x^1 + N^2(\xi)t_x^2 \qquad (1.4\text{-}62)$$

$$u_x(\xi) = N^1(\xi)u_x^1 + N^2(\xi)u_x^2$$

where $N^1(\xi) = 1/2\ (1-\xi)$,

$N^2(\xi) = 1/2\ (1+\xi)$, and

x^1, t_x^1, u_x^1, etc. are nodal values of position coordinate, traction and displacement components.

Similar expressions apply to the quantities $y(\xi)$, $t_y(\xi)$, and $u_y(\xi)$. Thus, considering a typical boundary element with nodes 1,2, a particular integral over the range S_e of the element is given by

$$\int_{S_e} T_x^{xi}\ u_x\ ds = u_x^1 \int_{-1}^{1} T_x^{xi} N^1(\xi)\ \frac{ds}{d\xi}\ d\xi + u_x^2 \int_{-1}^{1} T_x^{xi}\ N^2(\xi)\ \frac{ds}{d\xi}\ d\xi \qquad (1.4\text{-}63)$$

where $\frac{ds}{d\xi} = \left[\left(\frac{dx}{d\xi}\right)^2 + \left(\frac{dy}{d\xi}\right)^2 \right]^{1/2}$,

$$\frac{dx}{d\xi} = 1/2\ (x^2 - x^1)\ , \text{ and}$$

$$\frac{dy}{d\xi} = 1/2\ (y^2 - y^1)$$

Boundary Integral Equations

Integrals in Eq. (1.4-61) are evaluated by Gaussian quadrature procedures. Two cases occur in the integration which require special treatment. These cases relate to the load point occurring in the range of integration causing the integrand to be unbounded. When this occurs integration of the displacement-shape function product in the right hand integral involves a logarithmic singularity. This integral is evaluated using a quadrature formula proposed by Anderson (1965). Traction terms involving (1/r) singularities on the left hand side can be evaluated by interpreting the surface of integration in Eq. 1.4-60 to be composed of two parts as shown in Fig. 1.4-22. That is:

$$\int_S (T_x^{xi} u_x + T_y^{xi} u_y)\,dS = \lim_{\xi \to 0} \int_{S_\varepsilon} (T_x^{xi} u_x + T_y^{xi} u_y)\,dS$$

$$+ \lim_{\xi \to 0} \int_{S-S_\varepsilon} (T_x^{xi} u_x + T_y^{xi} u_y)\,dS \qquad (1.4\text{-}64)$$

$$= c_x^i u_x^i + c_y^i u_y^i + P.V. \int_S (T_x^{xi} u_x + T_y^{xi} u_y)\,dS$$

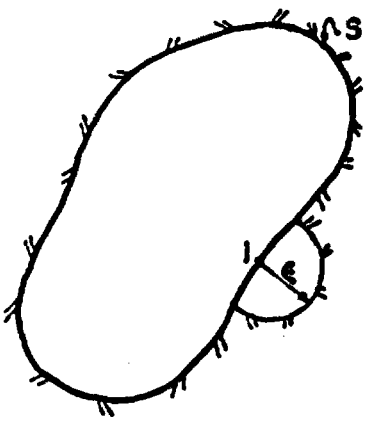

Fig. 1.4-22 Interpretation of Integrals Shown in Eq. (1.4-64)

It is shown in Section 1.4.5.4 that $c^i_x = 1/2$ and $c^i_y = 0$ if the load point is on a smooth boundary. The second integral is thus interpreted as a Cauchy principal value integral. The free terms $c_x{}^i u_x{}^i$ and $c_y{}^i u_y{}^i$ are evaluated in the numerical procedure by a method proposed by Cruse (1974). This procedure is equivalent to ensuring that static equilibrium is achieved over any closed surface in the medium.

Following integration over all boundary elements, Eq. (1.4-61) can be recast in terms of nodal values of traction and displacement, yielding

$$\sum_{j=1}^{n} \left(T^{xi}_{xj}\, u_{xj} + T^{xi}_{yj}\, u_{yj}\right) = \sum_{j=1}^{n} \left(t_{xj}\, U^{xi}_{xj} + t_{yj}\, U^{xi}_{yj}\right) \qquad (1.4\text{-}65)$$

where T^{xi}_{xj}, etc., represent the result of integration of the kernel-shape function products over the range of each element partitioned into components associated with each node j. An identical procedure is followed for a y-directional unit load applied at the particular boundary mode, to establish an expression similar to Eq. (1.4-65).

$$\sum_{j=1}^{n} (T_{xj}^{yi} u_{xj} + T_{yj}^{yi} u_{yj}) = \sum_{j=1}^{n} (t_{xj} U_{xj}^{yi} + t_{yj} U_{yj}^{yi}) \qquad (1.4\text{-}66)$$

The procedure is repeated for loads applied at all nodes i of the surface S, producing in each case equations similar to (1.4-65) and (1.4-66). These can be combined to form a set of 2n simultaneous equations, written in the form

$$[T]\{u\} = [U]\{t\} \qquad (1.4\text{-}67)$$

Conversion of Distributed Tractions to Nodal Point Forces

In the usual direct formulations of the Boundary Element Method, the boundary constraint equation (1.4-67) may be solved for unknown surface values of traction and displacement. However, for a coupled boundary element-distinct element algorithm, the boundary constraint equation must be modified to be compatible with the distinct element formulation. This requires that the boundary constraint equation be written in terms of nodal forces rather than tractions.

In the present boundary element formulation, tractions are assumed to vary linearly along the length of each element. Figure 1.4-23 shows an assumed distribution of tractions acting on elements 1 and 2 adjacent to node i.

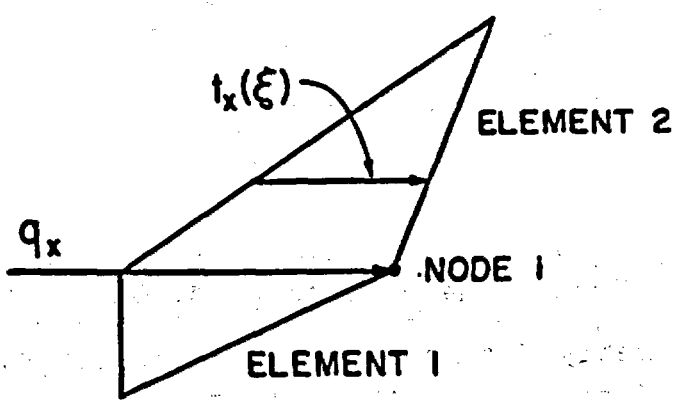

Fig. 1.4-23 Nodal Force Approximation Used in Linear Isoparametric Boundary Element Formulation

The nodal force, q, at i, equivalent to tractions acting on elements 1 and 2, may be approximated by

$$q_x^i = t_x^i \int_{-1}^{1} (N^2(\xi))_1 \left(\frac{dS}{d\xi}\right)_1 d\xi + \int_{-1}^{1} (N^1(\xi))_2 \left(\frac{dS}{d\xi}\right)_2 d\xi \qquad (1.4\text{-}68)$$

where subscripts 1,2 denote elements 1 and 2. A similar expression defines q_y^i in terms of t_y^i.

It should be noted that in most cases, a moment would result from replacing the tractions by a nodal force. The significance of neglecting this moment depends on the magnitude of the moment. Figure 1.4-24 shows the relative orientation and lengths of adjacent elements. For boundary elements only, neglecting this moment does not result in any significant errors for problems where the ratio of lengths of adjacent elements was three or less.

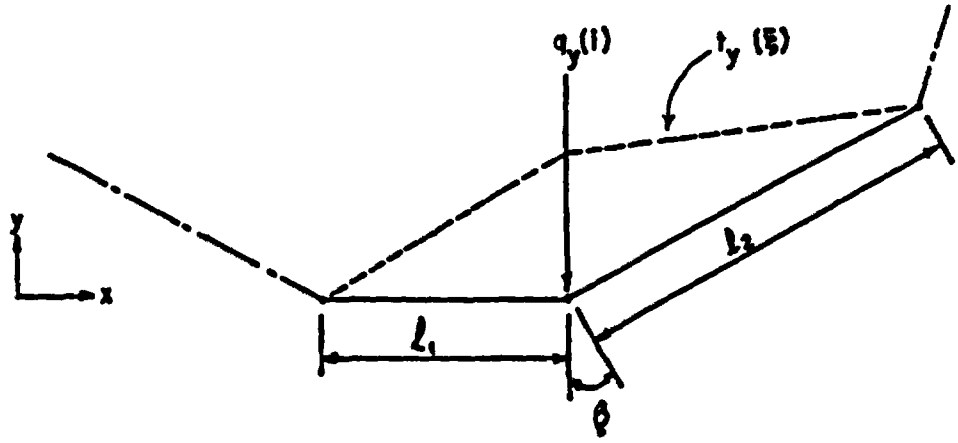

$$M(i) = t_y(i)\left[l_1^2 - l_2^2 \cos\theta\right]/6$$

Fig. 1.4-24 Geometry for Determining Resultant Moment at Typical Node i.

Expressions for nodal forces may be written as

$$q_x^i = a^i t_x^i$$

$$q_y^i = a^i t_y^i$$

or (1.4-69)

$$t_x^i = q_x^i / a_i$$

$$t_y^i = q_y^i / a_i$$

The factor a for each node can be evaluated directly from the geometry of adjacent elements. Thus, Eq. (1.4-67) may be written as

$$[T](u) = [U'](q) \tag{1.4-70}$$

where [U'] is obtained by dividing columns of [U] by the appropriate factor a_i for each node i.

Boundary Element Stiffness Matrix

Rearrangement of Eq. (1.4-68) yields

$$\{q\} = [U']^{-1}[T]\{u\} \tag{1.4-71}$$

or

$$\{q\} = [K_b]\{u\} \tag{1.4-72}$$

where $[K_b]$ represents the boundary element stiffness matrix for a hole in an elastic domain. The formation of $[K_b]$ in (1.4-72) is achieved in practice by using the Transpose Elimination Technique (Wassyng, 1982) to solve the system

$$[T]\ [K_b] = [U'] \tag{1.4-73}$$

For an excavation whose surface is traction free, Eq. (1.4-72) can be solved for the excavation induced displacements by using tractions determined from field stresses to calculate elements of {q}. Determination of boundary stresses, and stresses and displacements in the interior of the medium are discussed in the following sections.

Boundary Stresses

After solution of the boundary constraint equation [i.e., Eq. (1.4-67)], the values of excavation-induced tractions (t_x and t_y) and excavation induced displacements (u_x and u_y) are known at each node. Boundary stresses can be determined by finding the induced stresses at each element relative to the local axes for the element and then superimposing the field stresses. The process is initiated by determining the tangent at node i shown in Fig. 1.4-25. Next, tractions t_x and t_y are transformed to t_l and t_n. Element midpoint displacements at (a) and (b) are estimated by averaging displacements at the ends of the element. The estimated displacements at (a) and (b) are transformed to the local axes for node i. The coordinates for (a) and (b) are also transformed to the local axis for node i. The longitudinal strain at node i is estimated as

$$\varepsilon_{ll} = \frac{\Delta u_l}{\Delta l} = \frac{u_l(a) - u_l(b)}{\Delta l} \qquad (1.4\text{-}74)$$

For plane strain

$$\sigma_{ll} = \frac{E}{1-\nu^2}\varepsilon_{ll} + \frac{\nu}{1-\nu}\sigma_{nn} \qquad (1.4\text{-}75)$$

The total stress at each node is obtained by superimposing the field stresses.

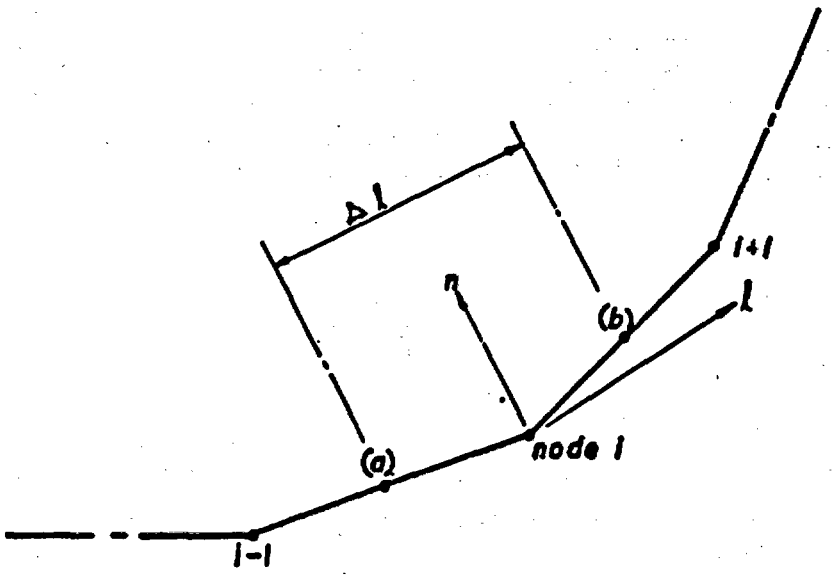

Fig. 1.4-25 Graphical Representation of Numerical Procedure Used to Determine Induced Tangential Stresses on Boundary of Boundary Element Domain.

Stresses and Displacements in the Boundary Element Domain

Displacements of points in the boundary element domain are determined directly from Somigliana's identity. The x-component of displacement at point i not on the surface S is given by

$$u_x^i = \int_S (t_x U_x^{xi} + t_y U_y^{xi}) dS - \int_S (T_x^{xi} u_x + T_y^{xi} u_y) dS \qquad (1.4\text{-}76)$$

or

$$u_x^i = \sum_{j=1}^{n} \int_{S_e} (t_x U_{xj}^{xi} + t_y U_{yj}^{xi}) dS - \sum_{j=1}^{n} \int_{S_e} (T_{xj}^{xi} u_x + T_{yj}^{xi} u_y) dS \qquad (1.4\text{-}77)$$

Induced stress components at points in the boundary element domain are determined by calculating induced strain components and applying appropriate stress-strain relation. Expressions for strain components are obtained from partial derivatives of the expression for displacement, for example

$$\varepsilon_{xx}^{i} = \frac{\partial u_x^i}{\partial x} \tag{1.4-78}$$

or

$$\varepsilon_{xx}^{i} = \int_S \left(\frac{\partial T_x^{xi}}{\partial x} u_x + \frac{\partial T_y^{xi}}{\partial x} u_y\right) dS - \int_S \left(t_x \frac{\partial U_x^{xj}}{\partial x} + t_y \frac{\partial U_y^{xi}}{\partial x}\right) dS \tag{1.4-79}$$

or

$$\varepsilon_{xx}^{i} = \sum_{j=1}^{n} \int_{S_e} \left(\frac{\partial T_{xj}^{xi}}{\partial x} u_x + \frac{\partial T_{yj}^{xi}}{\partial x} u_y\right) dS - \sum^{n} \int_{S_e} \left(t_x \frac{\partial U_{xj}^{xi}}{\partial x} + t_y \frac{\partial U_{yj}^{xi}}{\partial x}\right) dS \tag{1.4-80}$$

The state of stress is determined from the induced strains and the field stresses by superposition.

1.4.5.4.1 Fundamental Solution for Unit Load in an Infinite Elastic Plane

Expressions for displacements induced by a unit load in an infinite isotropic elastic continuum—i.e., Kelvin's problem, are given below for completeness. The displacements are for plane strain conditions.

(a) Unit load in the x-direction

$$U^{xi}_{xj} = - K_d[(3-4\nu)\ln(r) - x^2/r^2]$$

$$U^{xi}_{yj} = K_d\, xy/r^2 \qquad (1.4\text{-}81)$$

(b) Unit load in the y-direction

$$U^{yi}_{xj} = K_d\, xy/r^2$$

$$U^{yi}_{yj} = -K_d\,[(3-4\nu)\ln(r) - y^2/r^2] \qquad (1.4\text{-}82)$$

where the load is applied at point i, coordinates (x_i, y_i),

the point of interest is point j, coordinates (x_j, y_j),

$x = x_j - x_i$,

$y = y_j - y_i$, (1.4-83)

$r^2 = x^2 + y^2$, and

$K_d = 1/[8\pi\, G(1-\nu)]$.

1.4.5.4.2 Fundamental Solution for Unit Load in an Elastic Half-Plane

The fundamental solution for a unit load in an elastic half-plane can be decomposed into the sum of the infinite solution and a complementary part. Expressions for the complementary part, for the two-dimensional, plane strain case, are given by Telles and Brebbia (1981), and are reproduced here for completeness.

A unit load, acting at point i (Fig. 1.4-26), produces at a point j the displacements given below.

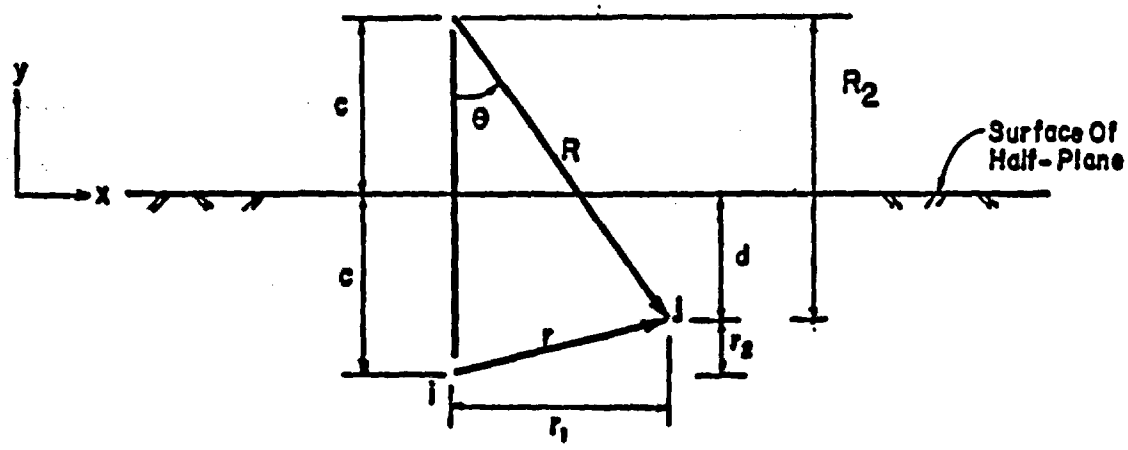

Fig. 1.4-26 Geometry for Complementary Expressions for Displacement Field Due to Unit Load in an Elastic Half-Plane

The complementary expressions for the displacement field are

(a) Unit load in the x-direction

$$U_{xj}^{xi} = K_d\{-[8(1-\nu)^2-(3-4\nu)]\ln R + [(3-4\nu)r_1^2+2cd]/R^2 - 4cdr_1^2/R^4\} \quad (1.4\text{-}84)$$

$$U_{yj}^{xi} = -K_d\{-(3-4\nu)r_1r_2/R^2 - 4cdR_2r_1/R^4 + 4(1-\nu)(1-2\nu)\theta\}$$

(b) Unit load in the y-direction

$$U_{xj}^{yi} = -K_d\{-(3-4\nu)r_1r_2/R^2 + 4cdR_2r_1/R^4 - 4(1-\nu)(1-2\nu)\theta\} \quad (1.4\text{-}85)$$

$$U_{yj}^{yi} = K_d\{-[8(1-\nu)^2-(3-4\nu)]\ln R + [(3-4\nu)R_2^2-2cd]/R^2 + 4cdR_2^2/R^4\}$$

where $K_d = 1/[8\pi G(1-\nu)]$, and

the other parameters are shown in Fig. 1.4-26.

1.4.5.4.3 Determination of "Free Terms" for Smooth Boundary

This section gives one method for determining the "free terms" in Eq. (1.4-64) for a smooth boundary. Only the coefficient c_x^i due to an x-directional unit force is determined. Similar expressions may be used to determine c_y^i and coefficients for a y-directional unit force. The procedure is initiated by writing the general expressions for stresses due to an x-directional unit force in an infinite isotropic plane.

$$\sigma_{xx} = k\{(1-2\nu)\, x/r^2 + 2x^3/r^4\}$$
$$\sigma_{xy} = k\{(1-2\nu)\, y/r^2 + 2x^2y/r^4\} \qquad (1.4\text{-}86)$$

where $k = -1/(4\pi(1-2\nu))$,

$x = x_j - x_i$,

$y = y_j - y_i$, and

$r^2 = x^2 + y^2$.

Equations (1.4-86) may be written in polar coordinates as

$$\sigma_{xx} = k\{2(1-\nu)\sin\theta - \sin\theta\cos2\theta\}/r$$
$$\sigma_{xy} = k\{2(1-\nu)\cos\theta - \cos\theta\cos2\theta\}/r \qquad (1.4\text{-}87)$$

The limiting value of the force, q_x, exerted over the semicircular arc AB, Fig. 1.4-27 as $\xi \to 0$ is given by

$$q_x = \lim_{\xi \to 0} \int_{S_e} T_x \, dS_e \qquad (1.4\text{-}88)$$

The traction, T_X, for an arbitrarily oriented increment length, dS, is found from the stress components in (1.4-87) and written as

$$T_X = k\{2(1-\nu) - \cos 2\theta\}/r \qquad (1.4\text{-}89)$$

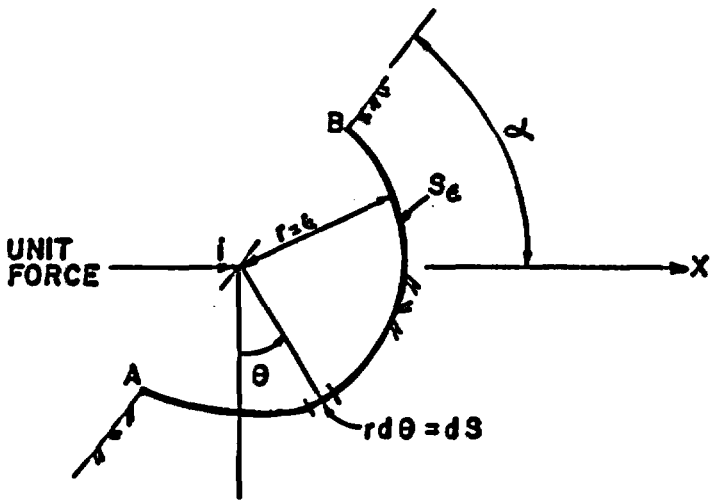

Fig. 1.4-27 Geometry for Calculation of "Free Term" on a Smooth Boundary

Referring to the geometry of Fig. 1.4-27 and replacing r by ε in Eq. (1.4-89) allows Eq. (1.4-88) to be rewritten as

$$q_X = \lim_{\xi \to 0} \int_{\alpha-\pi}^{2\pi} k\{2(1-\nu)\cos 2\theta\}d\theta \qquad (1.4\text{-}90)$$

or

$$q_X = c_X{}^i = 1/2$$

It is interesting to note that the physical significance of this result is that for a unit force applied at a boundary in an infinite elastic medium, half of the force is distributed to the interior of the problem and half is distributed to the exterior.

1.4.5.4.4 Determination of "Free Terms" by Rigid Body Considerations

This section gives an indirect method of calculating "free terms" in Eq. (1.4-64). This procedure, used in the boundary element formulation, is based on rigid body considerations and is adapted from Cruse (1974). The method is equivalent to ensuring that static equilibrium is achieved over any closed surface in the medium. Equation (1.4-60) may be rewritten by removing "free terms" and rearranging as

$$c_x^i u_x + c_y^i u_y = \int_S (t_x U_x^{xi} + t_y U_y^{xi}) dS = \int_S (T_x^{xi} u_x + T_y^{xi} u_y) dS \tag{1.4-91}$$

where the second integral on the right hand side is interpreted in the sense of the Cauchy principal value. Equation (1.4-91) is a specialization of

$$c_x^i u_x + c_y^i u_y = \int_S (t_x U_x^{xi} + t_y U_y^{xi}) dS + \int_{S_\infty} (t_x U_x^{xi} + t_y U_y^{xi}) dS_\infty \tag{1.4-92}$$

$$- \int_S (T_x^{xi} u_x + T_y^{xi} u_y) dS - \int_{S_\infty} (T_x^{xi} u_x + T_y^{xi} u_y) dS_\infty$$

where S_∞ is the boundary at infinity, and the integrations over these surfaces are zero. If, however, a rigid body translation equal to u_x or u_y is imposed on the system, then the tractions everywhere are zero. For $u_x = 1$ and $u_y = 0$, Eq. (1.4-92) becomes

$$c_x^i = - \int_S T_y^{xi} \, dS - \int_{S_\infty} T_y^{xi} \, dS_\infty \tag{1.4-93}$$

For $u_x = 0$ and $u_y = 1$, Eq. (1.4-92) becomes

$$c_y^i = \int_S T_y^{xi}\, dS - \int_{S_\infty} T_y^{xi}\, dS_\infty \qquad (1.4\text{-}94)$$

It can be shown for $\xi \to 0$, $\theta = 0$ to 2π that

$$\int_{S_\infty} T_x^{xi}\, dS_\infty = -1$$

$$\int_{S_\infty} T_y^{xi}\, dS_\infty = 0 \qquad (1.4\text{-}95)$$

Therefore, each unknown traction coefficient can be found explicitly from known off-diagonal traction coefficients.

1.4.5.5 Application

The boundary element coupling may be applied in any half-space or infinite body. The boundary elements must be placed outside the probable intact yield zone or joint slip region. The boundary elements are for static mechanical use only, and do not apply to fluid flow, heat transfer or dynamic analysis.

1.4.5.6 Numerical Method Type

The boundary element logic does not require any new or unique numerical method.

1.4.5.7 Derivation of Numerical Model

Section 4.4.4 presented the theoretical aspects of the boundary element method (BEM). In this section, we describe the coupling of the BEM to the distinct element method and how this is accomplished in UDEC.

The feasibility of coupling distinct elements and boundary elements was first demonstrated by Lorig and Brady (1982). This initial work used a static relaxation formulation for the distinct element domain and was limited mainly to validation studies for problems in isotropic elastic continua. Lemos (1983) used a simply deformable formulation in the distinct element domain to study stress distributions in jointed rock resulting from several loading episodes. Lorig and Brady (1983) used a hybrid code in initial studies to indicate applicability of the method in analyzing excavations in stratified rock.

Principles of Interfacing Boundary Elements and Distinct Elements

The nature of the coupled distinct element-boundary element system is shown in Fig. 1.4-28 with a set of Distinct Elements embedded in an elastic domain. The medium is subject to assumed in-situ initial stresses prior to excavation. Excavation eliminates traction on the surfaces defining the opening boundary. The condition to be satisfied on the interface between the Boundary Element Domain and the Distinct Element Domain is continuity of excavation induced displacements and equilibrium of the final state of stress. It is assumed that it is sufficient if these conditions are satisfied at the nodes defining interface between the two domains.

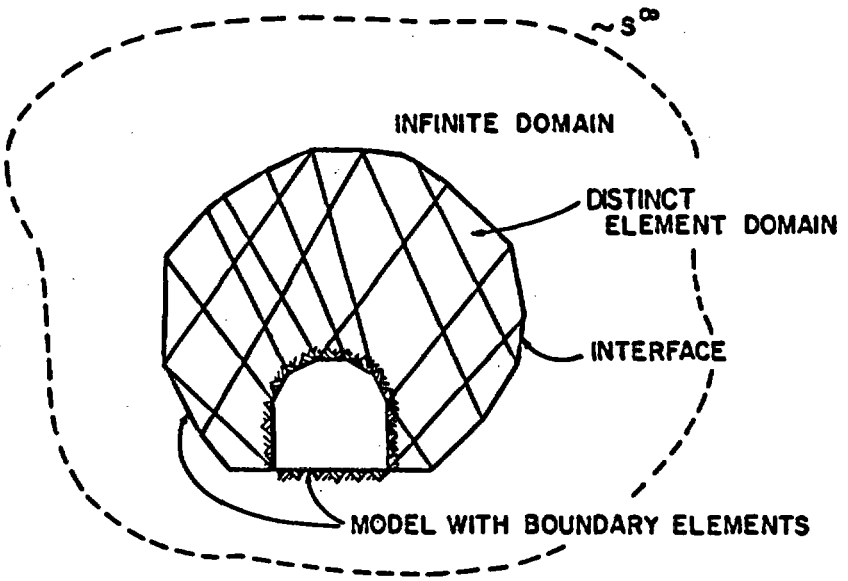

Fig. 1.4-28 Nature of Coupled Distinct Element-Boundary Element System

In the present formulation, boundary element nodes coincide with block corners on the periphery of the distinct element domain. Determination of induced displacements at each boundary element node permits direct determination of induced nodal force by multiplying the nodal displacement vector and the stiffness matrix for the boundary element domain [see Eq. (1.4-72)]. In Eq. (1.4-72), the vector (q) represents induced nodal forces which are related to the total nodal forces (q^t) by the expression

$$\{q^t\} = \{q^o\} + \{q\} \qquad (1.4\text{-}96)$$

where $\{q_o\}$ represents the initial nodal forces.

Thus, Eq. (1.4-72) may be rewritten

$$\{q^t\} = [K_b]\{u\} + \{q^o\} \qquad (1.4\text{-}97)$$

The nodal forces determined in this way can then be applied to appropriate block corners located on the periphery of the distinct element domain in the subsequent relaxation step or iteration. Thus, as the relaxation process continues, nodal displacements and forces are updated and used in the subsequent calculation cycle.

The boundary element stiffness matrix $[K_b]$ is computed using the x'-y' coordinate system as defined in Section 1.4.5.4. Consequently, elements of {u} determined from block displacements, must be converted to the x'-y' coordinate system. Following matrix multiplication, elements of {q} are converted back to the original x-y coordinate system.

Interface Conditions

As mentioned previously, coupling between the two domains must ensure that displacements and tractions at all nodal points are continuous across the interface. These conditions require that the non-linear material behavior zone be confined inside the distinct element domain. Surfaces of sliding or separation therefore cannot intercept the interface.

The boundary element formulation uses straight line elements and the distinct elements are defined by straight lines, so that physical compatibility is assured. Each iteration in the distinct element domain results in displacement and rotation of block centroids. Kinematic continuity at the interface is satisfied by identifying block corner displacements with nodal displacements in the boundary element domain. Since nodes correspond to the contact of two blocks, nodal displacements are taken as the average of two adjacent corner displacements. Since the contact between the corners of two blocks on the interface must be elastic, the difference of displacements is small and the averaging scheme is a reasonable approximation. As the variation of displacements is assumed linear, both in the boundary element domain and along the edge of a block, continuity of displacements across the interface is reasonably satisfied.

Induced nodal forces {q} results from multiplication of the boundary element stiffness matrix and nodal displacements as seen in Eq. (1.4-66). Since the vector {q} represents forces applied to the boundary element domain, the negative of this vector is applied to the corners of the blocks on the interfaces. Each pair of blocks corresponding to an interface node receive a fraction of the force proportional to the length of its edge along the interface. This procedure is consistent with the assumption of linear variation of tractions in the boundary element domain and satisfies the equilibrium conditions at the interface.

Elimination of Rigid Body Motions

In the hybrid distinct element-boundary element method, each iteration results in the interface displacements that are used to compute interface forces using the boundary element stiffness matrix. If gravity is included in the distinct element domain, removal of the distinct elements from within the distinct element domain to model an excavation leads to an imbalance in forces acting at the interface. This imbalance has the effect of causing the entire problem to experience an upward rigid body motion. Convergence of the iterative process requires that these interface displacements be related to some fixed nodal point in the boundary element domains. This is accomplished by modifying the stiffness matrix so that for every set of interface displacements, a selected interior point P has zero displacement. Lemos (1983) described a procedure for fixing a point in the boundary element domain. The discussion which follows is based on this work.

The procedure is initialized by giving the i^{th} entry of the interface displacement vector a unit displacement and setting all other entries equal to zero. The vector of interface forces corresponding to this displacement field is the i^{th} column of the stiffness matrix $[K_b]$ and can be denoted by $[F^i]$. The displacements at point P corresponding to the described displacement configuration are u_p^{oi} abd v_p^{oi} in the x- and y-directions, respectively.

Next, each of the interface nodes is given a unit displacement in the x direction, resulting in displacements u_p^{rx} and v_p^{rx} at P. The interface forces $\{F^{rx}\}$ for this condition are obtained by summing the elements of the odd numbered columns in each row of the stiffness matrix. Similarly, unit y-directed displacements are given to all interface nodes resulting in interface forces $\{F^{ry}\}$ and displacements u_p^{ry} and v_p^{ry} at P.

It is required that all boundary nodes be given an equal displacement a_x^i and a_y^i such that displacements u_p^{oi} and v_p^{oi} are eliminated. Superimposing on the i^{th} unit configuration the second displacement field will produce at P

$$u_p^i = u_p^{oi} + a_x^i\, u_p^{rx} + a_y^i\, u_p^{ry}$$
$$v_p^i = v_p^{oi} + a_x^i\, v_p^{ry} + a_y^i\, v_p^{ry} \qquad (1.4\text{-}98)$$

At the boundary nodes, the total displacement will be $u_b{}^i = a_x{}^i$ and $v_b{}^i = a_y{}^i$, except for the displacement at the i^{-th} entry where units must be added to the right hand side. The condition that P remains fixed relative to the boundary nodes can be expressed as

$$\begin{aligned} u_p{}^i - u_b{}^i &= 0 \\ v_p{}^i - v_b{}^i &= 0 \end{aligned} \qquad (1.4\text{-}99)$$

These preceding equations can be combined and rewritten as

$$\begin{aligned} u_p{}^{oi} + a_x{}^i \, (u_p{}^{rx-1}) + a_y{}^i \, (u_p{}^{ry}) &= 0 \\ v_p{}^{oi} + a_x{}^i \, (v_p{}^{rx}) + a_y{}^i + (v_p{}^{ry-1}) &= 0 \end{aligned} \qquad (1.4\text{-}100)$$

This system of equations can be solved for unknowns $a_x{}^i$ and $a_y{}^i$ to be superimposed on the i^{-th} configuration. The interface forces after superimposition become

$$\{F'^i\} = \{F^i\} + a_x{}^i\{F^{rx}\} + a_y{}^i\{F^{ry}\} \qquad (1.4\text{-}101)$$

The vector $\{F'^i\}$ is actually the i^{-th} column of the modified stiffness matrix. The process is repeated for all columns with i ranging from 1 to 2n, resulting in a new stiffness matrix $[K_b']$. This matrix gives forces for every set of interface displacements which are consistent with the assumption that P remains fixed.

For a given set of induced forces $\{q\}$, the differences in nodal displacements obtained by solving the system with $[K_b']$ instead of $[K_b]$ represents the rigid body motion of the problem domain. The rigid body motions are

$$\begin{aligned} a_x &= \sum_{i=1}^{2n} a_x^i d_i \\ a_y &= \sum_{i=1}^{2n} a_y^i d_i \end{aligned} \qquad (1.4\text{-}102)$$

where d_i are the induced nodal displacements.

When determining the final displacements at a point in the interior of the boundary element domain, these constant displacements must be added to account for the changed stiffness matrix. Internal stresses need not be corrected.

Implementation in UDEC

The primary functions of the BE coupling section of the program are as follows.

1. Generate the nodal points of the boundary elements from the outer boundary gridpoints of the distinct element finite difference grid.

2. Calculate influence coefficients from the nodal point geometry and far field rock properties.

3. Form a system of equations

$$[T]\{u\} = [U]\{t\} \qquad (1.4\text{-}103)$$

where [T], [u] are influence coefficient matrices for the tractions and displacement kernels, respectively, and,

{u}, {t} are the displacement and traction vectors, respectively.

[T] is saved in a temporary file on the hard disk called tape7.

[u] is saved in a temporary file on the hard disk called tape4.

4. The system of equations in (3), above, is altered to form a stiffness matrix [K] relating the incremental nodal displacements to incremental nodal forces:

$$\{f\} = [K]\ \{u\} \qquad (1.4\text{-}104)$$

where $[K] = [G][u]^{-1}[K]$, and

[G] is a geometry matrix for conversion of element tractions to equivalent forces lumped at the nodal points.

The stiffness matrix is written to a file = tape8, as it is being constructed, as well as the main program arrays.

5. During the problem solution, the boundary element coupling is performed every time step. This is accomplished in the following manner

   (a) Outer boundary incremental nodal displacements from the previous cycle are multiplied by the stiffness matrix, which is obtained from the main program array [i.e., Eq. (1.4-104)]:

   $$\{f\} = [K]\{u\}$$

   obtaining a new set of boundary incremental nodal forces.

   (b) These nodal forces are updated in the boundary force array for application to block boundary.

1.4.5.8 Location

All boundary element subroutines are located in a single file BE.FOR. The coupling is called in subroutine CYCLE, the main program explicit logic control routine. Updating of the boundary force array occurs in file BOUND.FOR. Saving and restarting of the problem is performed in file SAVE.FOR.

1.4.5.9 Numerical Stability and Accuracy

Presently, the boundary element coupling is performed every time-step—i.e., the boundary force vector is updated to reflect the presence of the infinite body. Performing this update every timestep insures stable convergence. No significant testing has been performed to examine the potential effects of coupling at wide-spaced intervals.

Numerical instabilities can occur if the lengths of adjacent boundary elements are widely different. Lorig (1984) observed instability when the ratio of lengths of adjacent elements was in the order of 100. In general, this condition will rarely occur, and usually the ratio of lengths should be around 10 or less.

The fixed point location was observed to have small effects on the final solution. Greater detail is given in Lorig (1984).

1.4.5.10 Alternatives

No specific alternative models for boundary element far-field coupling exist within the UDEC code.

1.4.6 Constitutive Laws for Intact Blocks

1.4.6.1 Purpose

The behavior of intact blocks of rock varies widely from rock mass to rock mass. In hard, brittle rocks such as granite, the intact blocks can generally be assumed to behave in a linearly-elastic, isotropic fashion. Here, any non-linear response of the rock under mechanical loading is generally attributed to the fractures. Other rocks, particularly softer materials such as sandstones, shales, etc., may exhibit intact rock failure characterized by plastic yield. The above description refers, in general, to static loading, however, in dynamic loading with high amplitude applied pressure, intact rock, including hard rocks, may exhibit extensive plastic yield. UDEC provides two constitutive model choices for intact rock: elastic and Mohr-Coulomb plasticity.

1.4.6.2 Assumptions and Limitations

The following assumptions and limitations are inherent in the elastic and/or Mohr-Coulomb plasticity models:

(1) isotropic rock mass;

(2) no rupture criterion provided for intact material undergoing plastic flow;

(3) plastic materials exhibit elastic-perfectly plastic behavior; and

(4) plane strain conditions.

The limitations of the constitutive models for representing rock behavior have been discussed by many authors, (e.g., Desai and Christian, 1977). The primary difference between the use of the distinct element method as opposed to continuum models is representing rock mass response. Continuum codes use constitutive models to represent the overall rock response. In most jointed rocks, the non-linearity in overall rock response is a result of the joints themselves and, to a lesser extent, the intact material. In the discontinuum approach, the joints themselves are modeled, and there is much less demand for examination of the applicability of intact constitutive laws or reproducing rock mass response.

The UDEC code does not account for the out-of-plane stress component in the Mohr-Coulomb model. For stress states in which the out-of-plane component does not fall between the principal stresses at that point, some error will result in the determination of the resulting yield zone. For the general two-dimensional plane strain or plane stress assumptions, this limitation is not considered to be a great restriction.

1.4.6.3 Notation

The notation for variable names and array offset locations for the elastic and Mohr-Coulomb models are given in Table 1.4-10.

Table 1.4-10

NOTATION USED IN ELASTIC AND MOHR-COULOMB CONSTITUTIVE RELATIONS FOR INTACT BLOCKS

Notation		Comments	Where Found
Algebraic	Computer		
x	KXG	Offset to x-coordinate in gridpoint data array	Main common block UDECOM
y	KXG	Offset to y-coordinate in gridpoint data array	"
$\dot{u}x$	KXDG	Offset to x-velocity in gridpoint data array	"
$\dot{u}y$	KYDG	Offset to y-velocity in gridpoint data array	"
ΣFx	KGFX	Offset to x-force sum in gridpoint data array	"
ΣFy	KGFY	Offset to y-force sum in gridpoint data array	"
$\Delta\sigma xx$	KZS11	Offset to xx-stress in zone data array	"
$\Delta\sigma xy$	KZS12	Offset to xy-stress in zone data array	"
$\Delta\sigma yy1$	KZS22	Offset to yy-stress in zone data array	"
θ	KZROT	Offset to zone rotation in zone data array	"

Table 1.4-10
(continued)

Notation		Comments	Where Found
Algebraic	Computer		
ρ	DENS(I)	Density of material I	Main common block UDECOM
K	BULK(I)	Bulk modulus of material I	"
G	SHEAR(I)	Shear modulus of material I	"
T	TENS(I)	Tensile strength of material I	"
λ	ALAM1(I)	Lame constant of material I	"
μ	ALAM2(I)	Lame constant of material I	"
ϕ	AMU(I)	Friction coefficient of material I	"
ψ	DILAT(I)	Dilation angle of material I	"
C	COH(I)	Cohesion of material I	"

1.4.6.4 Derivation

Elastic Model

The elastic model assumes a linear change in stress with strain on loading and unloading (Fig. 1.4-29).

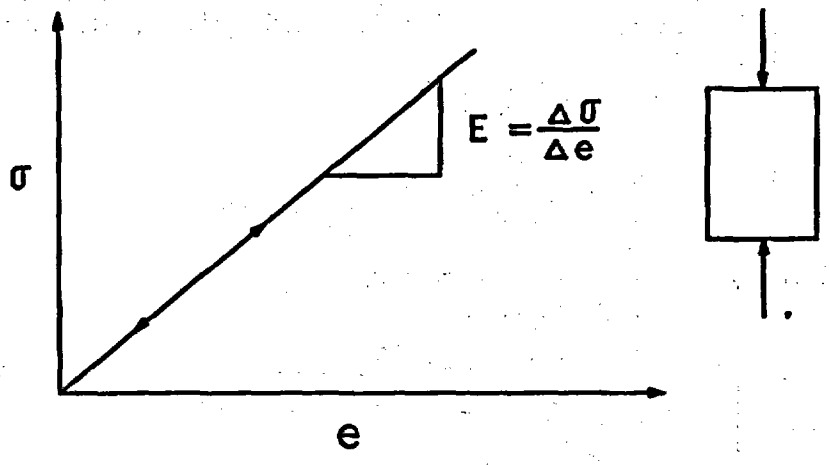

Fig. 1.4-29 Illustration of Linear Elastic Behavior of a Sample in Uniaxial Compression

The relation of stress to strain in incremental form is given by Hooke's law in plane strain as

$$\begin{aligned} \Delta\sigma_{11} &= \lambda\Delta e_{11} + \mu\Delta e_{22} \\ \Delta\sigma_{22} &= \mu\Delta e_{11} + \lambda\Delta e_{22} \\ \Delta\sigma_{12} &= 2G\Delta e_{12} \\ \Delta\sigma_{21} &= \Delta\sigma_{12} \end{aligned} \qquad (1.4\text{-}105)$$

where $\lambda = K + (4/3)G$,

$\mu = K - (2/3)G$, and

$\Delta\sigma$, Δe = incremental components of the stress strain tensors.

Mohr-Coulomb Plasticity

The formulation used assumes elastic/perfectly plastic with a linear Mohr-Coulomb yield condition and non-associated flow rule. Figure 1.4-30 illustrates the Mohr-Coulomb yield surface and associated terminology.

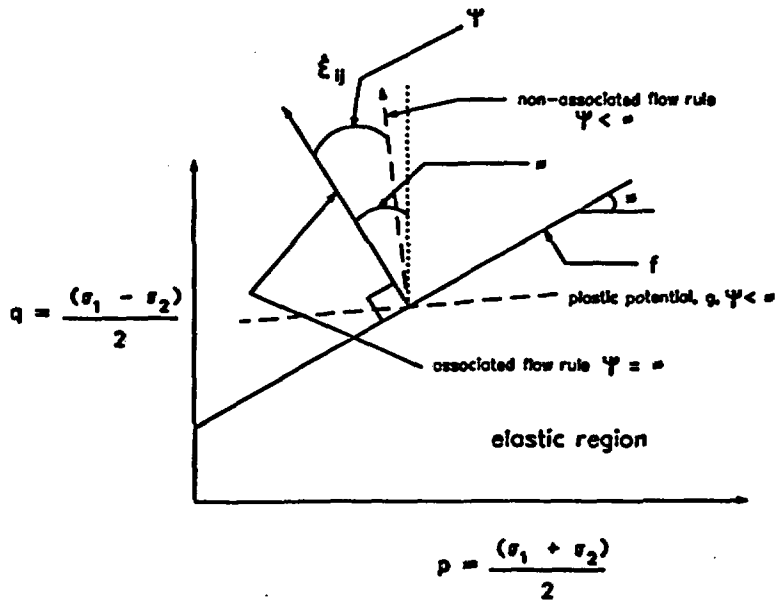

Fig. 1.4-30 Mohr-Coulomb Criterion (f) in q-p Space with Friction (Φ), Dilation (Ψ), Strain Rate Increment Vector and Plastic Potential (g) Shown

The total stain rate increments are assumed to be composed of elastic and plastic parts:

$$\dot{\varepsilon}_{ij} = \dot{\varepsilon}^{e}_{ij} + \dot{\varepsilon}^{p}_{ij} \qquad (1.4\text{-}106)$$

The Mohr-Coulomb yield criterion, f, and plastic potential, g, are written in terms of the principal stresses and material constants:

$$f = \sigma_1 - N_\phi \sigma_2 + 2C(N_\phi)^{1/2}$$
$$g = \sigma_1 - N_\psi \sigma_2 + 2C(N_\psi)^{1/2} \qquad (1.4\text{-}107)$$

where $\sigma_{1,2}$ = principal stress components,

$N_\xi = (1 + \sin\xi)/(1 - \sin\xi)$, and

$\xi = \phi$, ψ = friction, dilation angle.

The flow rule prescribes the angular relation between the stress and plastic strain increment tensors:

$$\dot{\varepsilon}_{ij}^{p} = \lambda \frac{\partial g}{\partial \sigma_{ij}} \qquad (1.4\text{-}108)$$

where λ is a multiplier determined from the stress state.

1.4.6.5 Application

The elastic model is applicable to any material which exhibits linear, isotropic behavior with no hysteresis upon loading/unloading. The Mohr-Coulomb model is applicable to any material which displays isotropic elastic-perfectly plastic behavior. This model is widely accepted as being applicable to geologic materials. The non-association of the flow rule is felt to be applicable to geologic materials in that volumetric strain in experimentation is generally far less than would be predicted from associated flow.

1.4.6.6 Numerical Method Type

The constitutive laws described above are implemented using the standard explicit finite difference logic described in Section 1.3. For the non-linear laws, initial, small elastic stress increments are used as input to the yield model at each timestep. The program determines whether yield has occurred and, if so, forces the stress state to lie on the yield surface. Stress corrections are determined based on the flow rule. No new or unique numerical methods are employed in this approach.

1.4.6.7 Derivation of the Numerical Method

Implementation of Finite Difference Logic for Triangular Zones

The finite difference logic for the triangular elements is based on work by Wilkins (1963). All constitutive laws for fully-deformable block use the same differencing logic. The following is adapted from Cundall (1989).

Gauss' theorem

$$\int_S n_i f \, dS = \int_A \frac{\partial f}{\partial x_i} \, dA \qquad (1.4\text{-}109)$$

is used to derive a finite difference formula for elements of arbitrary shape; here S denote the path around the element, A the element area, n_i the outward unit normal vector, x_i the position vector of a boundary point and f a scalar, vector or tensor.

Fig. 1.4-31 Typical Triangular Element with (a) Velocity Vectors; and, (b) Nodal Force Vector

Defining the average value of the derivative over A as

$$\left(\frac{\partial f}{\partial x_i}\right) = \frac{1}{A}\int_A \frac{\partial f}{\partial x_i}\, dA \qquad (1.4\text{-}110)$$

we obtain

$$\left(\frac{\partial f}{\partial x_i}\right) = \frac{1}{A}\int_S n_i f\, dS \qquad (1.4\text{-}111)$$

For a polygon, such as the triangular element shown in Fig. 1.4-31, the finite difference formula becomes

$$\left(\frac{\partial f}{\partial x_i}\right) \cong \frac{1}{A}\sum_s (f) n_i \Delta S \qquad (1.4\text{-}112)$$

where the summation is over the three sides and (f) is the mean value of f over a side.

This formula, suggested by Wilkins, enables the strain increments Δe_{ij}, for a zone, to be written in terms of nodal velocities, by substituting the velocity vector $\dot{u}_i$ for f in Eq. (1.4-112):

$$\frac{\partial \dot{u}_i}{\partial x_j} \cong \frac{1}{2A}\sum_s (\dot{u}_i(a) + \dot{u}_i(b)) n_j \Delta S$$

$$\Delta e_{ij} = \frac{1}{2}\left(\frac{\partial \dot{u}_i}{\partial x_j} + \frac{\partial \dot{u}_i}{\partial x_i}\right)\Delta t \qquad (1.4\text{-}113)$$

where Δt is the timestep and (a) and (b) denote two consecutive nodes on the boundary of the triangle [see Fig. 1.4-31(a)].

Since UDEC operates in large strain mode, finite rotations of zones produce changes in the stress components referred to a fixed frame of reference. The zone stresses are adjusted as follows, before invoking the constitutive law

$$\sigma_{ij} := \sigma_{ij} + (\dot{\omega}_{ik}\sigma_{kj} - \sigma_{ik}\dot{\omega}_{kj})\Delta t, \quad \dot{\omega}_{ij} = \frac{1}{2}\left(\frac{\partial \dot{u}_i}{\partial x_j} - \frac{\partial \dot{u}_i}{\partial x_i}\right) \tag{1.4-114}$$

Element stresses are now modified by application of the constitutive law, M:

$$\sigma_{ij} = M(\sigma_{ij}, \Delta e_{ij}) \tag{1.4-115}$$

For non-linear constitutive laws, small elastic stress increments are first determined for comparison to the yield surface. If the stresses lie above the yield surface, stress corrections are calculated based on the flow rule.

When stresses in all elements have been recalculated, nodal forces are summed from all surrounding elements. A typical expression is given below for the force on one node of the triangle shown in Fig. 1.4-31(b):

$$F_i = \frac{1}{2}\sigma_{ij}(n_j^{(1)}S^{(1)} + n_j^{(1)}S^{(2)}) \tag{1.4-116}$$

The summation of all such forces acting on a node is used to derive an acceleration that is integrated by central finite differences to provide new velocities:

$$\dot{u}_i^{(t+\Delta t/2)} = [\dot{u}_i^{(t-\Delta t/2)} * \alpha_1 + \left(\frac{\Sigma F_i(t)}{m} + g_i\right)\Delta t * \alpha_2 \tag{1.4-117}$$

where g_1 = gravitational acceleration,

α_1 = damping parameter, $1 - (1/2)\ \alpha\Delta t$, and

α_2 = damping parameter, $1/(1 + (1/2)\alpha\Delta t)$.

Elastic Model

The strain increments are used as input to Hooke's law as given in Eq. (1.4-105) to produce elastic stress increments.

Mohr-Coulomb Plasticity

The yield surface is given by:

$$f = \sigma_1 - N_\phi \sigma_2 + 2C\ (N_\phi)^{1/2} \qquad (1.4\text{-}118)$$

and the plastic potential function is given by

$$g = \sigma_1 - N_\psi \sigma_2 + 2C\ (N_\psi)^{1/2} \qquad (1.4\text{-}119)$$

where $N_\xi = (1 + \sin\xi)/(1 - \sin\xi)$ [$\xi = \phi$ or ψ],

C = cohesion (positive sign),

ϕ = friction angle,

ψ = dilation angle,

σ_1 = major principal stress, and

σ_2 = minor principal stress.

The strain increments are assumed to be composed of elastic and plastic parts:

$$\Delta e_1 = \Delta e_1^e + \Delta e_1^p$$
$$\Delta e_2 = \Delta e_2^e + \Delta e_2^p \qquad (1.4\text{-}120)$$

The plastic strain rates are given by the non-associated flow rule:

$$\dot{e}_1^P = \lambda \frac{\partial g}{\partial \sigma_1} = \lambda$$

$$\dot{e}_2^P = \frac{\lambda \partial g}{\partial \sigma_2} = - \lambda N_\psi \qquad (1.4\text{-}121)$$

where λ is the multiplier which must be determined from the stress state.

Multiplying by Δt, Eq. (1.4-121) becomes

$$\Delta e_1^P = \lambda \Delta t$$

$$\Delta e_2^P = - \lambda N_\psi \Delta t \qquad (1.4\text{-}122)$$

The incremental principal elastic stresses are given by:

$$\Delta \sigma_1 = (K + \frac{4}{3} G) \Delta e_1^e + (K - \frac{2}{3} G) \Delta e_2^e$$

$$\Delta \sigma_2 = (K - \frac{2}{3} G) \Delta e_1^e + (K + \frac{4}{3} G) \Delta e_2^e \qquad (1.4\text{-}123)$$

Substituting Eqs. (1.4-120) and (1.4-122) into Eq. (1.4-123),

$$\Delta\sigma_1 = (K+\frac{4}{3}G)\ (\Delta e_1-\lambda\Delta t) + (K-\frac{2}{3}G)\ (\Delta e_2 + \lambda N_\psi \Delta t)$$

$$\Delta\sigma_2 = (K-\frac{2}{3}G)\ (\Delta e_1 - \lambda\Delta t) + (K+\frac{4}{3}G)\ (\Delta e_2+\lambda N_\psi \Delta t) \quad (1.4\text{-}124)$$

Determining the initial elastic principal stresses by σ_1^I and σ_2^I, the corrected (for plasticity) stresses σ_1, σ_2 are given by

$$\sigma_i^I - \sigma_i = \Delta\sigma_i^I - \Delta\sigma_i \quad (1.4\text{-}125)$$

where i = 1 or 2.

The initial principal stress increments are given by

$$\Delta\sigma_1^I = (K+\frac{4}{3}G)\ \Delta e_1 + (K-\frac{2}{3}G)\ \Delta e_2$$

$$\Delta\sigma_2^I = (K-\frac{2}{3}G)\ \Delta e_1 + (K+\frac{4}{3}G)\ \Delta e_2 \quad (1.4\text{-}126)$$

By substituting Eqs. (1.4-124) and (1.4-126) into Eq. (1.4-125),

$$\sigma_1 = \sigma_1^I - \lambda\Delta t\ [(K+\frac{4}{3}G) - (K-\frac{2}{3}G)\ N_\psi]$$

$$\sigma_2 = \sigma_2^I - \lambda\Delta t\ [(K-\frac{2}{3}G) - (K+\frac{4}{3}G)\ N_\psi] \quad (1.4\text{-}127)$$

or, simplifying,

$$\sigma_1 = \overset{I}{\sigma_1} - \lambda\Delta t \ (\alpha_1 - \alpha_2 N_\psi)$$
$$\sigma_2 = \overset{I}{\sigma_2} - \lambda\Delta t \ (\alpha_2 - \alpha_1 N_\psi) \qquad (1.4\text{-}128)$$

Equation (1.4-128) gives the new principal stresses in terms of the trial initial stress, the material constants, and the multiplier, λ. The λ value can be found since σ_1 and σ_2 must lie on the yield surface (if a non-admissible stress state is detected). This is done by substituting Eq. (1.4-128) into the equation for the yield surface [Eq. (1.4-118)] and equating to zero:

$$\lambda\Delta t = \frac{\overset{I}{\sigma_1} - N_\phi \overset{I}{\sigma_2} - 2C N_\phi}{\alpha_2(1+N_\phi N_\psi) - \alpha_1(N_\phi + N_\psi)}$$
$$= \frac{f(\overset{I}{\sigma_1}, \overset{I}{\sigma_2}, C, N_\phi)}{\gamma} \qquad (1.4\text{-}129)$$

where $\gamma = \alpha_2(1 + N_\phi N\psi) - \alpha_1(N_\phi + N_\psi)$.

Substituting Eq. (1.4-129) into Eq. (1.4-128) yields the corrected principal stress components:

$$\sigma_1 = \overset{I}{\sigma_1} - (\alpha_1 - \alpha_2 N_\psi) \frac{f(\overset{I}{\sigma_1}, \overset{I}{\sigma_2}, C, N_\phi)}{\gamma}$$
$$\sigma_2 = \overset{I}{\sigma_2} - (\alpha_2 - \alpha_1 N_\psi) \frac{f(\overset{I}{\sigma_1}, \overset{I}{\sigma_2}, C, N_\phi)}{\gamma} \qquad (1.4\text{-}130)$$

The program first determines the σ_{xx}, σ_{yy} and σ_{xy} elastic stress increments and converts them to principal stresses. These components are then substituted into the equation for the yield surface [Eq. (1.4-118)]. If,

f<0, then the direction cosines of the principal stresses are found and the plastic corrections are made [Eq.(1.4-130)] to require conformity to the yield surface.

f>0, then no corrections are necessary.

The corrected principal stresses are then resolved back to the x,y coordinate plane by the direction cosines determined previously.

1.4.6.8 Location

The grid point velocities are determined in subroutine GPMOT, which is called from the main program control routine, CYCLE. The incremental strain tensor and stress rotation corrections are determined in subroutine ZSTRS, which calls the constitutive law routines. The elasticity and Mohr-Coulomb laws are found in subroutines CL1 and CL3, respectively. These routines return stress corrections which are added to existing stresses. The stresses are then converted to equivalent grid point forces before continued time stepping.

1.4.6.9 Numerical Stability and Accuracy

Numerical instabilities can occur if an attempt is made to define a non-sensible dilation angle. The energy change which occurs during yield is given by the dot product of the resultant stress and strain vectors.

$$E = \sigma \cdot \varepsilon \qquad (1.4\text{-}131)$$

This is shown in Fig. 1.4-32. In case a, the cohesion is zero, and any $\psi > \phi$ will produce E>0, or the model will produce energy rather than dissipate. For case (b), in which cohesion is present, some value of $\psi > \phi$ can occur before instability, depending on the value of cohesion.

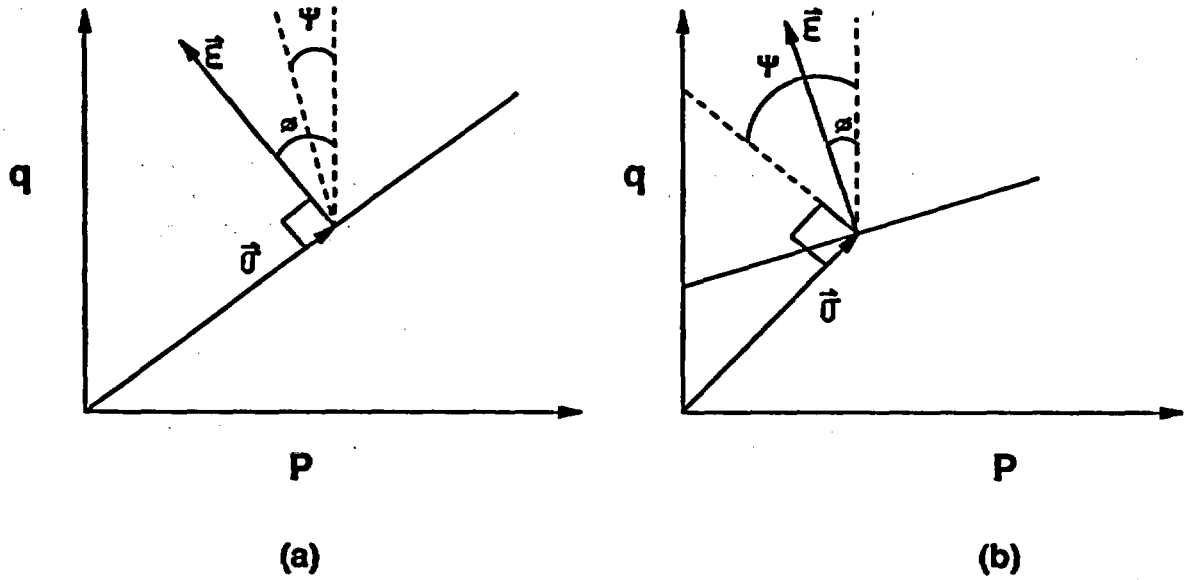

Fig. 1.4-32 Resultant Stress and Strain Vectors. (a) cohesion = 0, (b) cohesive and frictional material

The UDEC code may or may not become numerically unstable, depending on the boundary conditions, and there is no specific check in the code for values of ψ and ϕ.

The explicit solution routine is highly robust in enforcing nonlinear constitutive laws since no iteration or load stepping is necessary, as in explicit codes. Therefore, no "shear-locking" phenomena occur as is sometimes a problem in implicit procedures (e.g., Nagtegaal et al., 1974).

1.4.6.10 Alternatives

No specific alternative models of constitutive laws for intact blocks exist within the UDEC code. Models can be added to UDEC without great difficulty, provided they are mechanically sensible.

1.4.7 Constitutive Laws for Joints

1.4.7.1 Purpose

The jointing within a rock mass is the primary contributor to its overall non-linear behavior. The constitutive model used for the jointing controls both the normal and shear behavior which may contain elastic as well as irreversible strains. Two constitutive models are available in UDEC. The default model assumes linear normal stress-closure response and an elasto-plastic shear stress-shear displacement response. The second model, termed the "continuously-yielding" joint model (Lemos, 1987), attempts to provide realistic constitutive relations for progressive damage to the joint surface as a function of shear displacement. The model allows a variety of joint shear response ranging from elasto-plastic (as in the default model) to a peak strength-residual strength behavior (displacement-softening). One other model, the empirical Barton-Bandis model has been tested in UDEC, but is not included in the standard Version of ICG1.5 (see Barton et al., 1987). This model is not described here, although space for relevant input parameters to this model have been assigned in the main common block (UDECOM) in ICG1.5.

1.4.7.2 Assumptions and Limitations

Mohr-Coulomb Model

In this simple model, the joint behavior is described by linear shear and normal stiffness and constant friction and dilation angles. Because the actual joint surface is rough and non-planar, the normal stiffness will be non-linear and the asperities will shear off during shear deformation. This result is a peak shear strength followed by softening to some residual level. The Mohr-Coulomb model has been criticized for its lack of ability to model these phenomena.

Continuously-Yielding Model

This is an empirical model, the primary limitation of which is in specification of the input parameters. Seven parameters are required by the model, six of which can be determined from laboratory triaxial testing (and/or direct shear) of natural joints. A roughness parameter, R, is required which is not defined in formal detail sufficient to allow its experimental determination.

The user must therefore perform numerical experimentation with the model in comparison to laboratory results to empirically set the value of this parameter.

The model is also limited in that its base of application is somewhat limited at the present time. Lemos (1987) describes its use in analysis of dynamic problems involving cyclic loading; Hart et al., (1985) describe its use in the analysis of a large-scale in-situ block compression experiment in basalt.

1.4.7.3 Notation

Table 1.4-11 give the notation for variables and relevant parameters used in the Mohr-Coulomb and Continuously-Yielding models. As in previous sections, these variables may be in the form of offsets from addresses to the location of the variable position within one of the link-listed arrays used in UDEC.

Table 1.4-11

NOTATION FOR PARAMETERS AND VARIABLES USED IN THE JOINT CONSTITUTIVE MODELS

Notation		Comments	Where Found
Algebraic	Computer		
Variables Regarding Block Contacts Common to All Joint Constitutive Models			
x	KXC	X-contact coordinate offset	Contact data array
y	KYC	Y-contact coordinate offset	"
Δus	KCS	Relative shear displacement offset	"
Δun	KCN	Relative normal displacement offset	"
Fs	KCFS	Shear force offset	"
Fn	KCFN	Normal force offset	"
L	KCL	Contact length offset	"
n_x	KGNX	Contact normal cosine offset	"
n_y	KCNY	Contact normal cosine offset	"

Table 1.4-11
(continued)

Notation		Comments	Where Found
Algebraic	Computer		
Point Contact Model (JCONS = 1)			
Kn	AKN(I)	Contact normal stiffness, material I	Main common UDECOM
Ks	AKS(I)	Contact shear stiffness, material I	"
ϕ	AMU(I)	Contact friction, material I	"
C	COH(I)	Contact cohesion, material I	"
ψ	DILAT(I)	Contact dilation angle, material I	"
T_o	TENS(I)	Contact tensile strength, material I	"
Mohr-Coulomb Model (JCONS = 2, JCONS = 5)			
kn	AKNJ(I)	Joint normal stiffness, material I	"
ks	AKSJ(I)	Joint shear stiffness, material I	"
ϕ	AMUJ(I)	Joint friction, material I	"
C	COHJ(I)	Joint cohesion, material I	"
ψ	DILATJ(I)	Joint dilation angle, material I	"
T_o	TENSJ(I)	Joint tensile strength, material I	"

Table 1.4-11 (continued)

Notation		Comments	Where Found
Algebraic	Computer		
Continuously Yielding Joint Model (JCONS = 3)			
	KCJRE	Reversal indicator offset	Contact data array
	KCJDS	Old displacement increment offset	"
en	AKNJEX(I)	Normal stiffness exponent, material I	" UDECOM
es	AKSJEX(I)	Shear stiffness exponent, material I	"
R	SJR(I)	Joint roughness parameter, material I	"
ϕ_{eff}	AJGAM(I)	Joint bounding friction angle, material I	"
a_n	AKNJ(I)	Initial normal joint stiffness	"
as	AKSJ(I)	Initial shear joint stiffness	"
ϕ	AMUJ(I)	Intrinsic friction angle	"

1.4.7.4 Derivation

Review of Contact Logic

The joints in UDEC act as interfaces between blocks, acting essentially as a spring-slider system as shown in Fig. 1.4-33.

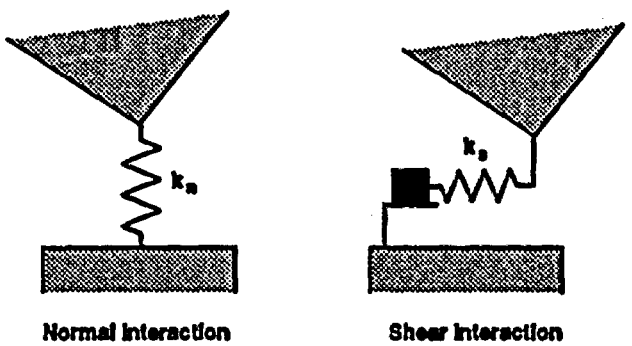

Fig. 1.4-33 Mechanical Representation of Interfaces in Distinct Element Method

In the model, spring-slider systems are located at contact points between blocks. The amount of penetration or overlap between two adjacent blocks can be defined directly from block geometry and block centroid translation and rotation for rigid blocks or grid point coordinates for fully-deformable blocks. The force-displacement relation at one contact is thus uncoupled from that at another on the same block.

The simplest force-displacement law relates incremental normal and shear forces (ΔF_n, ΔF_s) which develop at contacts directly to the amount of incremental relative displacement (Δu_n, Δu_s):

$$\Delta F_n = K_n \, \Delta u_n$$
$$\Delta F_s = K_s \, \Delta u_s \qquad (1.4\text{-}132)$$

where K_n and K_s are the contact normal and shear stiffnesses, as given previously in Table 1.4-11.

A constitutive model (JCONS = 1, see User's Manual, Volume II) is provided in UDEC which implements the above logic. This law applies primarily to particles or bodies in point contact, and does not adequately account for contact length. This model was originally intended for use with the rigid block logic. It has largely been superseded by the present Mohr-Coulomb model based on contact length and is not discussed further due to its limited applicability.

Contact between two block edges (Fig. 1.3-3) can be represented by two corner-edge contacts. The contact length, ℓ, calculated as

$$\sigma_n = \frac{F_n}{\ell}$$
$$\sigma_s = \frac{F_s}{\ell} \qquad (1.4\text{-}133)$$

and stress increments to be expressed in terms of the usual joint stiffnesses k_n and k_s [stress/length] as

$$\Delta\sigma_n = k_n \, \Delta u_n$$
$$\Delta\sigma_s = k_s \, \Delta u_s \qquad (1.4\text{-}134)$$

When blocks are discretized into a fine internal mesh, grid-points may be placed along the original edges [Fig. 1.3-3(c)]. These grid-points are treated as new corners, since the edge is now able to deform into a polygonal line. The same expressions (1.4-134) are used, with contact lengths defined as shown in Fig. 1.3-2(c).

The overlaps in Figs. 1.3-2(a) and 1.3.2(b) represent only a mathematically convenient way of measuring relative normal displacements. In finite element or displacement discontinuity models, joints are similarly assigned a zero thickness, with overlapping indicating compressive joint stresses and separation indicating tension. If normal joint stiffnesses are increased, overlaps can be made as small as desired.

At each timestep, the incremental stresses calculated by expressions (1.4-134) are added to the existing stresses, and the constitutive criteria are checked. In general, the joint constitutive relations must provide the stress increments as a function of the displacement increments, current stresses and possibly other state parameters

$$\Delta\sigma_n,\ \Delta\sigma_s = f(\Delta u_n, \Delta u_s, \sigma_n, \sigma_s, \ldots) \qquad (1.4\text{-}135)$$

In UDEC, the function f above, is limited to the Mohr-Coulomb or Continuously-Yielding model.

Mohr-Coulomb

Two forms of the Mohr-Coulomb law provided in UDEC utilize the following equations.

Normal Stress: $\sigma_n = \sigma^o_n + k_n \Delta u_n$, where σ^o_n = normal stress from previous timestep.

For joint constitutive model #2 (the default model), the normal stress is limited by the tensile strength of the joint in tension (i.e., $\sigma_n \leq T_o$, (compression positive) where T_o = tension strength = TENSJ(I)).

For joint constitutive model #5, the joint normal stress is initially limited to the tensile strength of the joint as above. However, once slip has been detected or the tensile strength is exceeded for a contact, it is assumed that the tensile strength is destroyed, and T_o is set equal to zero thereafter.

If the joint dilation angle is set (ψ_j=0 by default), the normal force is updated due to expansion of the joint upon shear:

$$F_n = F^o_n + k_n * \ell * abs(\Delta u_s) * tan(\psi_j) \qquad (1.4\text{-}136)$$

where F°_n = existing normal force,

ℓ = joint contact length,

Δu_s = shear displacement increment for slip only, and

$\tan(\psi_j)$ = tangent of the dilation angle of joint = DILATJ(I).

Shear Stress: $\sigma_s = \sigma^{\circ}_s + k_s \Delta u_s$, where the shear stress is limited by the Mohr-Coulomb law: $|\sigma_s| \leq C - \sigma_n \tan\phi$. σ°_s is the shear stress from the previous time-step.

For joint constitutive model #5, if slip is detected or the tensile strength is exceeded, the cohesion is assumed to be destroyed, and C is set to zero thereafter.

where C = joint cohesion (COHJ(I)),

$\tan\phi$ = joint friction (AMUJ(I)), and

σ_n is negative in compression.

Continuously Yielding-Model

The following description of the continuously-yielding model is taken from Lemos (1987).

Numerical modeling of practical problems may take the joints through rather complex load paths. Many empirical models only provide the response to simple loading conditions. More general situations require either interpolation between curves or other arbitrary assumptions. The continuously-yielding joint model, proposed by Cundall and Hart (1984), is intended to simulate the intrinsic mechanism of progressive damage of the joint under shear. This approach produces consistent responses in the varied conditions encountered in numerical modeling. The model also provides continuous hysteretic damping for dynamic simulations.

The response to normal loading is expressed incrementally as

$$\Delta\sigma_n = k_n \, \Delta u_n \qquad (1.4\text{-}137)$$

where k_n is the normal stiffness, given by $k_n = a_n \, \sigma_n^{en}$, a simple relation representing the observed increase of stiffness with normal stress, and

a_n and en are model parameters.

In general, zero tensile strength is assumed.

For shear loading, the model displays a continuous accumulation of plastic displacement from the onset of shearing. Figure 1.4-34 shows a typical stress-displacement curve for monotonic loading under constant normal stress. The shear stress increment is calculated as

$$\Delta\sigma_s = F \, k_s \, \Delta u_s \qquad (1.4\text{-}138)$$

where the shear stiffness can also be taken as a function of normal stress—for example,

$$k_s = a_s \, \sigma_n^{es} \qquad (1.4\text{-}139)$$

The instantaneous slope is governed by the factor F which depends on the distance from the actual stress curve to the "target" or bounding strength curve τ_m represented in the figure,

$$F = \frac{(1 - \sigma_s \, / \, \tau_m)}{(1 - r)} \qquad (1.4\text{-}140)$$

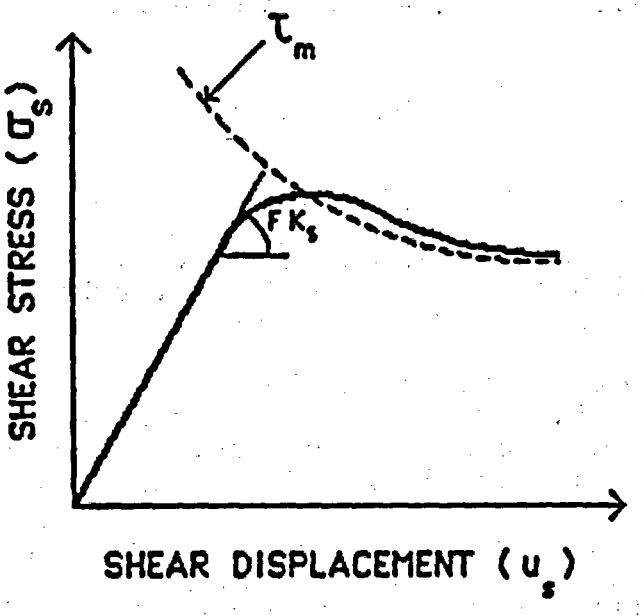

Fig. 1.4-34 Continuously-Yielding Joint Model: Shear Stress - Displacement Curve and Bounding Shear Strength

The factor r, which is initially zero, is intended to restore the elastic stiffness immediately after a load reversal. That is, r is set to σ_s/τ_m (and, therefore, F to 1) whenever sign (Δu_s) is not equal to sign(Δu_s^{old}). In practice, r is limited to 0.75 in order to avoid numerical noise when the shear stress is approximately equal to the bounding strength.

The bounding strength is given by

$$\tau_m = \sigma_n \tan \phi_{eff} \text{ sign}(\Delta u_s) \qquad (1.4\text{-}141)$$

The parameter ϕ_{eff} can be understood as the friction angle that would apply if no more asperities were sheared off. As damage accumulates, this angle is continuously reduced according to the equation

$$\Delta\phi_{eff} = - 1/R \; (\phi_{eff} - \phi) \; \Delta u_s^p \qquad (1.4\text{-}142)$$

where the plastic displacement is defined as

$$\Delta u_s^p = (1 - F)\ \Delta u_s \qquad (1.4\text{-}143)$$

ϕ is the basic friction angle of the rock surfaces, and

R is a material parameter (with dimension of length) which expresses the joint roughness.

A large value of R leads to a slower reduction of ϕ_{eff} and, therefore, to a larger peak. The peak is reached when the bounding strength equals the shear stress. After this point, the value of F becomes negative, and the joint enters the softening regime.

The above incremental relation for ϕ_{eff} is equivalent to

$$\phi_{eff} = \exp(-u_s^p/R)\ (\phi_{effo} - \phi) + \phi \qquad (1.4\text{-}144)$$

where ϕ_{effo} is the initial value of ϕ_{eff} and represents the in-situ state of the joint.

The dilatancy angle is calculated as

$$i = \tan^{-1}\ [|\sigma_s|/\sigma_n] - \phi \qquad (1.4\text{-}145)$$

—i. e., dilation takes place whenever the stress is above the residual strength level, and is obtained from the actual apparent friction angle.

Laboratory shear tests have shown that more damage is done under higher normal stress than at lower normal stress. This effect could be included by modifying the incremental equation governing the evolution of ϕ_{eff}. For example, parameter R could be multiplied by a factor of the form

$$\log_{10} (JCS/\sigma_n) \qquad (1.4\text{-}146)$$

as in the so-called Barton-Bandis model (Bandis et al., 1983).

1.4.7.5 Application

The applicability of the Mohr-Coulomb versus a displacement softening model such as the continuously-yielding model for mechanical analysis is not easily determined. It would appear that the primary features of joints which control the behavior of underground excavations are the joint spacing, orientation, number of joint sets, the peak friction, and dilation angles. The need to model softening behavior for failure analysis of confined rock (i.e., rock around excavations which is not kinematically free to move) subjected to straight ahead, quasi-static loading is not easily known, and may not be of particular importance. Softening behavior may be of greater importance when examining the behavior of rock under high normal stress in which blocks are kinematically free to move. Here, asperities may shear, resulting in significant decreases in shear capacity. Softening may also be significant in examination of the response of jointed rock to dynamic (cyclic) loading, or where energy release due to slip is important (e.g., rockbursting or earthquakes).

The normal stress-closure characteristics of joints are of importance when analyzing the flow of fluid through the joints. A non-linear relation of normal stress to closure (defined in the continuously-yielding model as a power law) is essential since the flow is a function of the joint aperture raised to the third power. The optional fracture logic which assumes that the tensile strength and cohesive shear strength drop to zero upon tensile or shear failure is probably the most physically reasonable Mohr-Coulomb model. Once failed, a joint does not regain tensile or shear strength.

1.4.7.6 Numerical Method Type

No new or unique numerical method types are required.

1.4.7.7 Derivation of the Numerical Model

Section 4.6.4 described the equations used for both joint models. The numerical implementation of these equations was previously described in Section 3. The interface constitutive laws are used to prescribe boundary forces to the blocks, (and finite difference zones in the case of fully-deformable blocks), which, in turn, used through the equations of motion to determine block relations and translations. The time stepping algorithm was described previously.

1.4.7.8 Location

The joint models are called from subroutine FORD. Constitutive model #1 is found in FORD, #2 in CLJ2, #5 in CLJ5 and the continuously yielding model in CLJ3.

1.4.7.9 Numerical Stability and Accuracy

The maximum joint stiffness (initial stiffness in the case of the standard Mohr-Coulomb model) is used to calculate the time step. The time step is determined from:

$$\Delta t = \text{FRAC}*2(m_{min}/k_{max})^{1/2}$$

where FRAC = user definable constant < 1,

m_{min} = minimum block or zone mass,

k_{max} = maximum stiffness

= $\max(k_{n,s}*l)$

where $k_{n,s}$ = normal or shear stiffness of joints, and

l = contact length.

For the continuously-yielding joint model, the code uses the initial joint stiffness value, JKN or JKS to determine the timestep.

The normal stiffness value may change dramatically as a function of normal stress. Therefore, numerical stability problems could occur at higher normal stresses, depending on the exponents en and es. Since UDEC does not dynamically recalculate the time-step, the user must manually adjust the FRAC parameter if numerical instability is encountered.

The present continuously-yielding formulation may produce unacceptable results when large variations of normal stress accompany reversals in the direction of shearing. For example, consider the case of shearing at a given σ_n, followed by a substantial reduction in normal stress without shear motion, and then by shearing in the opposite direction. If the change in σ_n causes a large drop in the bounding strength, or a stress-dependent shear stiffness is used, in principle it is possible for the unloading curve to be above the loading curve, leading to energy production. Applications to date have not involved load paths capable of producing such behavior. However, further research and modifications of the model are required to avoid this problem.

1.4.7.10 Alternatives

There are several suggested empirical (e.g., Barton-Bandis) and constitutive (e.g., Cook, 1988) laws for joint mechanical response. Models such as these can be added to UDEC without great difficulty, provided the law is mechanically sensible.

1.5 EXPERIENCE

The overall performance of UDEC is generally good. However, the following conditions have been identified under which the code is inefficient or may give poor results.

1.5.1 Disconnected Blocks

The data structure of UDEC was designed specifically to model compact rock masses (i.e., blocks tightly packed). The code can handle isolated cases where blocks lose contact with their neighbors by using "virtual contacts", which are fictitious links between particles. However, the code is not designed for multiple virtual contacts and, in this case, it becomes inefficient. It is suggested that these disconnected blocks be deleted if they are of no further interest.

1.5.2 Mixed Discretization

Constant-strain triangular zones such as those used in UDEC tend to inhibit incompressible plastic flow and may produce an excessively stiff and incorrect calculation for plastic flow. Nagtegaal et al. (1974) discuss procedures to improve the representation of plastic flow for triangular zones. One technique is the mixed-discretization procedure (Marti and Cundall, 1982), which reduces the constraints on plastic flow by using different numerical discretization for the isotropic and deviatoric parts of the strain tensor. This scheme works well for uniform grids composed of equal pairs of triangular zones.

Mixed-discretization is not used in UDEC because the creation of arbitrarily-shaped blocks makes the discretization of uniform grids of paired triangular elements difficult. However, quadrilateral blocks can always be discretized into uniform grids of diagonally exposed equal triangular zones using the **GEN QUAD** command. When such a grid is used for fully deformable blocks, UDEC results are generally good. Nagtegaal et al. (1974) showed that meshes composed of diagonally-opposed triangles produce a good representation for plastic flow.

1.5.3 Transient Fluid Flow

When modelling fluid flow with UDEC, there are a number of things to keep in mind.

1. The internal stresses should be generated physically, by allowing the system to come to equilibrium under the action of boundary stresses. Any in-situ pore pressure distribution can then be applied. For both these stages, some cycling is required in order to reach equilibrium. If the stresses are applied by the use of the **INSITU** command (without the optional keyword "NODIS"), joint displacements will be consistent with joint stresses, if joint numbers and material properties are previously assigned. If joint numbers and properties are not previously assigned, the hydraulic aperture will be incorrect for the intended stress level, since the joint aperture is derived from joint displacements. The optional INSITU keyword "NODIS" inhibits the calculation displacements for in-situ stresses. This keyword is useful, for example, if a non-linear joint stiffness is used in which case, the displacements are not correct. Note that the "fast flow" mode can be used for the equilibrium stage of the calculation.

2. There is a default limit on hydraulic aperture of five times the residual aperture. If a larger aperture is implied by the given effective stress level, then the **SET CAPRAT** command should be used to increase the limit.

3. The fluid continuity equation is satisfied at all domains, which represent lumped volumes. However, the volume of a domain at the intersection of two continuous joints can be very small, which would give rise to a tiny time step. Hence, there is a limit to the minimum domain volume, which is equal to A/2500, where A is the average block area. This limit appears to be undocumented and unchangeable, but it affects the transient response. If the actual joint volumes are less than the domain limit, then the response will be retarded. If in doubt, the domain volumes may be examined with the **PRINT DOM** command.

4. Joint displacements are computed in single precision. Since the permeability of a joint is highly sensitive to aperture (owing to the cubic law), a small error in displacement may give rise to a large flow error. Such a displacement error may be negligible for the mechanical response. If such an error is suspected, apertures may be checked directly with the **PRINT FLOW** command.

Items 3 and 4, together with the necessity for small timesteps when solving the flow equations explicitly, severely limit the usefulness of the current version of UDEC for modelling transient flow problems.

1.5.4 Contact Overlap

The most common execution error message is "Contact Overlap Too Great". It can occur during cycling if one block penetrates too far into another. The maximum amount of overlap allowed by the code is one-half the rounding length. If such an error occurs, it is usually necessary to restart the problem from an earlier state. However, before restarting, it is important to identify the cause of the error and correct it. Useful information concerning the contact location(s) where overlap occurred is given preceding the contact overlap message. The following possible causes for contact overlap can be identified.

Joint Normal Stiffness Too Low

If the joint normal stiffness is unrealistically low for the loads applied, the blocks will penetrate to far into each other. This cause can often be identified by (a) plotting a close-up of the affected area, or (b) printing contacts in the same area. The remedy for this cause is simply to increase the normal stiffness. The currently specified problem properties can be seen by typing **PRINT PROPERTIES**.

Numerical Instability

Numerical instabilities, characterized by increasing amplitude of oscillations, result from timesteps which are too large. History plots which show wild fluctuations are indicative of a numerical instability. The only way to correct a numerical instability without changing other problem parameters is to reduce the timestep by using the **FRAC** command.

Increasing mass damping parameters can often hide instability but will not likely eliminate it. UDEC automatically determines a timestep which is stable for most cases; however, situations may arise when this timestep is too large. Situations which have been identified as causing numerical instability are:

(1) use of stiffness proportional damping which is too great at high frequencies;

(2) use of high values of joint dilation;

(3) use of problem geometries in which one block contacts many (more than 3) other blocks on one side; and

(4) use of non-reflecting (i.e., viscous) boundaries in which the bounding material is significantly stiffer than the material in the problem domain.

If the cause of the contact overlap cannot be identified, it may be necessary to use the **SET CSCAN** command. This command causes the location of the center of rounded corners to be updated more frequently, resulting in more accurate calculation of contact and overlap.

Another procedure for eliminating this error is to increase the rounding length at the start of the problem. This procedure is useful if the original rounding length was very small and/or the problem geometry involved blocks with very acute angles.

1.6 REFERENCES

Anderson, D. G. "Gaussian Quadrature Formulation for $\int_0^1 \ln(x) f(x)\,dx$," Math. Comp., 19, 477-481 (1965).

Azuar, Debreuille, Habib, Londe, Panet, Rochet and Salembier. "Rock Mass Reinforcement by Passive Rebars," in Proc. 4th International Congress on Rock Mechanics, Vol. 1, pp. 23-30. 1979.

Bandis, S. C., A. C. Lumsden, and N. R. Barton. "Fundamentals of Rock Joint Deformation," Int. J. Rock Mech. Min. Sci., 20, 244-268 (1983).

Barton, N., S. Bandis and K. Bakhtar. "Strength, Deformation and Conductivity Coupling of Rock Joints," Int. J. Rock Mech. Min. Sci. & Geomech. Abstr., 22, 121-140 (1985).

Barton, N., A. Makurat, M. Christianson and S. Bandis. "Modeling Rock Mass Conductivity Changes in Disturbed Zones," Rock Mechanics: Proceedings of the 28th U.S. Symposium (Tucson, June-July 1987), pp. 563-574. Rotterdam: A. A. Balkema, 1987.

Bathe, K.-J. and E. L. Wilson. Numerical Methods in Finite Element Analysis. Englewood Cliffs, New Jersey: Prentice-Hall, Inc., 1976.

Belytschko, T. "An Overview of Semidiscretization and Time Integration Procedures," in Computational Methods for Transient Analysis," T. Belytschko and T.J.R. Hughes, Eds, pp. 1-65. 1983.

Biggs, J. M. Introduction to Structural Dynamics. New York: McGraw-Hill, 1964.

Bjurstrom, S. "Shear Strength on Hard Rock Joints Reinforced by Grouted Untensioned Bolts," in Proc. 3rd International Congress on Rock Mechanics, Vol 2, pp. 1194-1199. 1979.

Brady, B.H G. "A Direct Formulation of the Boundary Element Method of Stress Analysis for Complete Plane Strain," Int. J. Rock Mech. Min. Sci. & Geomech. Abstr., 16, 235-244 (1979).

Brady, B.H.G., and J. W. Bray. "The Boundary Element Method for Determining Stresses and Displacements Around Long Openings in a Triaxial Stress Field," Int. J. Rock Mech. Min. Sci. & Geomech. Abstr., 15, 21-28 (1978).

Brady, B.H.G., and A. Wassyng. "A Coupled Finite Element-Boundary Element Method of Stress Analysis," Int. J. Rock Mech. Min. Sci. & Geomech. Abstr., 18, 475-485 (1981).

Brierley, G. "The Performance During Construction of the Liner of a Large, Shallow Underground Opening in the Rock," Ph.D. Thesis, University of Illinois at Urbana-Champaign, 1977.

Consus, P., G. H. Golub and D. P. O'Leary. "A Generalized Conjugate Gradient Method for the Numerical Solution of Elliptic Partial Differential Equations," in Sparse Matrix Computations, J. R. Bunch and D. J. Rose, Eds., pp. 307-322. New York: Academic Press, 1965.

Cook, N.G.W. "Natural Joints in Rocks: Mechanical, Hydraulic and Seismic Behaviour and Properties Under Normal Stress," 1st Jaeger Memorial Lecture, University of Minnesota, 1988.

Crouch, S. L. "Analysis of Stresses and Displacements Around Underground Excavations: An Application of the Displacement Discontinuity Method," report to the National Science Foundation, University of Minnesota, 1976.

Crouch, S. L., and A. M. Starfield. Boundary Element Methods in Solid Mechanics. London: Allen and Unwin, 1983.

Cruse, T. A. "An Improved Boundary Integral Equation Method for Three-Dimensional Elastic Stress Analysis," J. Comp. and Struct., 4, 741-754 (1974).

Cundall, P. A. "A Computer Model for Simulating Progressive Large Scale Movements in Blocky Rock Systems," in Proceedings of the Symposium of the International Society of Rock Mechanics (Nancy, France, 1971), Vol. 1, Paper No. II-8. 1971.

Cundall, P. A. "UDEC - A Generalized Distinct Element Program for Modelling Jointed Rock," Peter Cundall Associates, Report PCAR-1-80, report to U.S. Army, European Research Office, Contract DAJA 37-79-C-0548, March 1980.

Cundall, P. A. "Adaptive Density-Scaling for Time-Explicit Calculations," in Proceedings of the 4th International Conference on Numerical Methods in Geomechanics (Edmonton, 1982), pp. 23-26. 1982.

Cundall, P. A. "Numerical Experiments on Localization in Frictional Materials" Ingenieur-Archiv, 59, 148-159 (1989).

Cundall, P. A. "Distinct Element Models of Rock and Soil Structure," Chapter 4, Analytical and Computational Methods in Engineering Rock Mechanics, E. T. Brown, Ed., pp. 129-163. London: George Allen and Unwin, 1987.

Cundall, Peter A., and Roger D. Hart. "Development of Generalized 2-D and 3-D Distinct Element Programs for Modeling Jointed Rock," Itasca Consulting Group, Inc., Final Technical Report to U.S. Army Engineers Waterways Experiment Station, 1983.

Cundall, Peter A., and Roger D. Hart. "Analysis of Block Test No. 1 Inelastic Rock Mass Behavior: Phase 2 - A Characterization of Joint Behavior (Final Report)," Itasca Consulting Group, Inc. report to Rockwell Hanford Operations, Subcontract SA-957, March 1984.

Cundall, P. A., H. Hansteen, S. Lacasse and P. B. Selnes. "NESSI - Soil Structure Interaction Program for Dynamic and Static Problems," Norwegian Geotechnical Institute, Report 51508-9, December 1980.

Cundall, P. A., J. Marti, P. J. Beresford, N. C. Last and M. I. Asgian. "Computer Modeling of Jointed Rock Masses," U.S. Army Engineer Waterways Experiment Station, Vicksburg, Mississippi, Tech. Report N-78-4, August 1978.

Desai, C. S. and J. T. Christian, Eds. Numerical Methods in Geotechnical Engineering. New York: McGraw-Hill, 1977.

Dight, P. M. "Improvements to the Stability of Rock Walls in Open Pit Mines," Ph.D. Thesis, Monash University, 1982.

Dixon, J. D. "Analysis of Tunnel Support Structure with Consideration of Support-Rock Interaction," U.S. Dept. of Interior, Bureau of Mines Investigation RI7297, 1971.

Donovan, K., W. E. Pariseau and M. Cepak. "Finite Element Approach to Cable Bolting in Steeply Dipping VCR Stopes," in Geomechanics Applications in Underground Hardrock Mining. New York: AIME, 1984.

Dowding, C. H., T. B. Belytschko and H. J. Yen. "A Coupled Finite Element-Rigid Block Method for Transient Analysis of Rock Caverns," Int. J. Num. Anal. Meth. Geomech., 7, 117-127 (1883a).

Dowding, C. H., T. B. Belytschko and H. J. Yen. "Dynamic Computational Analysis of Openings in Jointed Rock," J. Geotech. Div. ASCE, 109, 1551-1566 (1983b).

Fuller, P. G., and R.H.T. Cox. "Rock Reinforcement Design Based on Control of Joint Displacement — A New Concept," in Proc. 3rd Aust. Tunnelling Conference (Sydney, 1978), pp. 28-35. 1978.

Gerdeen, J. C., V. W. Snyder, G. L. Viegelahn and J. Parker. "Design Criteria for Roof Bolting Plans Using Fully Resin-Grouted Nontensioned Bolts to Reinforce Bedded Mine Roof," U.S. Bureau of Mines, OFR 46(4)-80, 1977.

Goodman, R. E. Introduction to Rock Mechanics. New York: John Wiley & Sons, 1980.

Haas, C. J. "Shear Resistance of Rock Bolts,"Trans. Soc. Min. Eng. AIME, 260(1), 32-41 (1976).

Hart R. D., P. A. Cundall and M. L. Cramer. "Analysis of a Loading Test on a Large Basalt Block," in Research and Engineering — Applications in Rock Masses (Proceedings of the 26th U.S. Symposium on Rock Mechanics, Rapid City, June 1985), E. Ashworth, Ed., Vol. 2, pp. 759-768. Boston: A. A. Balkema, 1985.

Itasca Consulting Group, Inc. UDEC (Universal Distinct Element Code) User's Manual, Version ICG1.5. Minneapolis, Minnesota: ICG, 1989.

Karlekar, B. V., and R. M. Desmond. Heat Transfer, 2nd Ed. St. Paul, Minnesota: West Publishing Co., 1982.

Kunar, R. R., P. J. Beresford and P. A. Cundall. "A Tested Soil-Structure Model for Surface Structures," in Proceedings of the Symposium on Soil-Structure Interaction (Roorkee University, India, January 1976), Vol 1, pp. 137-144. Meerut, India: Sarita Prakashan, 1976.

Lachat, J. C. and J. O. Watson. "Effective Numerical Treatment of Boundary Integral Equations: A Formulation for Three-Dimensional Elasto-Statics," Int. J. Numerical Methods Eng., 10, 991-1005 (1976).

Lemos, J. V. "A Hybrid Distinct Element-Boundary Element Computational Model for the Half-Plane," M.S. Thesis, University of Minnesota, 1983.

Lemos, José. "A Distinct Element Model for Dynamic Analysis of Jointed rock with Application to Dam Foundations and Fault Motion," Ph.D. Thesis, University of Minnesota, June 1987.

Littlejohn, G. S., and D. A. Bruce. "Rock Anchors—State of the Art. Part I: Design," Ground Engineering, 25-32 (May 1975).

Lorig, L. J. "A Hybrid Computational Model for Excavation and Support Design in Jointed Media," Ph.D. Thesis, University of Minnesota, August 1984.

Lorig, L. J. "Rock Reinforcement: Mechanical Representations and Use in Finite Element Schemes," in Underground Engineering 1988 (Proceedings of the International Symposium on Underground Engineering (New Delhi, April 1988), pp. 223-232. Roorkee, India: Central Building Research Institute, 1988.

Lorig, L. J., and B.H.G. Brady. "A Hybrid Discrete Element-Boundary Element Method of Stress Analysis," in Issues in Rock Mechanics (Proceedings of the 23rd Symposium on Rock Mechanics, Berkeley, August 1982), pp. 628-636. New York: Society of Mining Engineers, 1982.

Lorig, L. J., and B.H.G. Brady. "An Improved Procedure for Excavation Design in Stratified Rock," in Rock Mechanics--Theory-Experiment-Practice (Proceedings of the 24th U.S. Rock Mechanics Symposium, Texas A&M University, 1983), pp. 577-586. New York: Association of Engineering Geologists, 1983.

Louis, C. "A Study of Groundwater Flow in Jointed Rock and Its Influence on the Stability of Rock Masses," Imperial College, Rock Mech. Research Report No. 10, 1969.

Love, A.E.H. A Treatise on the Mathematical Theory of Elasticity (Reprint). New York: Dover Publications, 1944.

Lysmer, J., and R. Kuhlemeyer. "Finite Dynamic Model for Infinite Media," J. Eng. Mech. Div. ASCE, 95, EM4 (1969).

Lysmer, J., and G. Waas. "Shear Waves in Plane Infinite Structures," J. Eng. Mech. Div. ASCE, 98, 85-105 (1972).

Marti, J., and P. A. Cundall. "Mixed Discretisation Procedure for Accurate Solution of Plasticity Problems," Int. J. Num. Methods in Eng., 6, 129-139 (1982).

Monsees, J. E. "Station Design for the Washington Metro System," in Proceedings of the Engineering Foundation Conference—Shotcrete Support, ACI Publication SP-54, 1977.

Nagtegaal, J. C., D. M. Parks and J. R. Rice. "On Numerically Finite Element Solutions in the Fully Plastic Range," Comp. Meth. in Appl. Mech. & Eng., 4, 153-177, 1974.

Otter, J.R.H., A. C. Cassell and R. E. Hobbs. "Dynamic Relaxation," Proc. Inst. Civil Engrs., 35, 633-665 (1966).

Paul, S. L., A. J. Hendron, E. J. Cording, G. E. Sgouros and P. K. Saha. Design Recommendations for Concrete Tunnel Linings - Volume I: Results of Model Tests and Analytical Parameter Studies (Final Report). UMTA-MA-06-0100-83-1/DOT-TSC-UMTA-82-37, November 1983.

Pells, P.J.N. "The Behaviour of Fully Bonded Rock Bolts," in Proc. 3rd International Congress on Rock Mechanics, Vol. 2, pp. 1212-1217. 1974.

Roesset, J. M., and M. M. Ettouney. "Transmitting Boundaries: A Comparison," Int. J. Num. Anal. Meth. Geomech., 1, 151-176 (1977).

Seed, H. B., J. Lysmer and R. Hwang. "Soil-Structure Interaction Analysis for Seismic Response," J. Geotech. Div. ASCE, 101, 439-457 (1975).

St. John, C. M., and D. E. Van Dillen. "Rockbolts: A New Numerical Representation and Its Application in Tunnel Design," in Rock Mechanics — Theory - Experiment - Practice (Proceedings of the 24th U.S. Symposium on Rock Mechanics (Texas A&M University, June 1983), pp. 13-26. New York: Association of Engineering Geologists, 1983.

Sokolnikoff, I. S. Mathematical Theory of Elasticity, 2nd Edition, New York: McGraw-Hill, 1956.

Telles, J.C.F., and C. A. Brebbia. "Boundary Element Solution for Half-Plane Problems," Int. J. Solids and Struct. 17, 1149-1158, 1981.

U.S. Nuclear Regulatory Commission (NRC). "Final Technical Position on Documentation of Computer Codes for High-Level Waste Management", NUREG-0856, 1983.

Voegele, M. D. "An Interactive Graphics-Based Analysis of the Support Requirements of Excavations in Jointed Rock Masses," Ph. D. Thesis, University of Minnesota, Minneapolis, 1978.

Wassyng, A. "Solving Ax = b: A Method with Reduced Storage Requirements," Soc. Indust. Appl. Math. J. Num. Anal., 19(1), 197-204 (1982).

Watson, J. O. "Advanced Implementation of the Boundary Integral Equation Method for Two- and Three-Dimensional Elastodynamics," in Developments in Boundary Element Methods, P. K. Banerjee and R. Butterfield, Eds. London: Applied Science Publishers, 1979.

White, W., S. Valliappan and I. K. Lee. "Unified Boundary for Finite Dynamic Models," J. Eng. Mech., Div. ASCE, 103, 949-964 (1977).

Wilkins, M. "Calculation of Elasto-Plastic Flow," University of California, Lawrence Radiation Laboratory, Report UCRL 7322, 1963.

Wilkinson, W. L. Non-Newtonian Fluids: Fluid Mechanics, Mixing and Heat Transfer. London: Pergamon Press, 1960.

Williams, John R., and Graham G.W. Mustoe. "Modal Methods for the Analysis of Discrete Systems," Computers and Geotechnics, 4, 1-19 (1987).

Witherspoon, P. A., J.S.Y. Wang, K. Iawi and J. E. Gale. "Validation of Cubic Law for Fluid Flow in a Deformable Rock Fracture," Lawrence Berkeley Laboratory, University of California, Berkeley, 1979.

Wolf, J. P. Dynamic Soil-Structure Interaction. Englewood Cliffs, New Jersey: Prentice-Hall, 1985).

Zienkiewicz, O. C. The Finite Element Method, 3rd Edition. New York: McGraw-Hill, 1977.

Zimmerman, Roger M., Robert L. Schuch, Donald S. Mason, Michael L. Wilson, Michael E. Hall, Mark P. Board, Robert P. Bellman and Mark L. Blanford. Final Report: G-Tunnel Heated Block Experiment. Sandia National Laboratories, SAND84-2620, May 1986.

NRC FORM 335 (2-89) NRCM 1102, 3201, 3202

U.S. NUCLEAR REGULATORY COMMISSION

BIBLIOGRAPHIC DATA SHEET

(See instructions on the reverse)

1. REPORT NUMBER (Assigned by NRC, Add Vol., Supp., Rev., and Addendum Numbers, if any.)

NUREG/CR-5429
Vol. 1

2. TITLE AND SUBTITLE

UDEC (Universal Distinct Element Code)
Version ICG1.5

Software Summary

3. DATE REPORT PUBLISHED

MONTH: September YEAR: 1989

4. FIN OR GRANT NUMBER

FIN D1016

5. AUTHOR(S)

Mark Board

6. TYPE OF REPORT

Formal

7. PERIOD COVERED (Inclusive Dates)

8. PERFORMING ORGANIZATION – NAME AND ADDRESS (If NRC, provide Division, Office or Region, U.S. Nuclear Regulatory Commission, and mailing address; if contractor, provide name and mailing address.)

Itasca Consulting Group, Inc.
1313 5th Street S.E., Suite 210
Minneapolis, MN 55414

9. SPONSORING ORGANIZATION – NAME AND ADDRESS (If NRC, type "Same as above"; if contractor, provide NRC Division, Office or Region, U.S. Nuclear Regulatory Commission, and mailing address.)

Division of High Level Waste Management
Office of Nuclear Material Safety and Safeguards
U.S. Nuclear Regulatory Commission
Washington, DC 20555

10. SUPPLEMENTARY NOTES

11. ABSTRACT (200 words or less)

UDEC is a two-dimensional distinct element code written for analysis of static or dynamic, mechanical, thermomechanical and fracture fluid flow problems in jointed rock or soil. The body to be analyzed is subdivided into a series of blocks which are separated from their neighbors by interface planes which have friction, cohesion and dilation. The blocks themselves may behave as non-linear materials also. The code uses an explicit solution procedure for solving the dynamic equations of motion for the blocks. The large deformation formulation allows interaction between adjacent blocks including slip or separation. General heat transfer logic, fluid flow along the fractures and structural element support are optional features.

12. KEY WORDS/DESCRIPTORS (List words or phrases that will assist researchers in locating the report.)

UDEC, distinct element method, explicit procedure, dynamic, heat transfer, fluid flow, interface planes, large deformation structural elements

13. AVAILABILITY STATEMENT

Unlimited

14. SECURITY CLASSIFICATION

(This Page) Unclassified

(This Report) Unclassified

15. NUMBER OF PAGES

16. PRICE

*U.S. GOVERNMENT PRINTING OFFICE:1989-262-436:00279

UNITED STATES
NUCLEAR REGULATORY COMMISSION
WASHINGTON, D.C. 20555

OFFICIAL BUSINESS
PENALTY FOR PRIVATE USE, $300

SPECIAL FOURTH-CLASS RATE
POSTAGE & FEES PAID
USNRC
PERMIT No. G-67

D. Chery
4-H-3